The role of bridging microtubules in anaphase of cell division

Buđa, Renata

University of Zagreb

FACULTY OF SCIENCE
DEPARTMENT OF BIOLOGY

Renata Buđa

THE ROLE OF BRIDGING MICROTUBULES IN ANAPHASE OF CELL DIVISION

DOCTORAL DISSERTATION

Zagreb, year 2020

University of Zagreb

FACULTY OF SCIENCE
DEPARTMENT OF BIOLOGY

Renata Buđa

THE ROLE OF BRIDGING MICROTUBULES IN ANAPHASE OF CELL DIVISION

DOCTORAL DISSERTATION

Iva Tolić, PhD, Research Advisor

Zagreb, year 2020

Sveučilište u Zagrebu

PRIRODOSLOVNO-MATEMATIČKI FAKULTET
BIOLOŠKI ODSJEK

Renata Buđa

ULOGA PREMOŠĆUJUĆIH MIKROTUBULA U ANAFAZI STANIČNE DIOBE

DOKTORSKI RAD

dr. sc. Iva Tolić, Znanstvena savjetnica

Zagreb, 2020.

This work was done in laboratory of Iva Tolić, PhD, Research Advisor at Ruđer Bošković Institute, Zagreb, under supervision of prof. dr. sc. Iva Tolić. As a part of Postgraduate doctoral programme of Biology, this thesis is submitted for review to Department of Biology at Faculty of Science, University of Zagreb in order to achieve the academic degree doctor of biology.

Supervisor biography

Professor Iva Tolić was born in Zagreb, Croatia. She graduated Molecular biology at Faculty of Science, University of Zagreb, Croatia in 1996. During graduate studies, she worked as Research assistant in the group of Prof. Nenad Trinajstić, Ruđer Bošković Institute. Her PhD work was done with Prof. Ning Wang, Harvard School of Public Health, Boston, USA. She achieved the academic degree Doctor of biology at University of Zagreb in 2002. After this, she worked as a postdoctoral fellow with Prof. Kirstine Berg-Sørensen, Niels Bohr Institute, Copenhagen, Denmark and later with with Prof. Francesco Pavone, LENS - European Laboratory for Non-Linear Spectroscopy, Florence, Italy. From 2005 until 2014 she worked as a Research Group Leader at Max Planck Institute of Molecular Cell Biology and Genetics in Dresden, Germany. Her research areas are mitosis, mitotic spindle mechanics, microtubules, motor proteins and other processes in the cell that rely on cytoskeletal components and motor proteins. Professor Tolić has received 14 research grants including the prestigious projects funded by the European Research Council (ERC), *Consolidator* and *Synergy*. She has published more than 80 papers in peer-reviewed journals including *Science*, *Cell*, and *Nature Cell Biology*, cited more than 3500 times, and served as reviewer for these and various other journals. She has been elected to EMBO membership and received numerous awards such as the Ignaz Lieben Award of the Austrian Academy of Sciences and European Biophysical Societies Association (EBSA) Young Investigators' Medal and Prize. To this date she has mentored 8 PhD and 4 Master theses. As an invited speaker, she has participated in more than 100 conferences and research seminars worldwide. She organized several scientific meetings including the EMBO Conference on Meiosis in Hvar. Currently, professor Tolić is a Senior Research Group Leader with tenure at Ruđer Bošković Institute in Zagreb.

Acknowledgemets

I would like to express my gratitude to my supervisor Iva Tolić for an opportunity to work on this project, for the knowledge I gained during these years and for the experience I gathered that would help me in my future challenges.

I thank my family for the amazing support and love, my dad for teaching me to be patient and less stubborn, my mom for always being on my side and listening me even when I'm quite boring, my sister for being the most tender and optimistic person and my second mom. Most important, I thank my nephews, Luka and Mario, for constantly keeping me dynamic, for all the board games, great laughs and all the new things they have thought me. Their unconditional love was and is my biggest motivation.

Special thanks goes to my love and my best friend Dimitrij. Thank you for reminding me on how important it is to keep the inner child awaken and to appreciate the honesty and good in people. Because of you, I always feel exceptional.

To my friends, thank you for all the amazing moments while growing up, for all the new experiences, peculiar and pointless conversations and for accepting each side of me.

Big thanks to my lab colleagues and friends, particularly Ivana Šarić for the drawings and Ana Milas for help with photoactivation experiments in intact spindels. Special thanks to my lab partner Kruno, for giving me fundamental knowledge when I first started, for mutual learning, amazing patience and constant enthusiasm. Dear lab mates, you made that every challenge in the lab always looks achievable and fun.

University of Zagreb
Faculty of Science
Department of Biology

Doctoral thesis

The role of bridging microtubules in anaphase of cell division

Renata Buđa
Ruđer Bošković Institute

During cell division, microtubules of the mitotic spindle segregate chromosomes by exerting forces on kinetochores, protein complexes on the chromosomes. The central question is which forces drive chromosome segregation. The current model for anaphase in human cells includes shortening of kinetochore fibers and separation of spindle poles, processes that require kinetochore-pole connections. By combining laser ablation, photoactivation and protein depletion, we show that kinetochores can separate without the attachment to the pole. This separation requires the bridging fiber, which connects sister k-fibers whereby astral microtubules do not contribute to the separation. Bridging microtubules in intact spindles slide apart together with k-fibers, indicating strong crosslinks between them. Kinetochore segregation and pole separation is slower after depletion of MKLP1/KIF23 (kinesin-6), faster after depletion of KIF4a (kinesin-4), and unaffected by reduction of Eg5/KIF11 (kinesin-5) or KIF15/Hklp2 (kinesin-12). We assume that motor-generated sliding in the bridging fibers drives pole separation and pushes k-fibers poleward, thereby working together with k-fiber shortening to segregate chromosomes.

(108 pages, 64 figures, 1 table, 188 references, original in English)
Key words: anaphase, bridging fiber, chromosome segregation, laser ablation, MKLP1
Supervisor: Iva Tolić, PhD, Research Advisor
Reviewers: Juraj Simunić, PhD, Research Associate
Dubravko Pavoković, PhD, Assistant Professor
Thomas Surrey, PhD, Principal Investigator

Sveučilište u Zagrebu
Prirodoslovno-matematički fakultet
Biološki odsjek

Doktorski rad

Uloga premošćujućih mikrotubula u anafazi stanične diobe

Renata Buđa
Institut Ruđer Bošković

Tijekom stanične diobe, mikrotubuli u diobenom vretenu razdvajaju kromosome stvarajući sile na kinetohore, proteinske komplekse na kromosomima. Unatoč mnogim istraživanjima u ovom području, ostalo je upitno koje sile upravljaju segregacijom kromosoma. Trenutno prihvaćen model za anafazu u ljudskim stanicama obuhvaća skraćivanje kinetohornih mikrotubula i razdvajanje polova diobenog vretena, procese koji zahtijevaju vezu između kinetohore i pola. Primjenom laserske ablacije, fotoaktivacije i deplecije proteina, u ovom radu je pokazano da se kinetohore mogu razdvajati i kada nema veze sa polom diobenog vretena. Takvo razdvajanje zahtjeva antiparalelna premošćujuća vlakna, koja povezuju sestrinska kinetohorna vlakna i kližu jedan preko drugog, dok astralni mikrotubuli ne doprinose navedenom procesu razdvajanja. Također, premošćujuća vlakna u netaknutom diobenom vretenu kližu zajedno sa kinetohornim vlaknima, a to upućuje na snažnu povezanost između te dvije populacije vlakana. Brzine razdvajanje kinetohora i polova su manje nakon utišavanja MKLP1/KIF23 (kinezin-6), više nakon utišavanja KIF4a (kinezin-4) i nepromijenjene nakon inhibicije/utišavanja Eg5/KIF11 (kinezin-5) i/ili KIF15/Hklp2 (kinezin-12) proteina. Zaključak ovog rada je da premošćujući mikrotubuli kližu, vjerojatno uz pomoć motornih proteina, odgurujući tako kinetohorna vlakna sa kinetohorama, kao i polove, jedne od drugih. Takav mehanizam djeluje skupa sa skraćivanjem kinetohornih vlakana i posljedica njihovog zajedničkog djelovanja je razdvajanje kromosoma u ljudskim stanicama.

(108 stranica, 64 slike, 1 tablica, 188 literaturnih navoda, jezik izvornika engleski)
Ključne riječi: anafaza, premošćujuća vlakna, segregacija kromosoma, ablacija, MKLP1
Mentor: Dr. sc. Iva Tolić, Znanstvena savjetnica
Ocjenjivači: Dr. sc. Juraj simunić, Znanstveni suradnik
Dr. sc. Dubravko Pavoković, Docent
Dr. sc. Thomas Surrey, Principal investigator

Table of Contents

1 INTRODUCTION

The cell cycle of most eukaryotic cells is composed of interphase, followed by the mitotic phase. The main events of cell cycle appear during S phase (for synthesis), in which DNA replication occurs, and also during M phase when duplicated chromosomes divide into two daughter cells. In most cells, there are two G (for gap) phases, which separate the S phase and M phase events. G_1, S and G_2 phase belong to the interphase while the M phase consists of mitosis (nuclei division) and cytokinesis (cytoplasm division) (Alberts et al., 2014). The nuclear envelope breakdown at the end of first mitotic stage - prophase, in most eukaryotic cells, indicates the beginning of prometaphase in which microtubules (MTs) restructure, mitotic spindle formation occurs and chromosomes start to congress into metaphase plate. During metaphase, chromosomes are aligned at the central plane of the spindle whereby it is important that sister chromatids are properly connected to the opposite spindle poles. After proper chromosome congression, securin ubiquitination allows the sister chromatids to separate during anaphase. In telophase, chromosome decondensation occurs, nuclear envelope reappears and microtubule cytoskeleton reorganizes. Ultimately, the cell cytoplasm divides during cytokinesis (Alberts et al., 2014).

A mitotic spindle is a central structure of mitosis, composed of MTs and microtubule associated proteins, which enables chromosome division (Pavin and Tolic, 2016). MTs are microscopic protein tubes, formed by the polymerization of α- and β-tubulin, organized into a bundle of microtubules, termed fibers, in the mitotic spindle. Microtubule ends with α-subunits exposed are named minus (-) ends, while microtubule ends with the β-subunits exposed are named plus (+) ends, respectively (Alberts et al., 2014). Depending on the MT orientation, we can distinguish between parallel and antiparallel fibers. Kinetochore fibers (k-fibers) are the most stable and the most important fibers which attach with their (+) ends to the kinetochores, the protein complexes on the chromosome (Musacchio and Desai, 2017). Such k-fiber attachments enable chromosomes to link with the mitotic spindle. Electron microscopy has shown that k-fibers in human cancer cells contain 12-22 parallel MTs linked together (Wendell et al., 1993). Beside k-fibers, a mitotic spindle contains two more kinds of MTs – interpolar and astral MTs. Interpolar MTs are organized into antiparallel bundles as they overlap at the center of the spindle and astral microtubules extent from spindle poles into the cytoplasm where they interact with the cell cortex thereby participating in spindle positioning inside the cell (Alberts et al., 2014).

The ultimate goal of mitotic spindle machinery is to properly segregate chromosomes during anaphase. Anaphase relies on multiple mechanisms, even in an individual cell. However, in most model systems, chromosome separation includes poleward chromosome movement (anaphase A) and spindle elongation (anaphase B) (Asbury, 2017; Pavin and Tolic, 2016). One of the mechanisms contributing to anaphase A is "Pac-Man" mechanism where kinetochores stimulate k-fiber depolymerization at their (+) ends (Mitchison et al., 1986). Another mechanism, “poleward flux”, refers to k-fiber poleward movement due to depolymerisation at their (-) ends (Mitchison, 1989). The sliding of overlap MTs at the centre of the spindle (Saxton and McIntosh, 1987) combined with pulling of astral MTs from the cell cortex (Aist et al., 1993) could lead to spindle pole and chromosome separation in anaphase B.

Furthermore, previous research on anaphase in human cells has marked the importance polymerization and depolymerization of k-fibers in chromosome motion (Ganem et al., 2005; Sikirzhytski et al., 2014; Stumpff et al., 2008), while the contribution of forces acting from the central spindle or the cell cortex remained unknown. According to the classical structural model of mitotic spindle, only MTs within k-fibers, which directly interact with kinetochores, can generate forces on kinetochores. On the other side, interpolar MTs do not interact with kinetochores and the interaction with k-fibers is weak and exists only in the vicinity of the spindle poles (Alberts et al., 2014). However, the electron microscopy experiments of mitotic spindle in different model systems, including human cells, have shown non-kMTs in the vicinity of k-fibers (McDonald et al., 1992; Nixon et al., 2017; Ohi et al., 2003). Also, the recent laser ablation experiments have shown the strong interaction between k-fibers and interpolar antiparallel MTs named briding MTs (Kajtez et al., 2016). The bridging MTs bridge sister k-fibers and balance the tension between sister kinetochores (Milas and Tolic, 2016). Likewise, recent work has shown that almost all interpolar MT bundles are associated with kinetochores and act as a bridge between sister k-fibers in metaphase (Polak et al., 2017). Because of their antiparallel organization and their attachment to sister k-fibers, bridging fibers may have a role in anaphase chromosome separation.

Despite intense research on anaphase in a variety of model organisms, the mechanisms driving chromosome segregation in human cells are not well known. Previous research has shown that spindle pole separation could be explained by a variety of mechanisms. In diatoms, fission yeast, grasshopper and *Drosophila* embryo, the pole-pole separation occurs by outward sliding of interpolar MTs (Brust-Mascher et al., 2009; Khodjakov et al., 2004; Leslie and Pickett-Heaps, 1983; Tolic-Norrelykke et al., 2004). On

the contrary, severance of the spindle midzone accelerated pole separation during anaphase B in *Nectria haematococca*, PtK2 cells, and *C. elegans.* This suggested that midzone microtubules serve as a brake on pole-to-pole separation and demonstrates a contribution from cortical pulling (Aist et al., 1991; Aist et al., 1993). Therefore, anaphase relies on multiple mechanisms among different model systems. In human cells, one mechanism or a combination of them could influence chromosome segregation. My hypothesis on anaphase revisits the old ideas that force for anaphase movement can be generated in the midzone by MT sliding and pushing, and transmitted along the entire k-fiber (Belar, 1929). Östergren proposed that these forces are produced all along the k-fiber rather than only at its ends (Östergren, 1951). Also, Mcintosh et al. suggested that MT sliding moves the chromosomes apart (McIntosh et al., 1969). Although such ideas have been mentioned in several works, they have not been directly tested in human cells and remain largely unappreciated.

To answer some of the questions, the motivation of this research is to examine a possible role of bridging microtubules in anaphase of human cells. Also, if the role of the bridging microtubules is confirmed, it is important to determine if the bridging microtubules are essential for normal anaphase dynamic. Furthermore, the goal is to describe closer the mechanism in which bridging microtubules influence the anaphase movement and how such mechanism cooperates with other known anaphase mechanisms in human cells.

To obtain experimental data for the ideas outlined above, we will use live-cell imaging, laser cutting of MT bundles, photoactivatable GFP experiments and inhibition of candidate motor proteins. First experimental step is the imaging of control U2OS cells without laser ablation as the reference measurements for anaphase dynamic and in order to exclude the possible negative effect from laser ablation. Next, we will combine live imaging and laser ablation where the latter is going to be performed on the outermost k-fiber in the spindle, 2-3 μm from the kinetochore. Laser ablation refers to removal of specific structures or parts of structures, in this case microtubule fibers. Outermost k-fibers are selected for ablation because they move away from the spindle after the cut. This way it is easier to distinguish a single kinetochore pair and the associated microtubules from their neighbors. The distance of 2 - 3 μm away from the kinetochore is chosen to preserve the connection between the bridging fiber and the k-fiber (Kajtez et al., 2016). After laser ablation, it is necessary to determine if the bridging fiber between displaced kinetochores remained preserved during anaphase and if they are similar to the previously described bridging fibers in metaphase (Kajtez et al., 2016). Furthermore, their antiparallel nature will be examined with PRC1 protein which binds to antiparallel overlap regions, in this case bridging fibers. If

the bridging fibers remain preserved after ablation and kinetochores segregate properly, another set of experiments will combine the above mentioned experiment with photoacivation of bridging fibers in order to observe the bridging fibers behavior during anaphase. Also, one of the approaches includes cutting of bridging fiber with laser ablation after the severing of k-fiber or an indirect removal by cutting a k-fiber close to the kinetochore (in order to disrupt the connection between the bridging fiber and the k-fiber). These types of experiments would verify the necessity of bridging fibers in chromosome segregation after laser ablation. In order to estimate the importance of bridging microtubules on a whole mitotic spindle scale, all bridging fibers in the center of the spindle will be removed. After each experimental approach, the velocities for kinetochores and spindle poles during anaphase will be calculated and compared with controls. The experimental data from modified cells is going to be obtained on a large number of cells, showed both, graphically and statistically, and compared to control cells.

The main conceptual advance of this work is the finding of novel mechanisms which contribute to chromosome segregation in human cancer cells and were not previously included in existing anaphase models. These novel findings will contribute to better understanding of anaphase mechanism and potentially help its manipulation and regulation in future.

2 OVERVIEW OF LITERATURE

2.1 Cell cycle

The cell cycle of most eukaryotic cells can be roughly divided into interphase and the mitotic phase (M phase) and its duration is 24h hours. As interphase is set between two mitotic divisions, during this time cell reorganizes its interior, grows and prepares for the next mitosis. The main changes of cell cycle appear during S phase of interphase, in which deoxyribonucleic acid (DNA) replication occurs. G_1 and G_2 phase also belong to the interphase and during these phases the cell doubles its mass of proteins and organelles (Alberts et al., 2014). It is also possible for cell to enter G_0 phase from G_1 phase, which is a resting period that can even last for a longer period of time before the cell cycle resumes. Most of the cells return to the G_1 phase from G_0 but there are cells called post-mitotic cells, like neurons for example, that are metabolically active but do not divide (Lodish et al., 2000). G phases mark the gap phase between S and M phase as they give the cell time to feed, grow and control the accuracy of on-going events. During M phase, which consists of mitosis and cytokinesis, cell divides to form two identical daughter cells. Interestingly, M phase lasts for about 1 hour and the cell spends more than 95% of the time in the interphase (**Figure** 1) (Alberts et al., 2014).

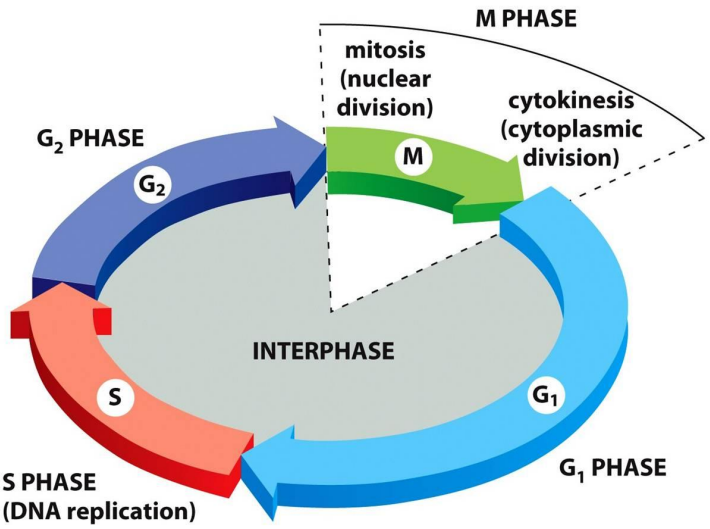

Figure 1 The phases of the cell cycle. Interphase consists of three phases: S phase which includes DNA replication, G_1 phase as the gap between M phase and S phase and G_2 phase as the gap between S phase and M phase. The M phase consists of mitosis and cytokinesis (Alberts et al., 2014).

Cell cycle regulation depends on the different signals from the inside and outside of the cell. If the cell experiences unfavorable conditions or it cannot complete a specific cell cycle phase, a regulation system is going to prevent the cell cycle to enter the next phase. Therefore, three control points or checkpoints occur in the interphase of the cell cycle - the G_1 checkpoint at the G_1/S transition, the S checkpoint during S phase, the G_2 checkpoint at the G_2/M transition. The spindle assembly checkpoint (SAC) is active during mitotic phase, at the transition from metaphase to anaphase (Cooper and Hausman, 2003). S phase checkpoint regulates progress through the cell cycle, DNA repair and DNA replication itself and assures the fidelity of DNA replication before cells enter M-phase (Longhese et al., 2003). The G_1 cell cycle checkpoint controls the passage of cells from the first 'gap' phase (G_1) into the DNA S phase. This is a point where cells typically arrest the cell cycle if environmental conditions are unfavorable for cell division, such as the presence of DNA damage or lack of growth factors (Yang, 2018). The G_2 checkpoint prevents cells from entering mitosis when DNA is damaged, providing an opportunity for repair and stopping the proliferation of damaged cells (Stark and Taylor, 2004). The spindle assembly checkpoint (SAC) activates when kinetochores are not properly attached to the spindle and blocks cell cycle progression (**Figure** 2) (Nezi and Musacchio, 2009).

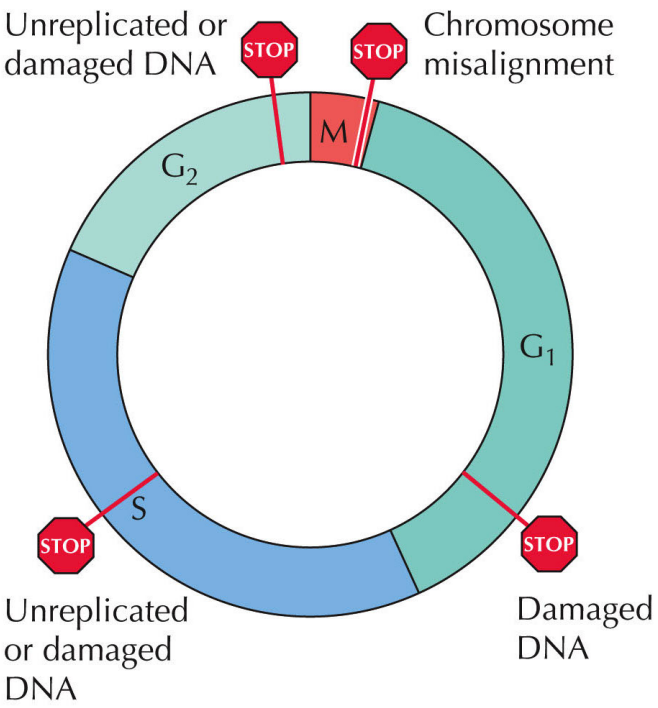

Figure 2 Four control points or checkpoints in the cell cycle - the G_1 checkpoint at the G_1/S transition, the S checkpoint during S phase, the G_2 checkpoint at the G_2/M transition during Interphase. Spindle assembly checkpoint (SAC) during M phase (Cooper and Hausman, 2003).

Major components of the cell cycle regulation system are cyclin dependent kinases (CDKs). By phosphorylating certain intracellular proteins, they regulate major events in the cell cycle such as DNA replication, mitosis and cytokinesis (Alberts et al., 2014; Galderisi et al., 2003). Cyclin dependent kinases are present in a cell at a constant level but are cyclically active. The catalytic subunits are in molar excess, but lack activity until bound by their cognate cyclin subunits and form cyclin-CDK complex (Alberts et al., 2014; Barnum and O'Connell, 2014). The four major mechanisms of CDK regulation are cyclin binding, CDK-activating kinase (CAK) phosphorylation, regulatory inhibitory phosphorylation, and binding of CDK inhibitors (CKIs) (Alberts et al., 2014). Cyclins are proteins that vary in quantity throughout the cell cycle. They are synthesized during a specific phase of the cell cycle and broken down after they fulfill their purpose. When the cyclins and CDKs that are expressed in a specific form a complex and became activated, they phosphorylate the serine and threonine residues of a target protein. The phosphorylated target protein executes the events occurring in the respective phases of the cell cycle (Asashima et al., 2010).

At the end of G_1 phase, the cell checks the quality of the DNA, the presence of specific growth factors and cell size which is controlled by cyclin D-CDK 4/6 and cyclin E-CDK 2. The control of the integrity of DNA continues during S phase with cyclin A-CDK 2 as the regulator. At the end of G_2 phase, the cell checks that all the proper structures are there and ready for cell division. This is especially important for the microtubules and replicated DNA from the S phase. If these conditions are not fulfilled, cells enter in an inactive state where DNA repair or apoptosis can occur. This checkpoint is controlled by G_2/M-phase cyclin and G_2/M-phase CDK (cyclin B-Cdc2 complex) (**Figure** 3) (Asashima et al., 2010; Cooper and Hausman, 2003). When the cell passes G_2 checkpoint, nuclear membrane breakdown and chromosome formation starts and this indicates the start of M phase (Asashima et al., 2010).

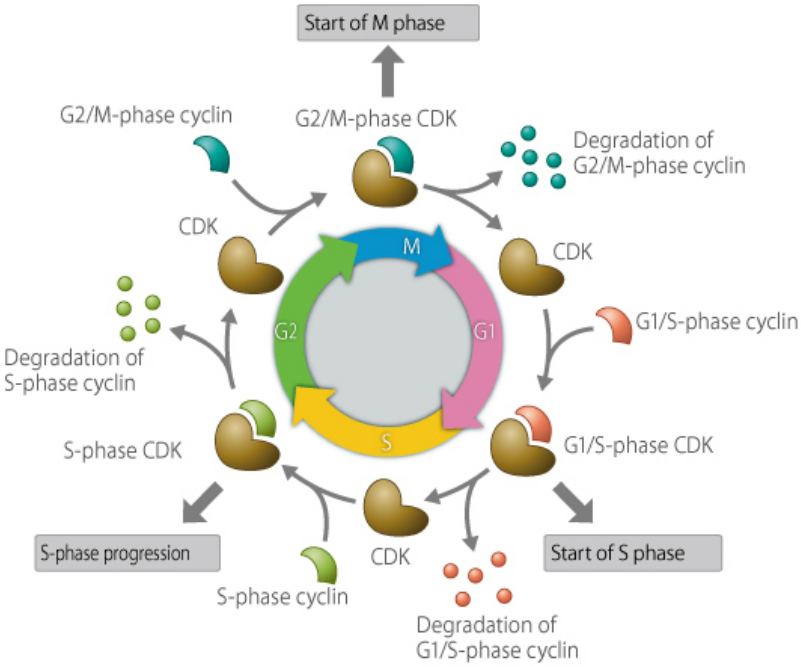

Figure 3 CDKs as the main cell cycle regulators. The cell cycle is controlled at checkpoints in G_1/S phase, in S phase and in G_2/M phase by different cyclins (Asashima et al., 2010).

2.2 Mitotic phase

Mitosis is a stage in cell cycle during which condensed chromosomes migrate to the center of the cell and segregate into two daughter nuclei before cytokinesis (cell division) with the aid of a dynamic mitotic spindle (Yanagida, 2014). There are five phases during

nuclei division of M phase – prophase, prometaphase, metaphase, anaphase and telophase followed by cytoplasmic division – cytokinesis (**Figure** 4).

The first phase of mitosis is prophase, marked by the chromatin condensation into individual chromosomes, which contain centromere regions where kinetochores assemble. Each chromosome decreases the length and increases the thickness as prophase progresses, individualizing the strands of DNA into noticeable units. As chromatin condenses, the nucleolus disperses (McIntosh, 2016). Also, during prophase, the nuclear envelope is intact and the mitotic spindle begins to form outside nuclear envelope from microtubule organizing centers (MTOCs) usually called centrosomes (Wayne, 2010). Centrosomes begin to migrate to the opposite poles of the cell as the microtubules grow which results in the formation of the bipolar spindle (Wayne, 2010).

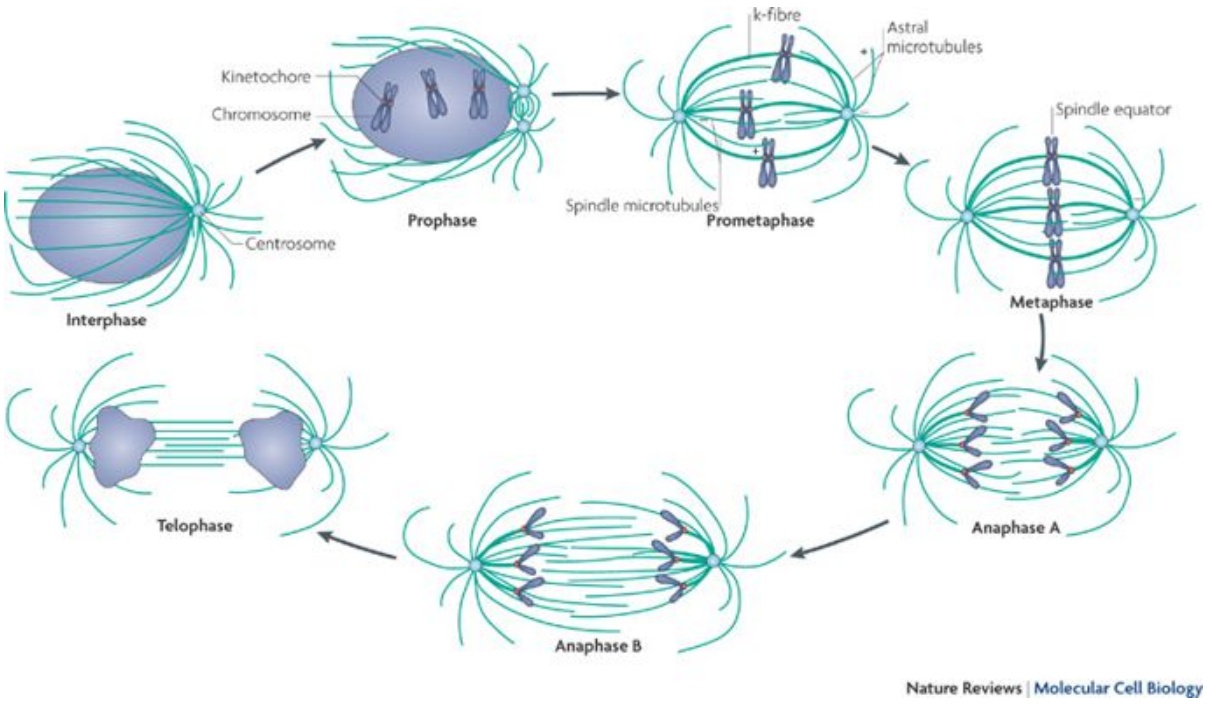

Figure 4 Phases of mitosis. Nucleic cell division of mitosis is divided into five phases – prophase, prometaphase, metaphase, anaphase and telophase (Walczak et al., 2010).

Just before the next phase of mitosis, prometaphase, the spindle undergoes contractions and the oscillations and beginning of prometaphase is marked by the nuclear envelope breakdown (NEBD). During this phase, multiple proteins associate with the kinetochore within the centromeres, and microtubules attached at the kinetochores (kinetochore microtubules) begin to move chromosomes to the center of the cell (**Figure** 5) (Goodman, 2008).

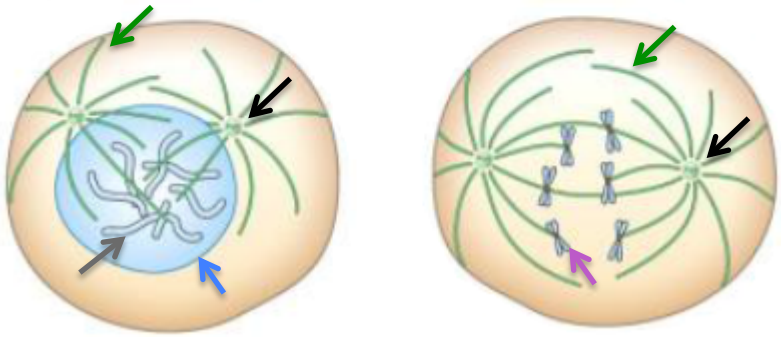

Figure 5 From prophase to prometaphase. In prophase, chromation condenses and centrosomes start to migrate to opposite sides. The nuclear envelope breaks down in prometaphase and MTs attach to the kinetochores. Arrows: blue – nuclear envelope, green – MT, black – centrosome, grey – chromatin, purple - chromosome (Alberts et al., 2014).

Metaphase is evident when all of the chromosome pairs are fully condensed, attached to the mitotic spindle microtubules and aligned at the central metaphase plate. The kinetochore fibers exert forces on the kinetochores through the cohesin, a protein complex associated to chromosomes, in order to pull them towards the opposite spindle poles and to generate the tension which indicates that the sister chromatids have achieved appropriate biorientation. The cell constantly monitors the attachments of microtubules to the chromosomes ensuring that the sister chromatids are properly aligned at the metaphase plate (**Figure** 6) (Malumbres, 2020; Musacchio and Salmon, 2007; Sacristan and Kops, 2015). This process is the foundation of the mitotic stage checkpoint called the spindle assembly checkpoint (SAC, see above). If one of sister kinetochores does not properly attach to a kinetochore microtubule, the transition to anaphase is inhibited. The main protein involved in this process is Mad2, which attaches to the kinetochores that are not attached to microtubules and becomes activated. It interacts with the protein Cdc20 in order to inhibit Cdc20 activity. Since Cdc20 is an activator of anaphase-promoting complex/cyclosome (APC/C) that is required to initiate anaphase, transition to anaphase will be inhibited as long as Mad2 protein

is present (Asashima et al., 2010). In cultured mammalian cells, there is an interval of ≈ 20 min between the establishment of proper microtubule attachment on the last chromosome and the onset of anaphase (Rieder et al., 1995).

Anaphase is one of the most spectacular phases of the cell cycle, when coordinated segregation of the sister chromatids occur (**Figure** 6).

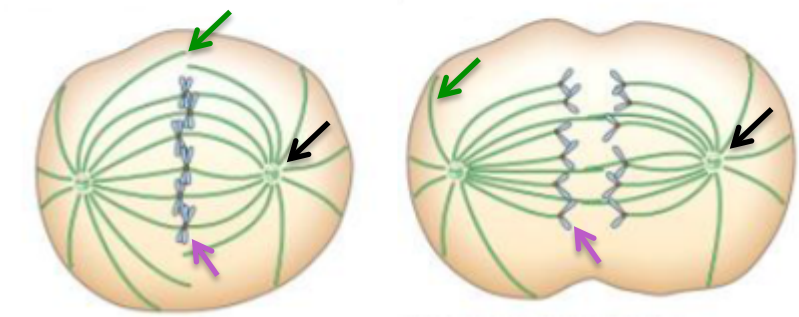

Figure 6 From metaphase to anaphase. During metaphase, chromosome pairs allign at the center of the mitotic spindle that are later segregated during next phase, anaphase. Arrows: green – MT, black – centrosome, purple - chromosome (Alberts et al., 2014).

It is divided into two phases: anaphase A where chromosomes move poleward as a consequence of the k-fiber depolymerization at the a plus and at the minus end (Mitchison et al., 1986), and anaphase B where the spindle elongates to additionally increase the distance between chromosomes (Asbury, 2017; Scholey et al., 2016). Since the process of anaphase is the foundation of this study, it is going to be described in more detail in the following sections.

The last stage of mitotic nuclear division is telophase. During telophase, sister chromatids reach the opposite poles and the nuclear envelope around opposite groups of chromosomes starts to form. As the nuclear envelopes re-form, the chromosomes begin to decondense (McMillan, 2018). To complete the cell cycle, the invagination of the cell membrane, cleavage furrow, pulls the plasma membrane toward the cell center, pinching the cytoplasm into two lobes that are subsequently separated into two cells during cytokinesis (**Figure** 7) (Glotzer, 2004).

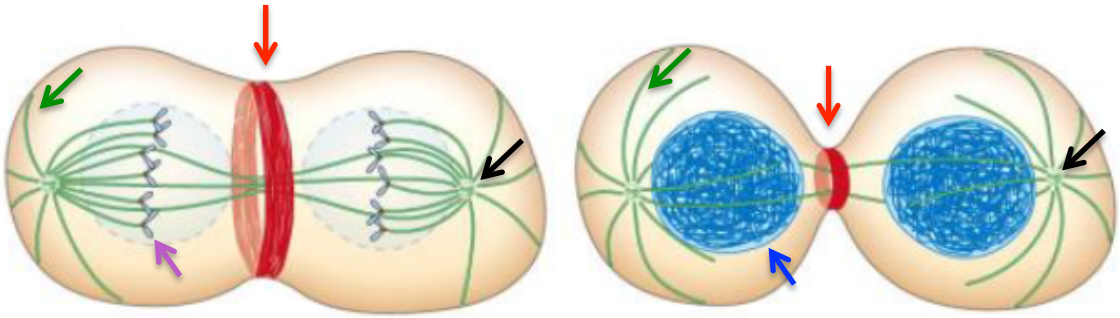

Figure 7 Telophase and cytokinesis. Nuclei division is completed during telophase. The last mitotic phase, cytokinesis indludes cytoplasm division. Arrows: green – MT, black – centrosome, purple – chromosome, red – cleavage furrow, blue – chromosome decondensation (Alberts et al., 2014).

2.3 Cytoskeleton and microtubules

All eukaryotic cells contain a three-dimensional network of cytoplasmic protein filaments called the cytoskeleton. The cytoskeleton is composed of actin filaments (microfilaments), intermediate filaments and microtubules that that are under the influence of proteins that regulate their length (**Figure** 8), polymerization state and level of cross-linking (Alberts et al., 2014; Goodman, 2008; Stringham et al., 2012). For example, protein members of the myosin family move vesicles along actin microfilaments, whereas members of the kinesin and dynein families move cargo along microtubule tracks and play essential roles in the formation and function of the mitotic spindle. Such dynamic and multifunctional structure of cytoskeleton and associated-proteins enables some of the fundamental processes including chromosome segregation, cell migration, cell polarity, subcellular organelle distribution and intracellular trafficking (Goodman, 2008; Stringham et al., 2012).

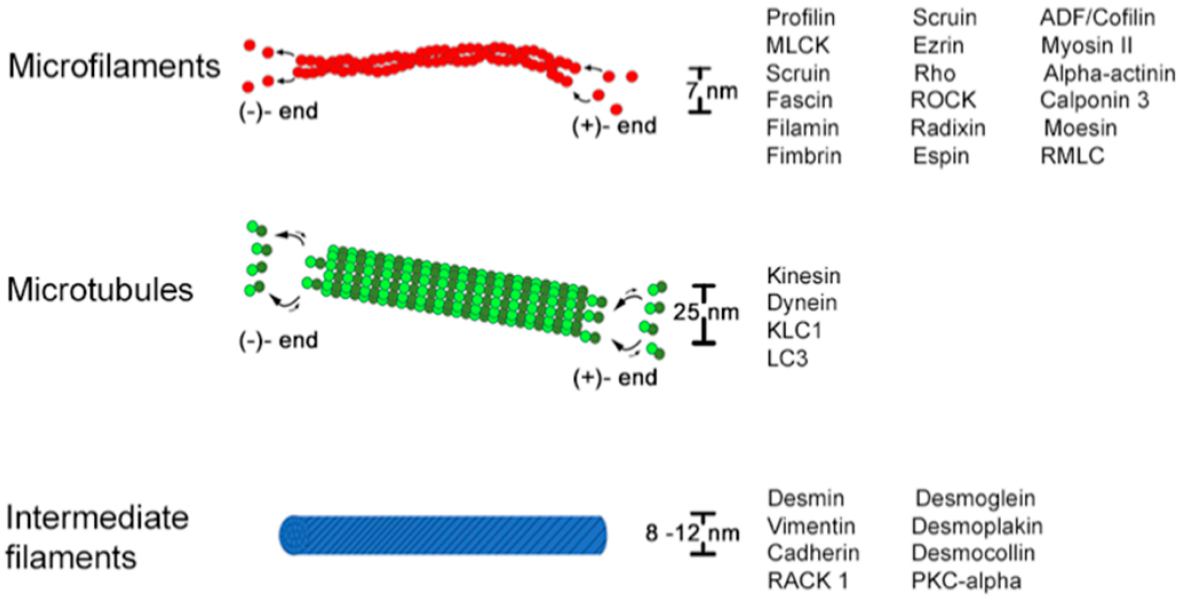

Figure 8 Cytoskeleton components and the associated proteins (Tarau et al., 2019)

The major cytoskeletal protein of most cells is actin, which polymerizes to form actin filaments, flexible fibers approximately 7 nm in diameter and up to several micrometers in length. Within the cell, they are organized into bundles especially abundant beneath the plasma membrane, where they form a network that provides mechanical support, determines cell shape, and allows movement of the cell surface (Cooper, 2000). Additionally, the interaction of filamentous actin with myosin forms the basis of muscle contraction (Dominguez and Holmes, 2011).

Each actin monomer (G actin) has tight binding sites that mediate head-to-tail interactions with two other actin monomers, so actin monomers polymerize to form filaments (filamentous F actin) (Cooper, 2000; Feher, 2012). Adenosine triphosphate (ATP) hydrolysis by F actin is one of the main factors regulating the transition between G and F actin. Basically, actin monomers join the fast-growing barbed end (plus end) of the filament in the ATP state, hydrolysis takes place in the filament, and ADP-actin monomers dissociate faster from the pointed end (minus end) (Wegner and Isenberg, 1983). The concentration of G actin in the local environment determines if a filament is going to grow on both ends (high concentration), shrink at both ends (low concentration) or grow at the plus end while shrinking at the minus end. This state achieved at a particular concertation, when polymerization and depolymerization are balanced, is known as steady state, whereby a constant filament length is maintained (**Figure** 9) (Carlier et al., 1987; Cooper, 2000).

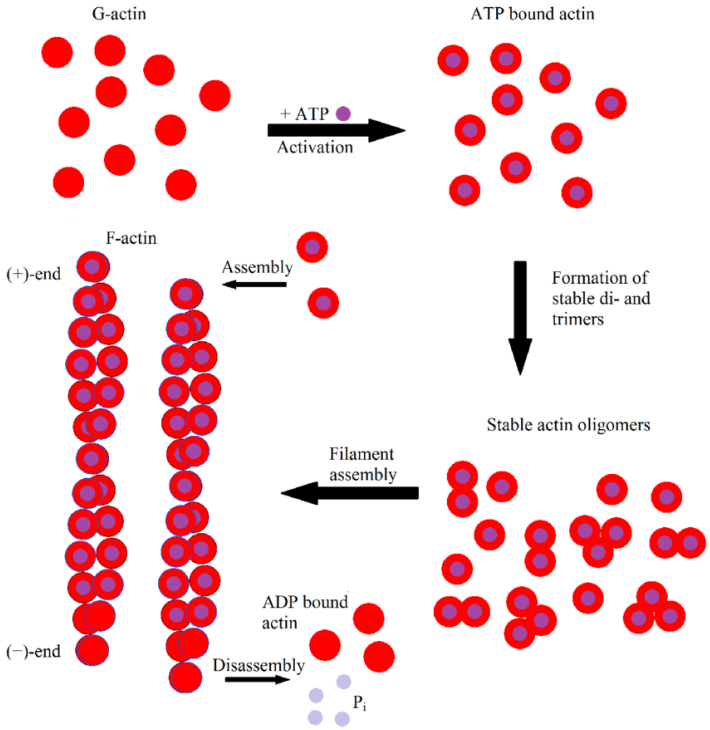

Figure 9 Scheme of actin filament formation. F actin filaments elongate by addition of G actin monomers. Hydrolysis of ATP to ADP leads to a distinction between the fast growing (+)-end and the slower growing or dissociating (−)-end (Hohmann and Dehghani, 2019).

Intermediate filaments are strong but flexible polymers with 10 nm diameter that provide mechanical support for the cells. They were first recognized between thick and thin filaments in the striated muscles after which they were eventually named intermediate (Pollard et al., 2017). Intermediate filaments are classified into five major types based on their structure and sequence homology. The first four types (I–IV) are cytoplasmic, whereas type V resides in the nucleus. Types I and II are the acidic and neutral-basic keratins, typically found in epithelial cells (Lowery et al., 2015; Moll et al., 2008). Type III is composed of vimentin, desmin, peripherin, or glial fibrillary acidic protein (GFAP). Vimentin is typically expressed in fibroblasts, desmin is the major intermediate filament protein of smooth, skeletal, and cardiac muscle, peripherin is found mainly in neurons of the peripheral nervous system and GFAP is located in astrocytes and glial cells. Type IV includes those expressed in the nervous system and type V includes the nuclear lamins (lamin A/C, B_1, and B_2) (Fuchs and Coulombe, 1992; Lowery et al., 2015).

Interestingly, intermediate filaments differ from microtubules and actin filaments. Unlike microtubules and actin filaments, they lack the polymerization mechanism of monomeric proteins since they are made of elongated and thin rod-like dimers, which align parallel to the filament axis thereby determining the filament width (**Figure** 10). Due to such structural difference, dissociation of intermediate filament dimers can occur all along the length of the filament and not only at their ends. Finally, intermediate filaments have no structural polarity because individual monomers are oriented in both directions along the axis of the filament (Feher, 2012).

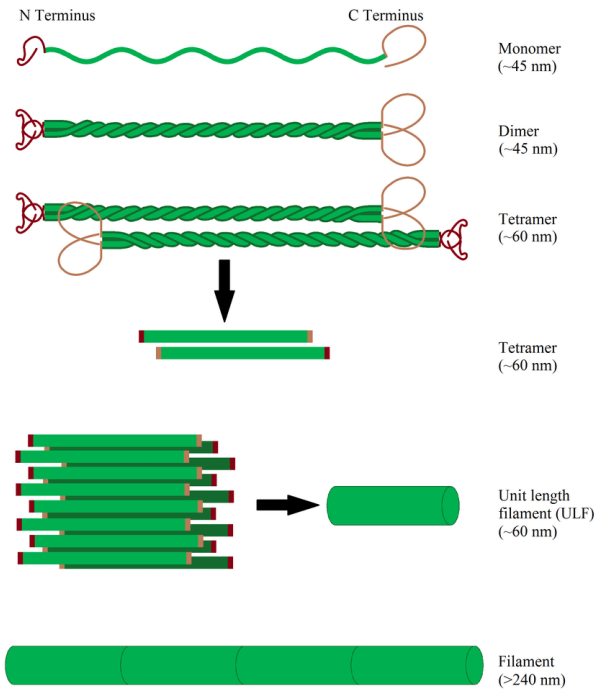

Figure 10 Illustration of intermediate filament assembly. Intermediate filaments arise from the monomers spiraling around each other to form dimers. Two dimers aggregate to a tetramer and eight tetramers to a unit length filament. Unit filaments form the final filament via end-to-end aggregation (Hohmann and Dehghani, 2019).

Lastly, microtubules are the largest of cytoskeletal filaments, approximately 25 nm in diameter, constructed from protofilaments resulting from the polymerization of heterodimers of α- and β-tubulin. Tubulin binds head-to-tail along protofilaments, forming longitudinal interactions. Microtubules are polar and they have a plus- and a minus-end. Most of them consist of 13 protofilaments that interact laterally to form a hollow tube. Since they associate laterally to one another with the same polarity, microtubule ends with α-subunits exposed are named minus (-) ends, while microtubule ends with the β-subunits exposed are named plus (+) ends, respectively (Alberts et al., 2014). Heterodimers added to the plus end of microtubules contain guanosine triphosphate (GTP) in both subunits. After incorporation into a microtubule, GTP is hydrolyzed into guanosine diphosphate (GDP) and subsequent hydrolysis of GTP encourages a conformational change in the heterodimer that is opposed by the geometry of the microtubule, thus trapping energy in the lattice (Alberts et al., 2014; Howard and Hyman, 2007). This difference in the free energy of GTP/GDP-bound polymers is the cause of microtubule dynamic instability. The presence of unhydrolyzed GTP at the plus end of microtubules promotes further polymerization/growth while GDP induces

depolymerization/shrinkage (**Figure** 11) (Erickson and O'Brien, 1992; Howard and Hyman, 2009).

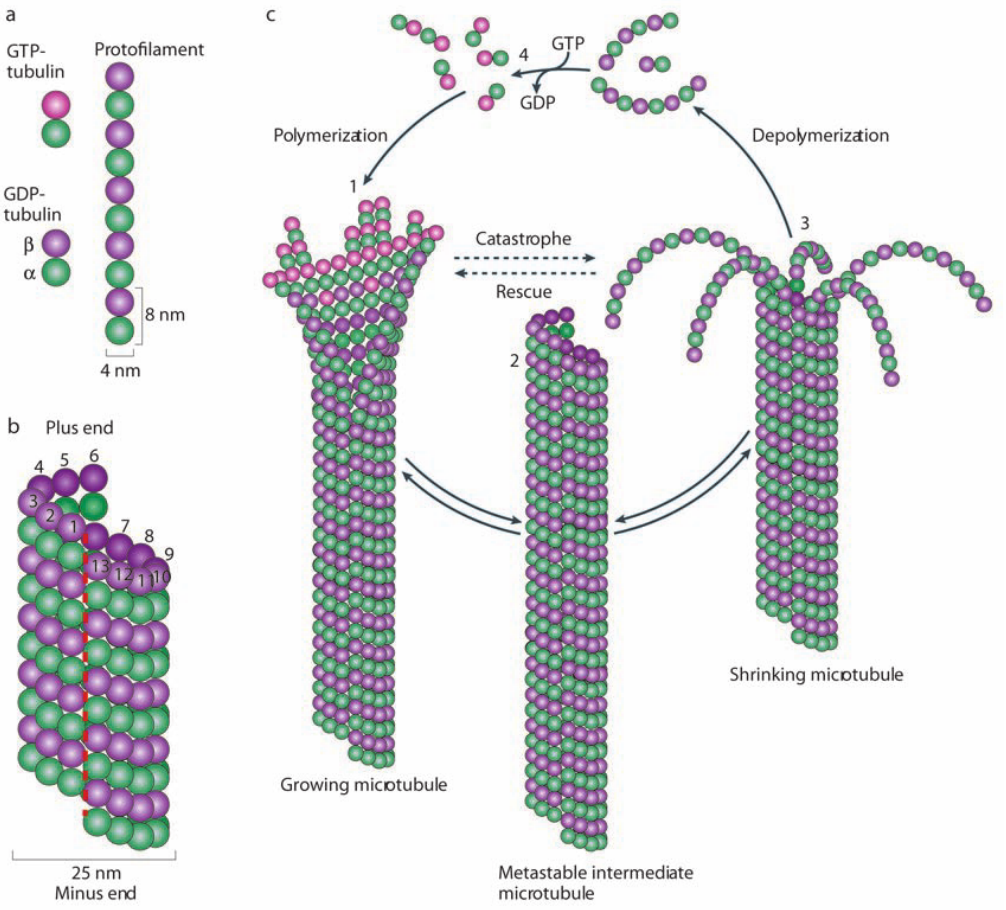

Figure 11 Microtubule assembly and disassembly. Each protofilament of microtubule is a tubulin heterodimer made of α- and β-monomer bound to one GTP molecule. Protofilaments laterally associate into a stiff hollow tube, a microtubule. GTP hydrolization into GDP causes depolymerization (des Georges, 2008).

This occasional switching to rapid shrinkage is also called microtubule catastrophe, wherby the switching back from shrinkage to growth is commonly called microtubule rescue (Alberts et al., 2014). The purpose of this dynamic instability is to allow the cell to rapidly reorganize the microtubular cytoskeleton when necessary (**Figure** 12).

Microtubules have several functions. They provide tracks for motor proteins in order to move organelles (e.g., mitochondria), provide structural support to the cells and they are

major components of cilia and flagella (cellular locomotory projections). Last but not least important, they are structurally and functionally the main component of the mitotic spindle during cell division (Britannica, 2019).

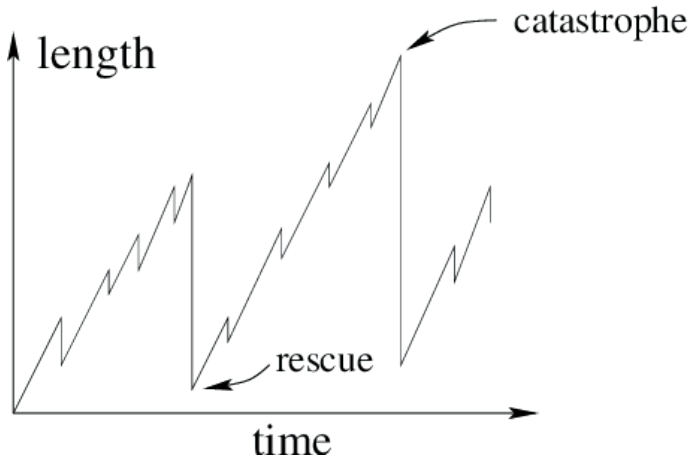

Figure 12 Schematic illustration of the growth and catastrophe shrinkage of a microtubule as a function of time (Antal et al., 2007).

2.4 Mitotic spindle

In most cell types, the mitotic spindle formation starts when microtubules nucleate from microtubule-organizing centers (MTOCs) (Luders and Stearns, 2007). The main MTOC in animal cells is the centrosome that defines the spindle pole composed of two orthogonal centrioles enclosed by an amorphous mass of pericentriolar material (Luders and Stearns, 2007; Waters and Salmon, 1997). Mitotic spindle is a highly organized structure composed of microtubules and microtubule associated proteins, required for segregation of the genetic material into two daughter cells (Pavin and Tolic, 2016). The spindle proteins that are associated with MTs or chromatin can be divided into several classes – molecular motors from the kinesin and dynein families that convert chemical energy stored in ATP to do mechanical work such as kinesin-6, passive proteins that crosslink spindle MTs such as PRC1, and various protein regulators such as kinases (Verhey and Hammond, 2009).

There are different populations of MTs regarding their structure, dynamics, and function which can be divided into kinetochore MTs and non-kinetochore MTs (Alberts et al., 2014). Kinetochore MTs form parallel bundles known as kinetochore fibers (k-fibers) because they interact with protein complexes at the centromere of each chromosome, called kinetochores, and connect them with the spindle poles. Non-kinetochore MTs can be grouped into interpolar and astral MTs, where interpolar extend from the opposite spindle poles to the

center of the spindle forming an antiparallel bundle and astral MTs grow from the pole towards the cell cortex (**Figure** 13) (Tolic, 2018).

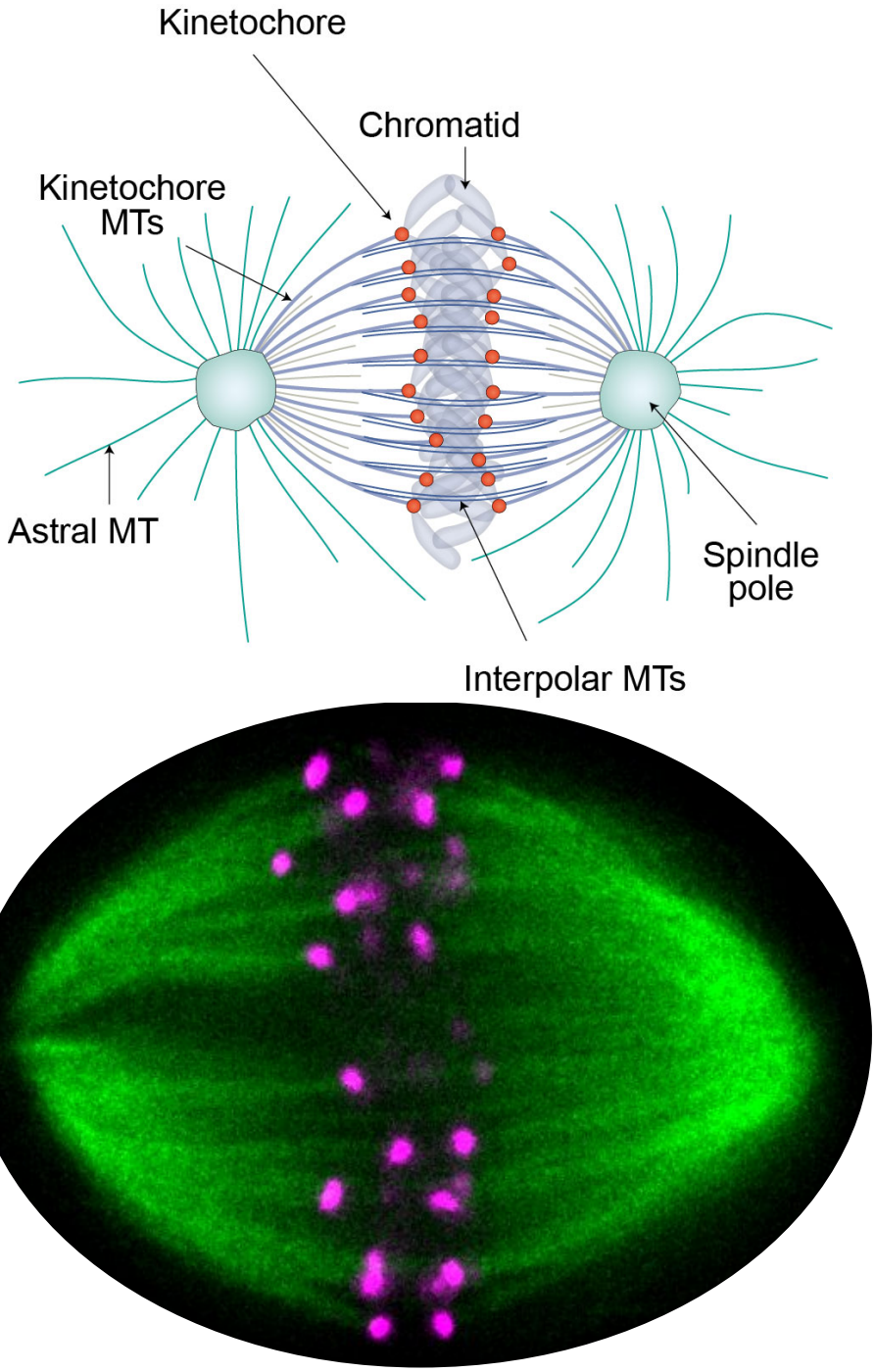

Figure 13 Scheme of the mitotic spindle. Kinetochore MTs interact interact with protein complexes, kinetochore, at centromere of each chromatid. Non-kinetochore MTs consist of interpolar, and astral MTs (top) (Vukusic, Buđa et al., 2019b). STED image (single z-plane) of anaphase spindle in a live U2OS cell expressing CENP-A-GFP (magenta). Microtubules are labelled with silicon SiR-tubulin (green) (bottom) (image taken by Patrik Risteski).

2.5 Mechanisms of anaphase

Anaphase is one of the most spectacular phases of the cell cycle, when coordinated splitting of the replicated chromosomes and segregation of the sister chromatids occur. Like almost every aspect of mitosis, the anaphase movements are accomplished by the mitotic spindle (Pavin and Tolic, 2016).

Chromosome segregation in human cells begins with a rather abrupt transition that is initiated by the proteolytic severing of cohesion links between sister chromatids, and is known as the anaphase onset (Hauf et al., 2001). Anaphase can be divided into separate phases marked by distinct anaphase events regarding poleward movement, anaphase A, and spindle elongation, anaphase B (**Figure** 14) (Su et al., 2016).

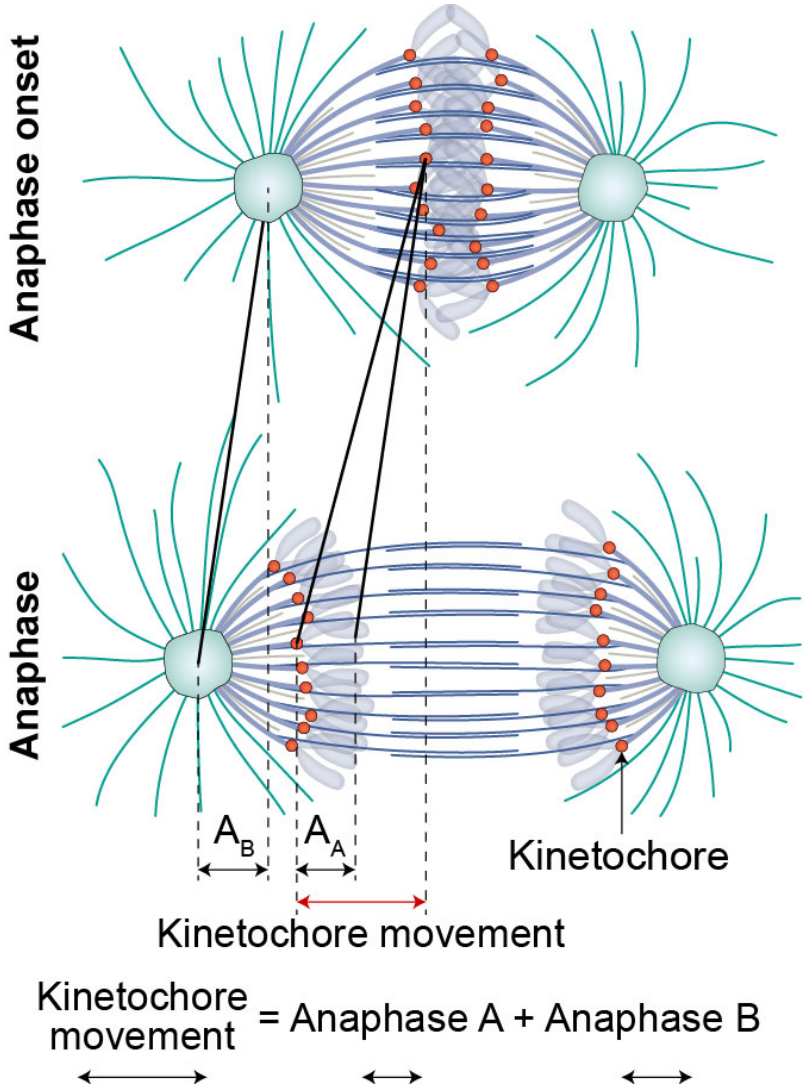

Figure 14 The scheme of anaphase mitotic spindle shows anaphase A and B (A_A and A_B) contribution to total kinetochore movement (red double-headed arrow) (Vukusic, Buđa et al., 2019b).

2.5.1 Anaphase A

The most important structures for anaphase A movements are k-fibers, whose kinetochore-attached MTs drive poleward movement of kinetochore-bound chromosomes (Maiato and Lince-Faria, 2010) by k-fiber depolymerization at the plus and at the minus end. By using electron microscopy, it was shown that depolymerization occurs at the kinetochore concomitantly with the chromosome poleward movement in anaphase (Mitchison et al., 1986). In support of these experiments, by using photobleaching marks on k-fibers, it was shown that chromosomes always approach and invade the bleached domains, indicating that depolymerization of k-fibers takes place at kinetochores (**Figure** 15a) (Gorbsky et al., 1987). Later micromanipulation studies in grasshopper spindles, in which a polar region was removed, showed that chromosomes continued to move poleward in anaphase as long as the k-fiber stub was longer than 1 μm (Nicklas, 1989) indicating that the primary site of force generation in anaphase A is on or near kinetochores. In addition, it was shown that energy for poleward movement of isolated chromosomes and MTs *in vitro* is derived solely from MT depolymerization at kinetochore (Koshland et al., 1988). The chromosome movement coupled to MT disassembly at a kinetochore is known today as the Pac-Man model (**Figure** 15a and b) (Cassimeris et al., 1987), named after a popular arcade game at the time, since Pac-Man is reminiscent of a kinetochore chewing a fiber in order to decrease its length.

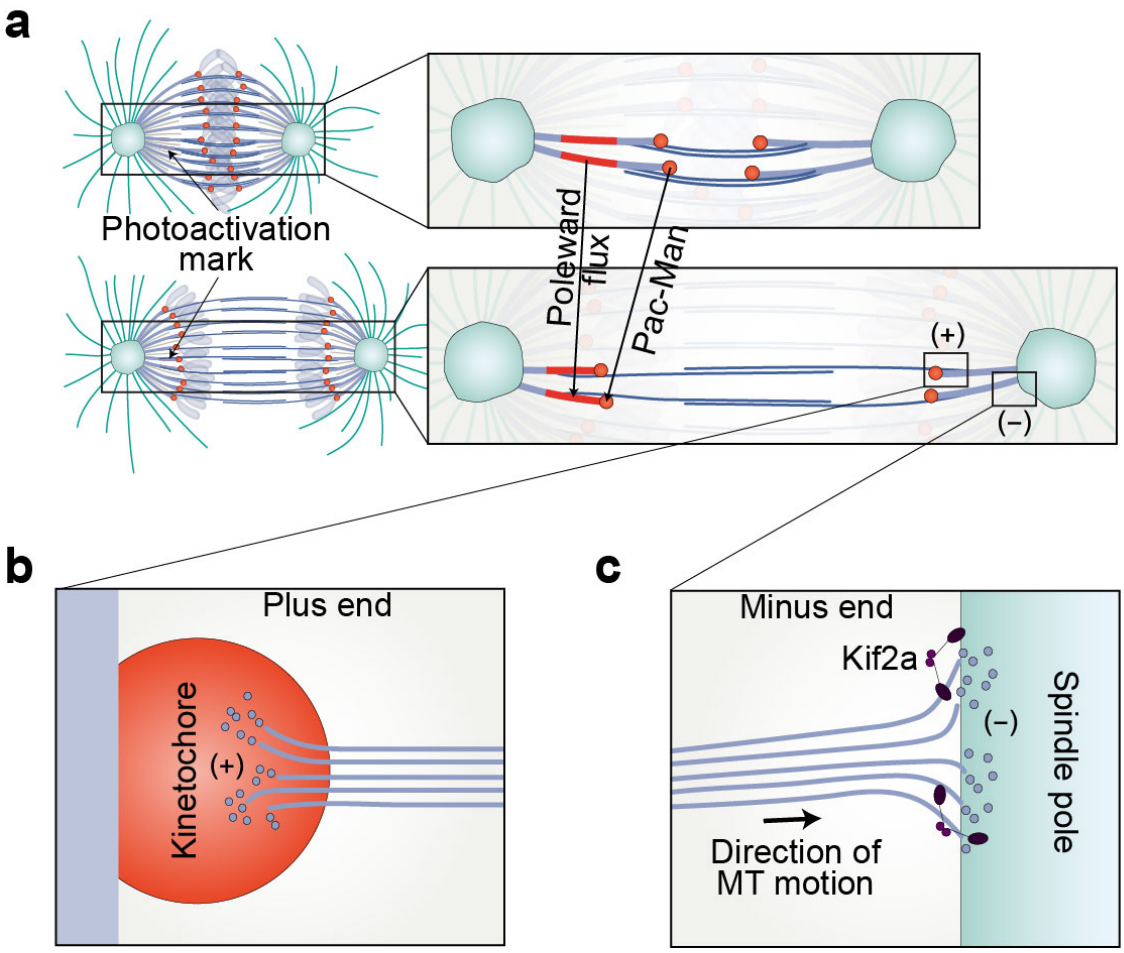

Figure 15 Anaphase A mechanisms. (a) Mechanisms of k-fiber depolymerization. (b) Pac-Man contributes more than the MT poleward flux to the poleward chromosome movement (top). (c) k-fiber minus-end depolymerization (Vukusic, Buđa et al., 2019b).

Regarding depolymerization at the k-fiber minus end, pioneering experiments were first conducted in metaphase where it was shown, in mammalian BSC1 fibroblasts, that microinjected biotinylated tubulin incorporates at k-fiber plus-ends and subsequently extends towards the pole indicating a poleward flux of MT subunits accompanied by the depolymerization at the pole (**Figure** 15a and c) (Mitchison et al., 1986). The same phenomenon was observed in anaphase, in newt lung cells, using photoactivation marks where it was noticed that the poleward movement of tubulin was slowing down as the anaphase progressed (Mitchison and Salmon, 1992). This observation constitutes the modern version of Traction fiber model (Inoue and Ritter, 1975) in which the polymerization at the kinetochore decreases after anaphase onset and the depolymerization at the pole pulls the k-fiber, along with the kinetochore, polewards.

2.5.2 Anaphase B

Anaphase B spindle elongation initiates shortly after anaphase A onset (Su et al., 2016). It is characterized by sliding of overlap MTs (Saxton and McIntosh, 1987) and pulling from the cortex on astral MTs (Aist et al., 1993; Grill et al., 2001) in order to drive spindle pole separation thereby contributing to kinetochore separation.

2.5.2.1 Astral MTs

In most vertebrates, spindle poles initiate MTs that grow away from the spindle pole. These astral MTs can be long enough to interact with proteins in the cell cortex, the actin layer beneath the inner surface of the plasma membrane (**Figure** 16) (McIntosh et al., 2012).

Even though not all the cells have astral MTs (Bannigan et al., 2008; Dumont et al., 2010) and they seem to be non-essential for mitosis, they can contribute to spindle positioning in some systems, most notably *C. elegans* embryo (Grill et al., 2003; Grill and Hyman, 2005). Regarding human mitotic spindles, it has been shown that the position of the mitotic spindle is partially controlled by dynein-dependent cortical pulling forces exerted on astral MTs (Kiyomitsu and Cheeseman, 2012). It has been demonstrated that dynein/dynactin complex is recruited to the cell cortex in anaphase by parallel pathways including LGN and 4.1 family proteins, both interacting with NuMA, and that depletion of both pathways results in unequally-sized daughter cells after cell division and defects in the spindle centering relative to cell boundaries (Kiyomitsu and Cheeseman, 2013).

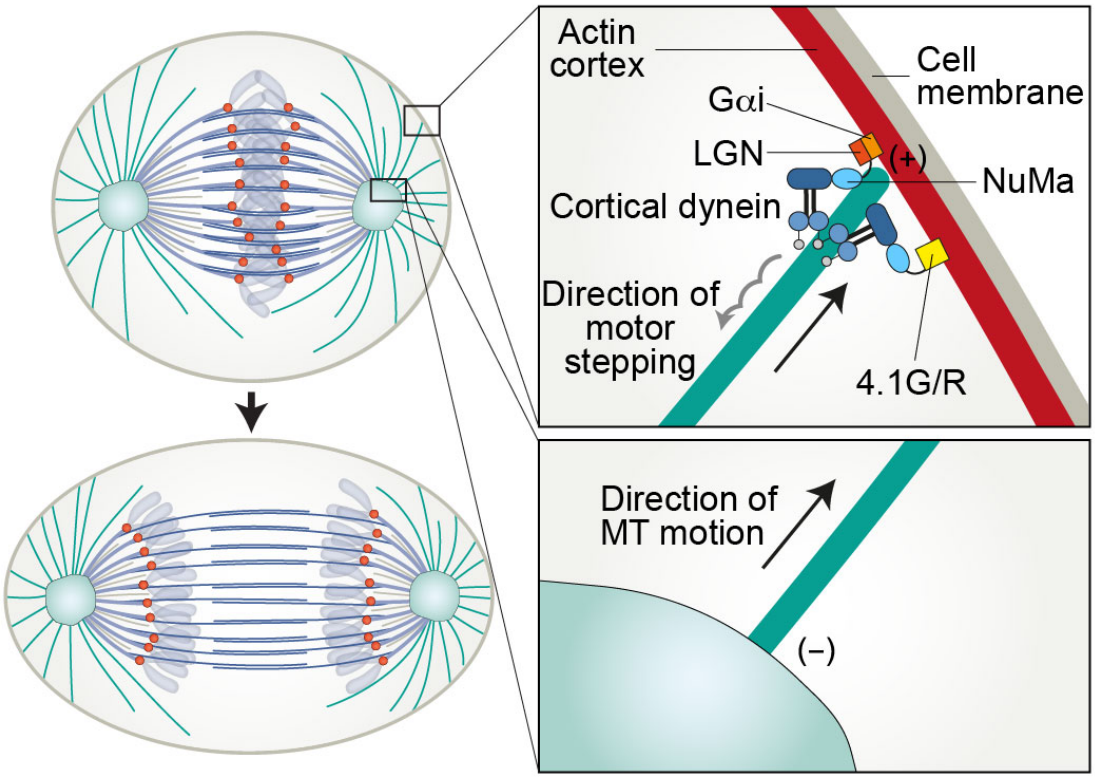

Figure 16 Astral MTs. Cortical forces are mediated by cortical dynein and its adaptors connecting astral microtubules (MTs) to the cell cortex (magnified region, top), and transmitted to the spindle pole (magnified region, bottom) (Vukusic, Buđa et al., 2019b).

In some organisms, however, there is evidence that supports the existence of external pulling forces that pull on the spindle poles in order to elongate the spindle (Aist et al., 1993; Grill et al., 2001). Potential mechanisms explaining such force generation include depolymerization of the plus ends of astral MTs (Grishchuk et al., 2005) or pulling by cortical dynein walking towards the minus end of astral MT (Ananthanarayanan et al., 2013; Pavin and Tolic-Norrelykke, 2013). This suggests the requirement for direct contact between astral MTs and cell cortex (Kozlowski et al., 2007). Nevertheless, the removal of both LGN and 4.1G.R by siRNA did not affect rates of sister chromatid separation in HeLa cells (Kiyomitsu and Cheeseman, 2013) arguing against their role during spindle elongation in human cells.

2.5.2.2 Interpolar MTs

Previous studies have shown, that antiparallel interpolar MTs slide apart during anaphase (**Figure** 17) while the tubulin subunits are added to their plus ends (Saxton and McIntosh, 1987). The sufficiency and necessity of pushing from spindle midzone for spindle elongation has also been confirmed by laser ablation of interpolar MTs in diatom (Leslie and Pickett-Heaps, 1983) and fission yeast (Khodjakov et al., 2004; Tolic-Norrelykke et al., 2004). The outward sliding of interpolar MTs could exert forces on the poles to push them apart leading to anaphase spindle elongation in human cells.

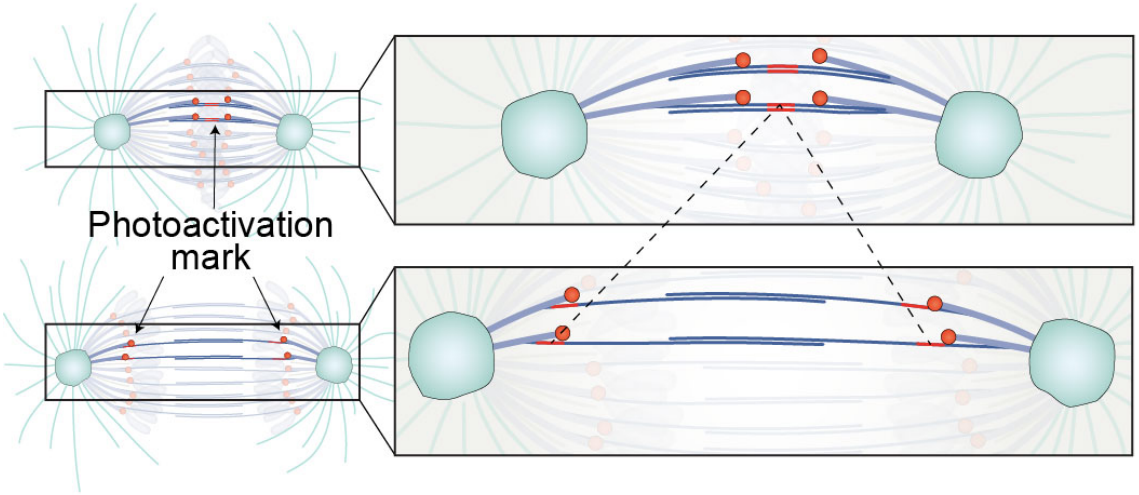

Figure 17 Interpolar microtubules (MTs) slide apart during ahaphase. Sliding mechanism is indicated as the separation of the photoactivated spot into two spots (red marks) (Vukusic, Buđa et al., 2019b).

The first possibility is that the forces from sliding of interpolar MTs are directly transmitted on the spindle poles via interpolar MTs minus-ends in order to push them apart (**Figure** 18a). However, a direct linkage with centrosomes has been shown to be redundant in anaphase as chromosomes continued to move poleward even after centrosome removal (Hiramoto and Nakano, 1988; Nicklas, 1989; Sikirzhytski et al., 2014; Yu et al., 2019b). Also, in Ptk1 spindles (Mastronarde et al., 1993), the minus ends of the most interpolar MTs do not reach the poles suggesting that direct pushing of interpolar MTs on spindle poles is not likely scenario in this system as well as it was shown in human cells (Yu et al., 2019b). However, of the direct linkage between spindle poles and interpolar microtubules is rarely observed in human spindles, a second possibility would include indirect pushing of spindle poles through

connections with k-fibers and other polar MTs that are tethered with spindle poles but that remains yet to be tested (**Figure** 18b).

Interestingly, in some organisms, interpolar antiparallel MTs could also serve as negative regulators of anaphase dynamics through a braking mechanism produced by molecular friction or crowding effects (**Figure** 18c) (Collins et al., 2014; Saunders et al., 2007). For example, the ablation experiments of interpolar MTs in Ptk2 (Aist et al., 1993), *C.elegans* (Grill et al., 2001) and *Nectria haematococca* (Aist et al., 1991), accelerated pole separation during anaphase B, revealing that midzone MTs are dispensable and instead act as a brake in spindle elongation while astral MTs exert pulling forces.

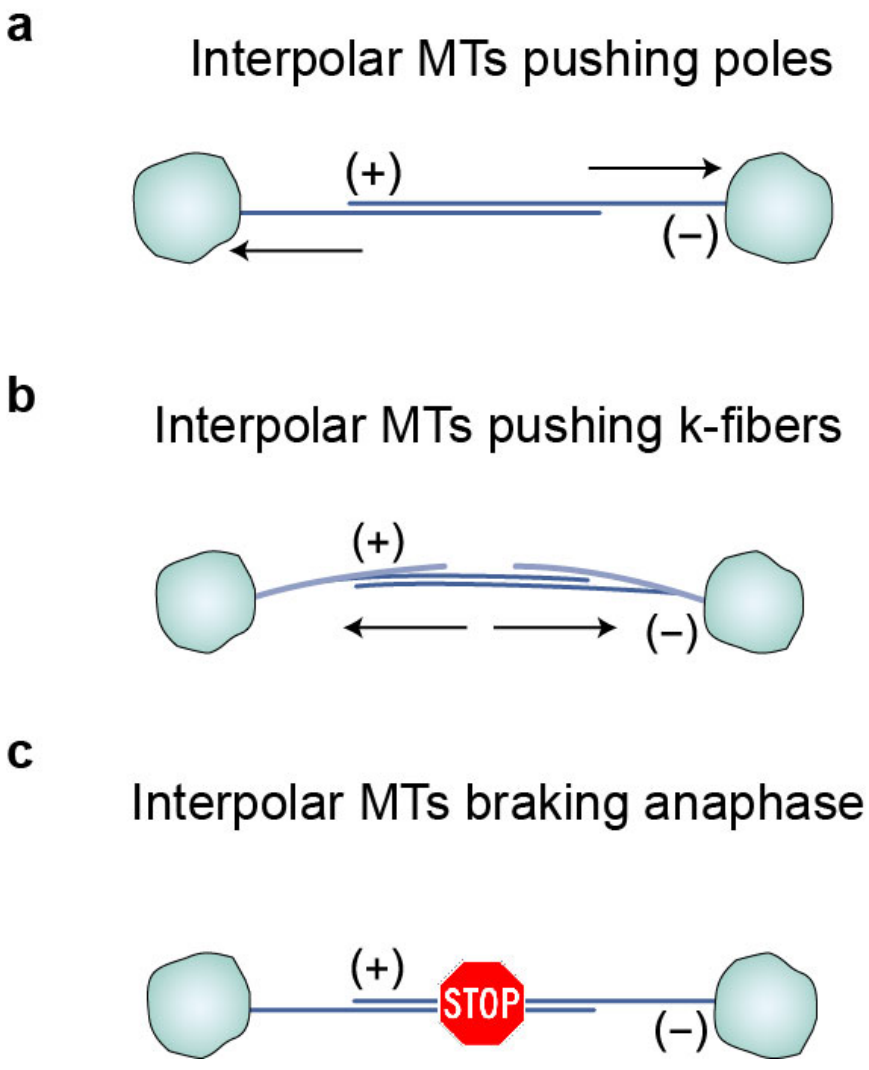

Figure 18 Interpolar MTs can be involved in spindle elongation by different mechanisms (Vukusic, Buđa et al., 2019b).

2.5.2.3 Motor proteins in anaphase B

Spindle elongation during anaphase B is a well-established motor-dependent process, with an increased sensitivity to the lack of ATP when compared to anaphase A (Cande, 1982; Lee, 1989). Although the identity of potential motor candidates, responsible for sliding within interpolar bundles is largely unknown in human cells, there are experimets from different model systems pointing out some of the candidates based on their localization or sliding activity (**Figure** 19).

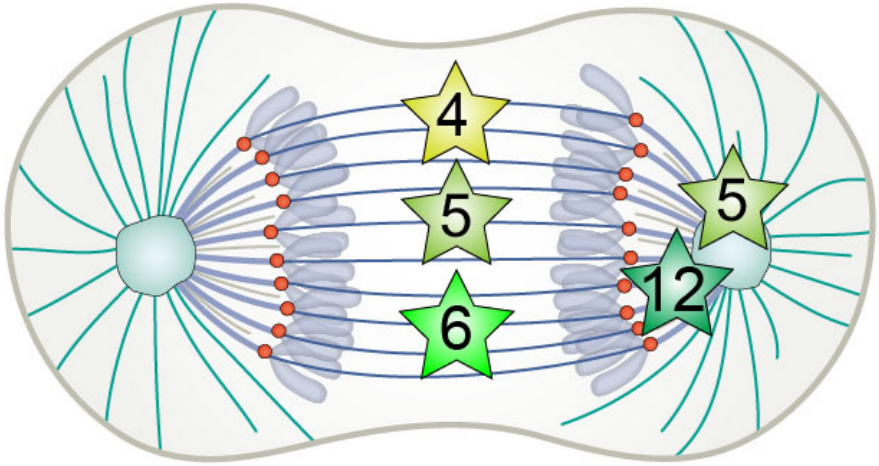

Figure 19 Localization of motor proteins candidates. Scheme represents the localization of KIF4a (4), Eg5 (5), MKLP1 (6) and KIF15 (12) in anaphase spindle.

The main candidates involved in regulating spindle length in metaphase are plus end directed motors, Eg5 (kinesin-5/Kif11) and Kif15 (kinesin-12) (Tanenbaum et al., 2009; van Heesbeen et al., 2014). The localization of Eg5 is primarily on antiparallel MTs and spindle poles in the mitotic spindle (**Figure** 20). It was previously shown that Eg5 crosslinks and slides antiparallel microtubules (**Figure** 21) extending from each centrosome, generating an outward-directed force during bipolar spindle formation (Collins et al., 2014; Kapitein et al., 2005; Sawin et al., 1992; Sharp et al., 1999). Also, its depletion harms centrosome separation, during prophase or prometaphase, that results in monopolar spindle formation (Ferenz et al., 2010). Considering KIF15 protein, it plays a non-essential role in the establishment and maintenance of spindle bipolarity, in close cooperation with Eg5. Only the

overexpression of Kif15 can drive bipolar spindle assembly when Eg5 is fully inhibited (Tanenbaum et al., 2009; Vanneste et al., 2009). Regardless of the Eg5 and KIF15 role during early mitosis, their contribution to spindle elongation in anaphase remains unexplored

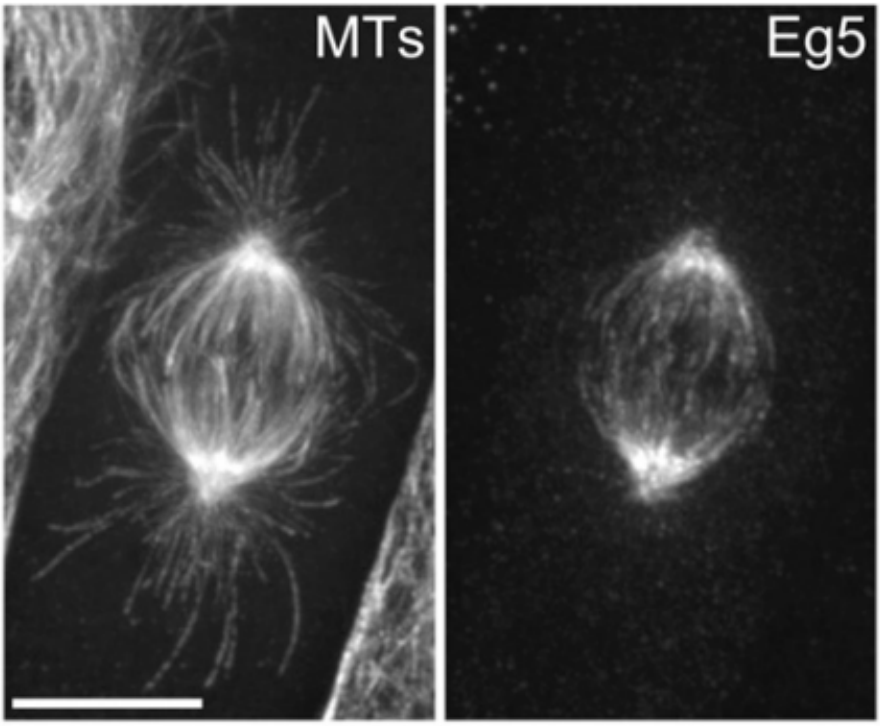

Figure 20 Localization and activity of Eg5 in mammalian cells. Immunofluorescence of an LLC-Pk1 cell stained with antibodies to tubulin (MTs) and Eg5 (Ferenz et al., 2010).

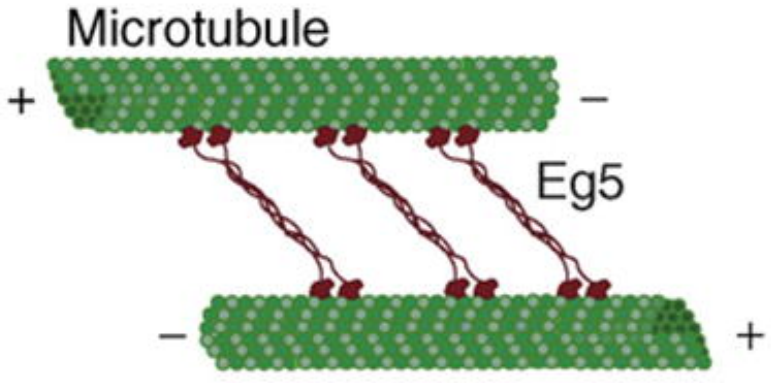

Figure 21 Eg5 can slide two MTs apart. Scheme represents Eg5 crosslinking two anti-parallel microtubules (Valentine and Gilbert, 2007).

Interestingly, kinesin-6 (MKLP1/Kif23), a part of centralspindlin complex, has been shown to drive spindle elongation in fission yeast (Kruger et al., 2019) and slide antiparallel MTs *in vitro* (Nislow et al., 1992). The studies in human cells have shown that kinesin-6 is involved in cell cortex elongation (Hickson et al., 2006) and in regulation of spindle midzone length (Figure 22) (Hu et al., 2011).

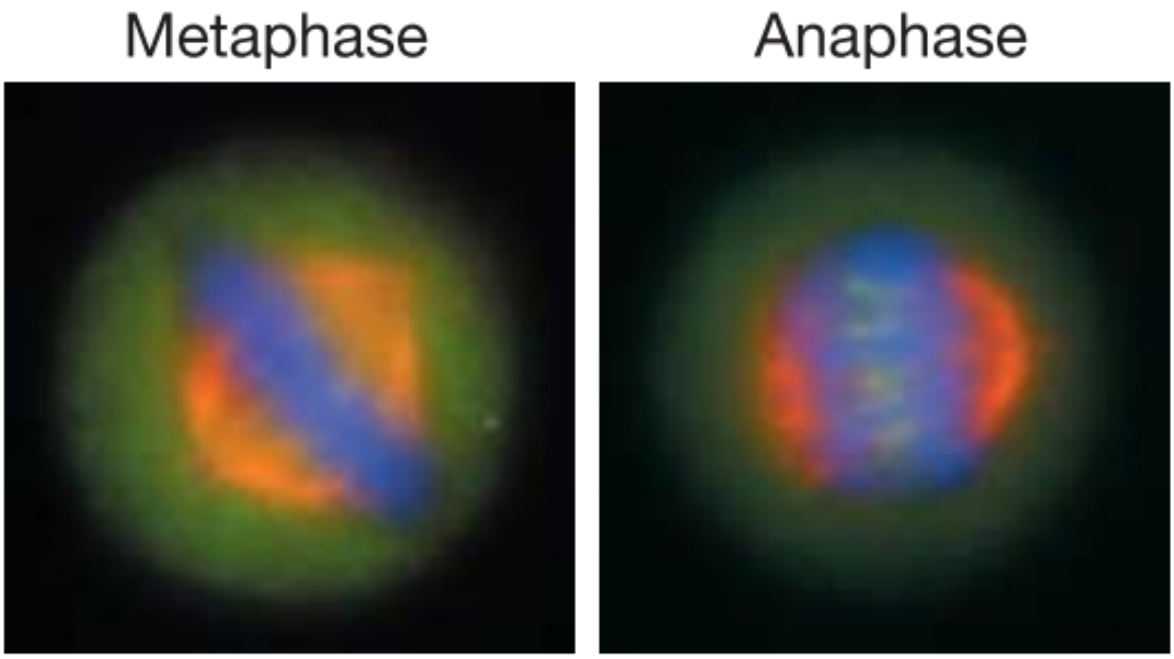

Figure 22 Localization of MKLP1 in HeLa cells. MKLP1 (green) accumulates on the central spindle upon anaphase onset (Mishima et al., 2004).

Regarding motor proteins that can regulate dynamics of the interpolar MTs in anaphase, kinesin-4 members have been tested so far. KIF4a has been shown to block midzone from growing continually during cytokinesis by inhibiting plus-end polymerization of interpolar MTs (**Figure** 23). However, the velocity of midzone elongation during fanaphase was not changed in the absence of KIF4a (Hu et al., 2011), meaning that KIF4a has some role in regulation of overlap length during cytokinesis. In conclusion, the anaphase B

motors that are involved in force generation and their precise regulators in human cells are yet to be elucidated.

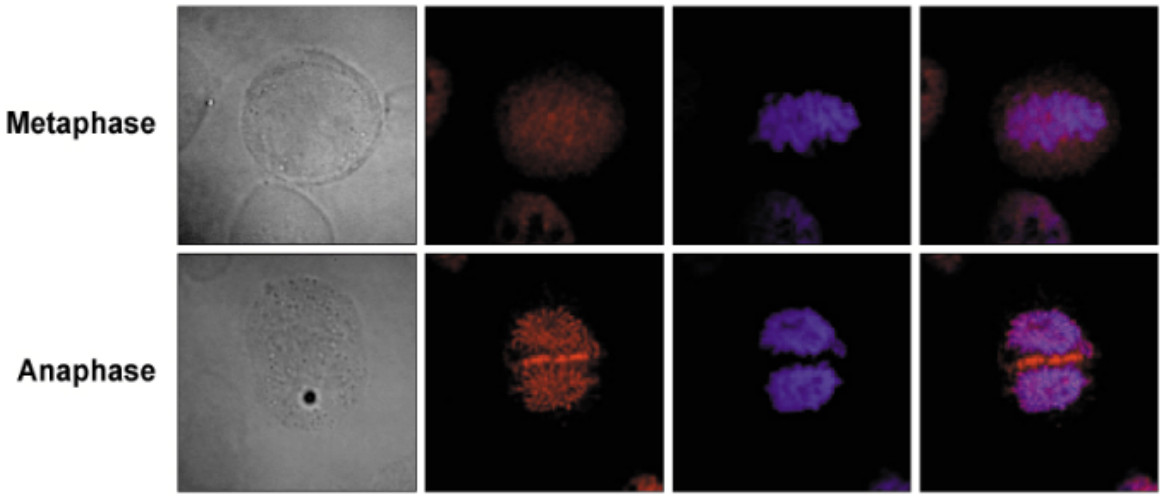

Figure 23 Localization of KIF4a. Fixed cell images of HeLa cell. Red – anti-KIF4a antibody, blue – DAPI (Lee and Kim, 2004).

2.5.2.4 Non-motor regulator of anaphase B – PRC1

The region of interpolar MTs also contains a PRC1 protein that cross-links anti-parallel MTs and provides the structural support in cytokinesis (**Figure** 24) (Mollinari et al., 2005). In mammalian cells, PRC1 is transported to the midzone of the spindle by KIF4a (Mollinari et al., 2002a) and is required to set up the central spindle before a number of other kinesins locate to the spindle. These kinesins include motors involved in finishing the assembly of the central spindle and in cytokinesis such as Kif14 and MKLP1 (Glotzer, 2004). PRC1 is negatively regulated through the phosphorylation by cyclin dependent kinase 1 (Cdk1) which limits its bundling activity until later stages of mitosis.

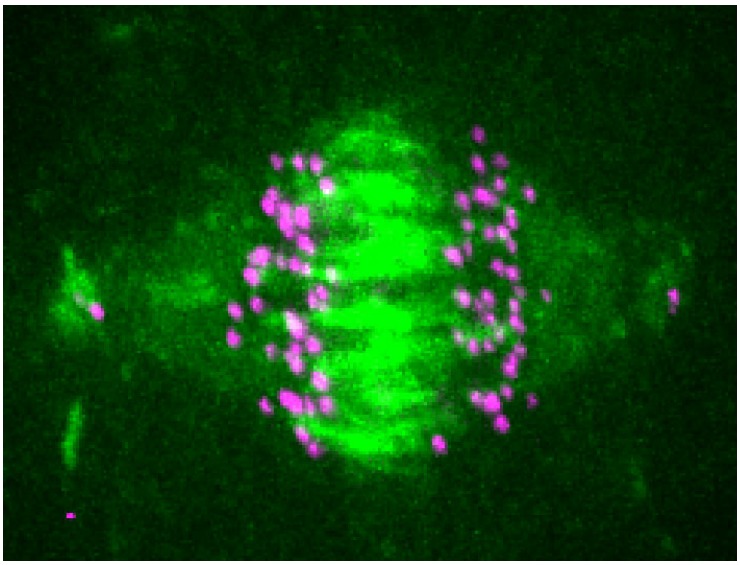

Figure 24 Localization of PRC1. Immunofluorescence (IF) images of fixed RPE-1 cells stably expressing CENP-A-GFP and centrin1-GFP (magenta) stained with AlexaFluor594 conjugated with PRC1 antibody (green) (Vukušić, Buđa et al., 2019a).

In the absence of PRC1, human cells progressed normally to metaphase and chromatid segregation was not affected in anaphase, although abscission step in cytokinesis was blocked (Mollinari et al., 2005). However, cells lacking PRC1 always showed aberrant spindle morphology in late anaphase where interpolar MTs were generally absent between the two half spindles (Mollinari et al., 2002b). That could explain the effect where the depletion of PRC1 caused accelerated spindle elongation only after cytokinesis furrowing, not effecting fast phase of spindle elongation (Uehara et al., 2016).

2.5.2.5 Bridging MTs

The classical view of the mitotic spindle places the origin of the forces mainly on the k-fibers predicting that interpolar microtubules do not interact with kinetochores or the k-fibers unless in the vicinity of the spindle pole (Tolić, 2017). However, the lack of interactions between k-fibers and interpolar MTs cannot explain the curved shape of k-fibers in the mitotic spindle of various species (Simunic and Tolic, 2016; Tolic and Pavin, 2016). In support to this idea, a recent study has found a bundle of interpolar MTs that connects a pair of sister k-fibers in the form of a bridge and termed this fiber bridging fiber (**Figure** 25 and **Figure** 26a). The model described two k-fiber and the bridging fiber as elastic rods, which merge at two junction points 1 – 2 μm from kinetochores whereby balancing the tension between sister kinetochores and supporting a rounded shape of the spindle (**Figure** 26b) (Kajtez et al., 2016).

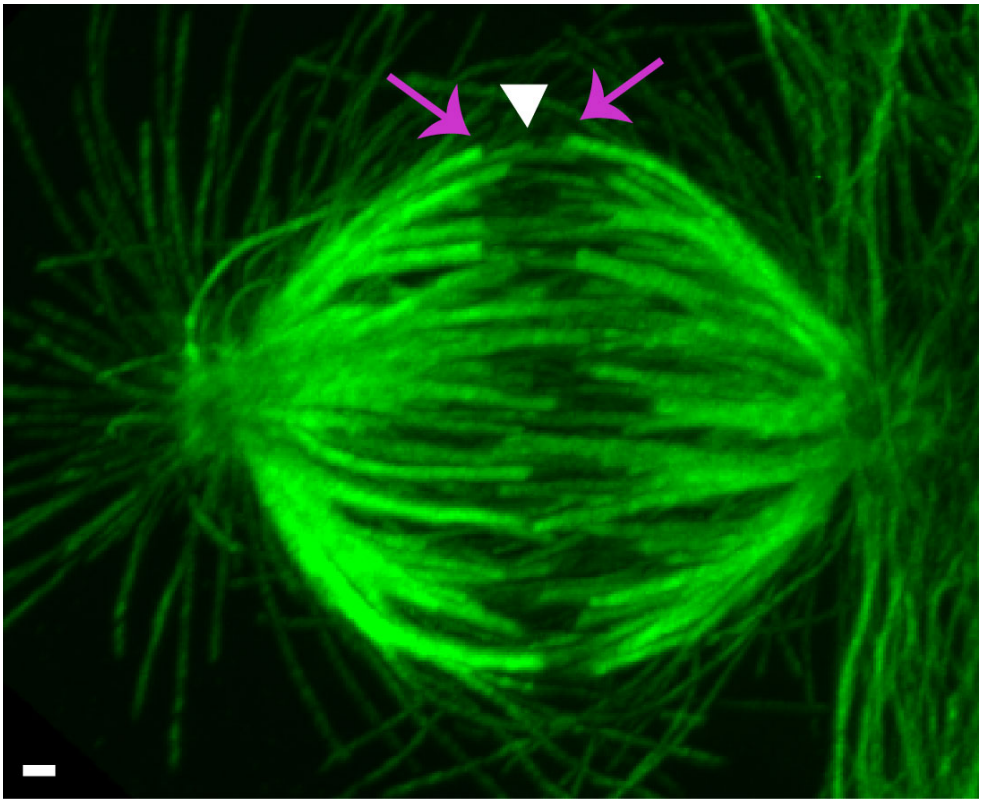

Figure 25 Bridging MTs in metaphase. Expansion microscopy images RPE-1 cell stained with AlexaFluor594 conjugated with α-tubulin antibody. Expansion factor is estimated from spindle length to be 2.3x. Magenta arrows indicate sister k-fibers (+) end, white arrowhead indicate bridging fiber between them. Scale bar 1 μm (imaged by Ivana Ponjavic).

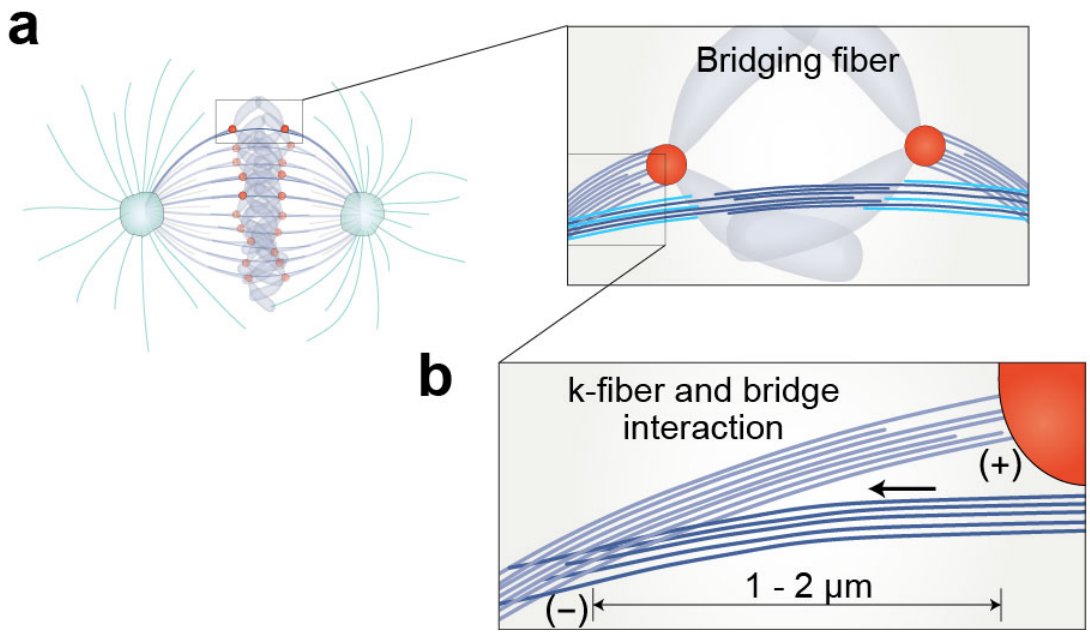

Figure 26 Bridging fiber interaction with k-fibers. (a) magnified rectangular region from the mitotic spindle indicates a bridging fiber connecting a pair of sister k-fibers. (b) magnified region from (a) shows the interaction of the k-fiber and the bridging fiber 1-2 um from the kinetochore (Vukusic, Buđa et al., 2019b).

By using a laser ablation assay (Buda et al., 2017), it was shown that bridging fibers moved together with sister kinetochores and their k-fibers, indicating strong crosslinking between these structures during metaphase (Kajtez et al., 2016). Furthermore, localization of PRC1 protein in the central part of the bridging fiber indicates overlap regions of antiparallel MTs (Kajtez et al., 2016; Milas and Tolic, 2016; Tolic, 2018; Tolic and Pavin, 2016).

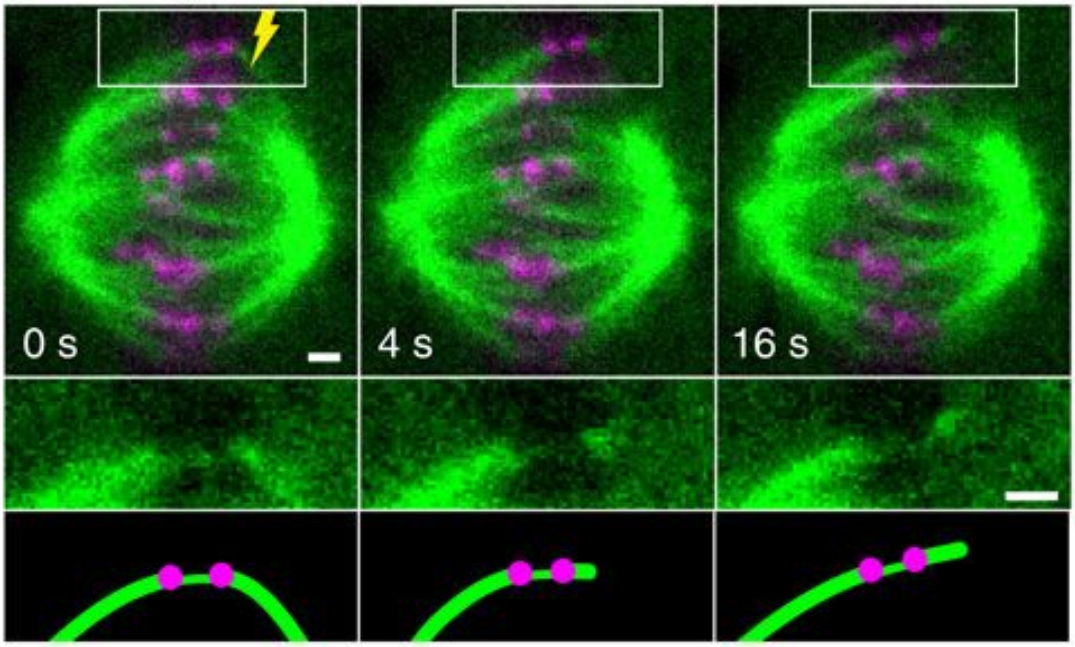

Figure 27 Characterization of the bridging fiber after laser ablation. Live images of HeLa cell after the cut (yellow) show that the bridging fiber moves together with sister kinetochores. Time 0 represents the cut onset. Scale bar, 1 μm (Kajtez et al., 2016).

Likewise, several studies based on electron microscopy reported non-kinetochore MTs that extend along the k-fiber to the region between sister kinetochores in metaphase spindles of human cells (McIntosh and Landis, 1971; Nixon et al., 2017).

In agreement with these results, recent large-scale electron tomography reconstructions of spindles in human cells revealed three classes of interpolar MTs during anaphase: those with two free ends between chromosomes, those with one free end between chromosomes and the other contacting chromosomes and the last class with one end between chromosomes and the other between chromosomes and the poles (around 1 μm from the chromosome) (Yu et al., 2019a). Interestingly, MTs that extend all the way from the pole to the region between chromosomes were not observed. All three classes of MTs were tightly associated into bundles contacting k-fibers, with the last class being the most abundant one in the spindle (**Figure** 28) (Yu et al., 2019a), which likely correspond to bridging MTs (Kajtez et al., 2016).

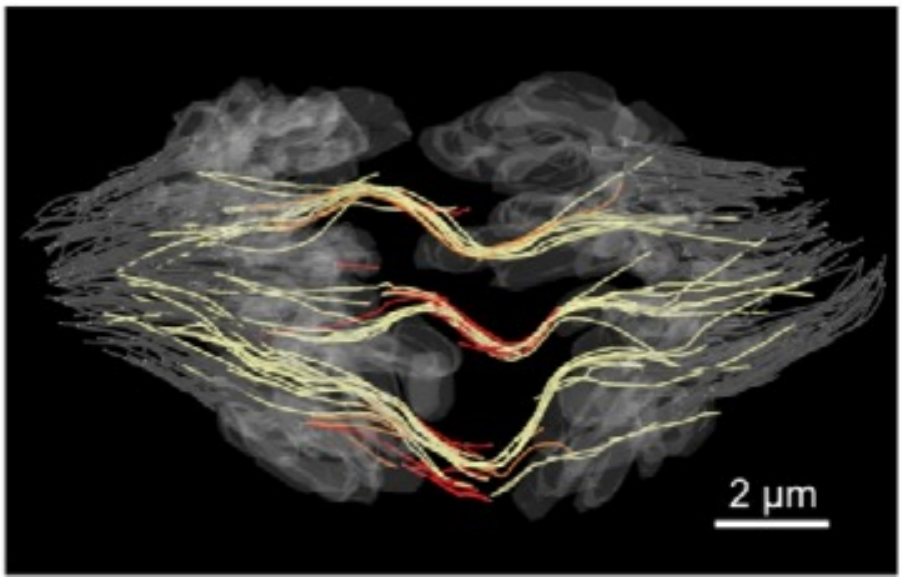

Figure 28 Interpolar MTs during anaphase. Electron tomographic reconstruction of selective microtubule bundles consisting of the three classes of microtubules (red, orange, and yellow) in anaphase (Yu et al., 2019b).

The crosslinks between the bridging fiber and the k-fibers open an interesting possibility that the bridging fiber may provide a structural support for poleward movement of kinetochores or sliding of k-fibers (McIntosh et al., 2012). Moreover, MTs in the bridging fibers may slide apart and actively generate forces for chromosome segregation during anaphase.

2.6 Laser ablation

To move forward in the understanding of main forces acting in mitotic spindle, experiments in recent years have been focused on mechanical perturbations of mitotic spindle *in vivo*. The underlying idea of all perturbation techniques is to perform controlled modifications of a selected structure and to observe its reaction to those alterations, which allows the interpretation of the forces acting on the selected structure in an unperturbed system.

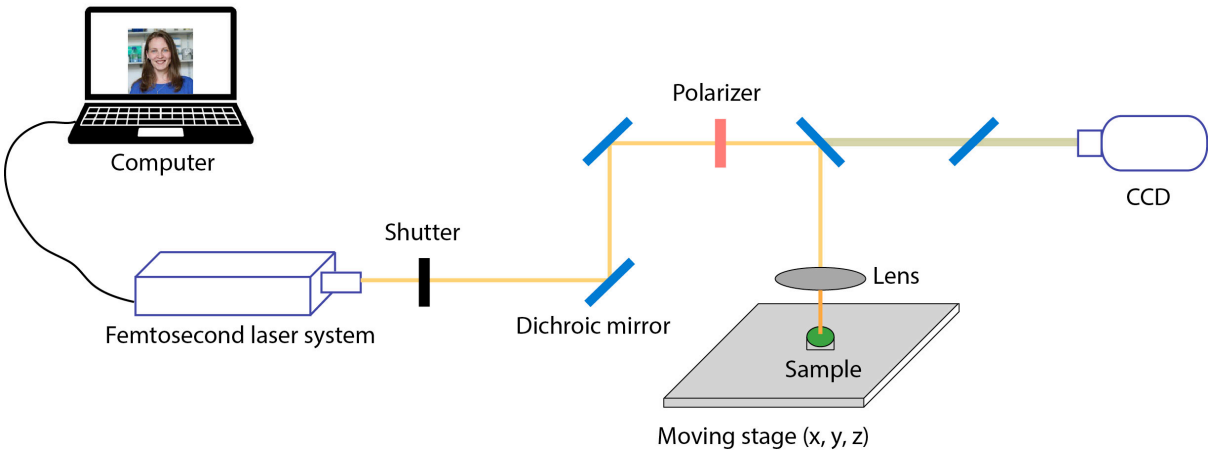

Figure 29 The simplified schematic illustration of the experimental setup of the femtosecond laser ablation.

During last decades, optical manipulation became one of the main tools for introducing perturbations on a very small scale (Magidson et al., 2007). This is due to many advantages of optical over non-optical manipulation techniques including easy integration with standard microscopy systems, high spatial and temporal resolution and finally minimal interaction with the sample (Maghelli and Tolic-Norrelykke, 2010, 2011). As a result, many studies have been performed using optical techniques such as laser cutting in diverse model systems, including *Schizosaccharomyces pombe* (Guarino et al., 2014; Khodjakov et al., 2004; Raabe et al., 2009; Rumpf et al., 2010; Tolic-Norrelykke et al., 2004; Vogel et al., 2009), *C.elegans* (Bringmann and Hyman, 2005; Yanik et al., 2004), *Dictyostelium* (Brito et al., 2005), *Drosophila* (Maiato et al., 2005; Maiato et al., 2004), mammals (Botvinick et al., 2004; Cojoc et al., 2016; Colombelli et al., 2005a; Colombelli et al., 2005b; Elting et al., 2014; Goudarzi et al., 2012; Kajtez et al., 2016; Klingner et al., 2014; La Terra et al., 2005; Milas and Tolić, 2016; Sikirzhytski et al., 2014; Stiess et al., 2010), and plants (Reinhardt et al., 2005; Stiess et al., 2010).

Specifically, a manipulation technique based on laser ablation with near-infrared (NIR, 1030 nm) femtosecond laser pulses (**Figure** 29) enables specific ablation of submicron-scale structures *in vivo* with minimal collateral damage (Steinmeyer et al., 2010; Vogel et al., 2005). The use of high-speed electro-optic modulator unit (EOM) and high repetition rate laser provide the flexibility in optimizing laser-pulse repetition rates. Lower pulse repetition rates yield reduced heat accumulation in the specimen, and therefore less collateral damage (Steinmeyer et al., 2010; Vogel et al., 2005). The ablation with femtoseconds pulse duration

occurs through non-linear multiphoton absorption (Vogel et al., 2005) and has been widely used to study the function of microtubules (Botvinick et al., 2004), mitochondria (Watanabe et al., 2004) and other organelles in cultured cells as well as in tissues and whole organisms (Shen et al., 2005; Stiess et al., 2010; Vogel et al., 2007).

By applying this method, one structure of interest could be easily severed without causing any significant collateral damage, in order to study the role of specific structures in the force balance of the mitotic spindle.

2.7 U2Os cell line

The cell line used in this study is U2OS which is one first created cell lines used frequently in various research areas (**Figure** 30). It is characterized by chromosomal instability, structural rearrangements and alterations and high incidence of aneuploidy (Niforou et al., 2008). The U2OS cell line, originally known as the 2T line, was cultivated from the bone tissue of a fifteen-year-old human female suffering from osteosarcoma. Established in 1964, the original cells were taken from a moderately differentiated sarcoma of the tibia (Nikon Microscopy, 2020).

Human osteosarcoma is a primary malignant tumor of the bone. It affects people between the age of 15 and 29, as well as in later life at the age >60 (Niforou et al., 2008). Due to lack of response to drugs and radiation therapies, the prognosis of osteosarcoma is very unfortunate, and despite advances in medicine and chemotherapy, the 5-year survival rate remains at 60–70% for patients with localized disease and 20–30% for patients with metastases (Lauvrak et al., 2013; PosthumaDeBoer et al., 2011)

Although the trigger for osteosarcoma is unspecified, its development is related to irradiation, genetic influences and rapid bone growth (Niforou et al., 2008). Despite the intensive research, the knowledge on human cancer cells is very limited and it is therefore important to better understand the underlying mechanisms of cancer cells division and ultimately the tumor progression.

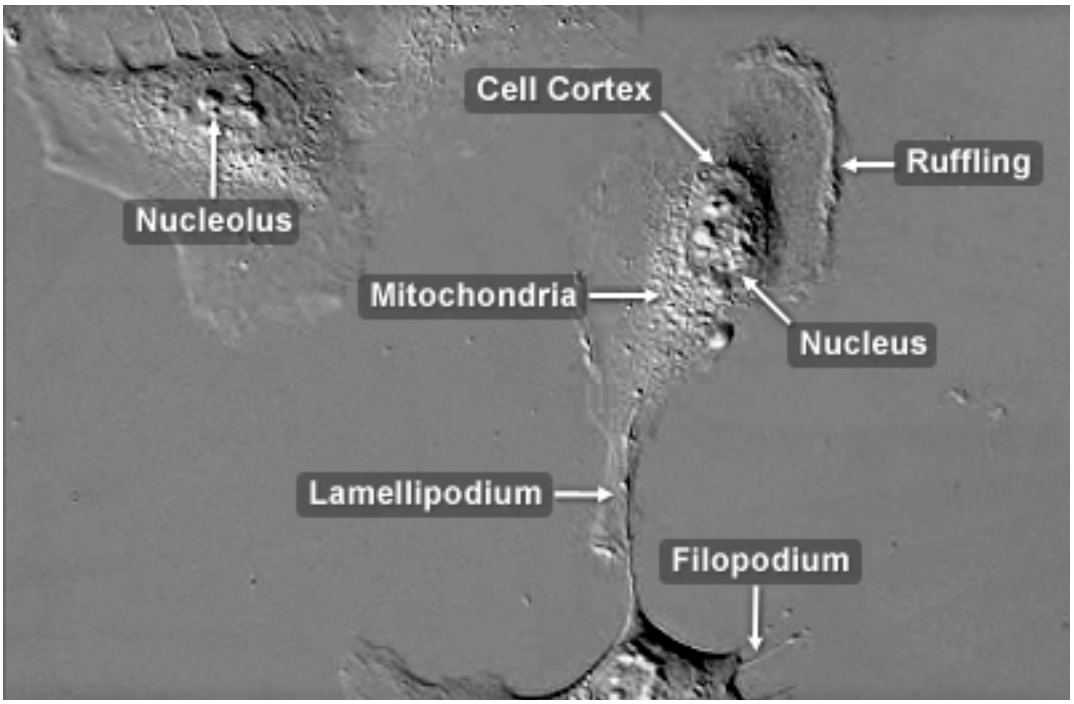

Figure 30 Human osteosarcoma epithelial cells. White arrows indicate parts of the U2OS cell (Nikon Microscopy, 2020).

3 MATERIALS AND METHODS

3.1 Cell culture and sample preparation

The cell line used is human osteosarcoma U2OS permanently transfected and stabilized using CENP-A-GFP (protein of kinetochore complex), mCherry-α-tubulin, photoactivatable (PA)-GFP-tubulin, which was a gift from Marin Barišić and Helder Maiato (Institute for Molecular Cell Biology, University of Porto, Portugal). Cells were grown in flasks in Dulbecco's Modified Eagle's medium (DMEM) (1 g/l D-glucose, L-glutamine, pyruvate) (Lonza, Basel, Switzerland) supplemented with 10% of heat-inactivated Fetal Bovine Serum (FBS) (Sigma-Aldrich, St Louis, MO, USA), 50 μg/ml geneticin (Life Technologies, Waltham, MA, USA) and penicillin/streptomycin solution (Lonza) to a final concentration of 100 I.U./mL penicillin and 100 μg/mL streptomycin. The cells were kept at 37 °C and 5% CO_2 in a Galaxy 170s humidified incubator (Eppendorf, Hamburg, Germany).

When cells reached 80% confluence, DMEM medium was removed from the flask and the cells were washed with 5 mL of 1% PBS. Afterward, 1 mL of 1% Trypsin/EDTA (Biochrom AG, Berlin, Germany) was added and the cells were incubated at 37 °C and 5% CO2 in a humidified incubator (Eppendorf). After 5 min incubation, Trypsin was blocked by adding 5 mL of DMEM medium. Cells were counted using the Improved Neubauer chamber (BRAND GMBH + CO KG, Wertheim, Germany) and $4.5x10^5$ cells were seeded and cultured in 2 ml DMEM medium with same supplements (as above) at 37 °C and 5% CO_2 on 35 mm glass coverslip uncoated dishes with 0.17mm (#1.5 coverglass) glass thickness (MatTek Corporation, Ashland, MA, USA). After one-day growth, 3h prior to imaging, the medium was replaced with Leibovit's (L-15) CO2-independent medium (Life Technologies), supplemented with 10% FBS (Life Technologies), 100 I.U./mL penicillin and 100 μg/mL streptomycin.

3.1 Immunostaining

Cells were fixed in ice-cold methanol (100%) for 2 min and washed with PBS. To permeabilize cell membranes, cells were incubated in triton (0.5% in PBS) for 25 min at room temperature. Unspecific binding of antibodies was blocked in blocking solution (1% normal goat serum (NGS) in PBS) for 1 h at 10°C. Cells were incubated in 250 μL of primary antibody solution (4 μg/ml in 1% NGS in PBS) for 48 h at 10°C. Rabbit polyclonal anti-a-

tubulin C-terminal antibody (SAB4500087, Sigma-Aldrich) was used. After washing of primary antibody solution, cells were incubated in 250 ml of the secondary antibody solution (4 μg/ml in 2% NGS in PBS; Alexa Fluor-405 F-conjugated donkey anti-rabbit IgG, ab175649; Abcam, Cambridge, UK) for 1 h at room temperature, protected from light. After each incubation step, washing was performed three times for 5 min in PBS softly shaken at room temperature.

3.2 Transfection and SiR-tubulin staining

U2OS cells were transiently transfected by electroporation using Nucleofector Kit R (Lonza, Basel, Switzerland) with the Nucleofector 2b Device (Lonza, Basel, Switzerland), using X-001 program. Transfection protocol provided by the manufacturer was followed. Cells were transfected with mCherry-PRC1 plasmid provided by Casper C. Hoogenraad (Utrecht University, Utrecht, Netherland). 1×10^6 cells were electroporated with 1.5 μg of plasmid DNA. Transfection of U2OS cells was performed 25–35 h before imaging.
For live-cell staining SiR-tubulin (Cytoskeleton Inc., Denver, CO, USA) was added to 1 mL of cells in a DMEM medium to a final concentration of 100 nM 5h before imaging together with efflux pump inhibitor verapamil (Cytoskeleton Inc.) to a final concentration of 10 μM.

3.3 Protein depletion and inactivation experiments

For all siRNA treatments, 2×10^5 and 1×10^5 cells were seeded and cultured in 2 ml DMEM medium with same supplements (as above) at 37 °C and 5% CO2 on 35 mm glass coverslip uncoated dishes with 0.17mm (#1.5 coverglass) glass thickness. After one-day growth, at □50–60% confluency cells were transfected with 100 nM (except Kif15: 60 nM) raw targeting or non-targeting siRNA constructs diluted in a Opti-MEM medium (Life Technologies, Waltham, MA, USA). Transfection was performed using Lipofectamine RNAiMAX Reagent (Life Techologies). The constructs used were as follows: human MKLP-1 siRNA (sc-35936), human KIF15 siRNA (sc-78517) and control siRNA-A (sc-37007), from Santa Cruz Biotechnology (Santa Cruz, CA, USA). 3h prior to imaging, the medium was replaced with Leibovit's (L-15) CO2-independent medium (Life Technologies), supplemented as above. The cells were imaged 24 or 48 hours after transfection. To inhibit Eg5, STLC (Sigma-Aldrich) was added to cells in L15 (see previous paragraph) 5 min before imaging at

40 μM (10 mM DMSO stock). To probe bipolar spindles with inhibited Eg5, we added 40 μM STLC after spindle formation (in metaphase), which preserves bipolarity (Cameron et al., 2006). All protein depleted cells were imaged by acquiring 8-12 focal planes with 0.5 μm z-spacing. Time interval between Z-stacks was 15 s. All other imaging parameters were the same as described for laser ablation experiments. We observed that inhibition of MKLP1 blocked normal progression of cytokinesis that resulted in formation of binucleated cells. We have observed an increase of 81% in the number of binucleated/multinucleated cells in MKLP1 siRNA-treated samples (calculated from 88 cells) after 48h in comparison with the samples treated with control siRNA (calculated from 92 cells), similar to previous observations (Fontijn et al., 2001). In experiment where KIF15 was inhibited by siRNA treatment, we observed rapid collapse of metaphase spindle upon 40 μM STLC treatment, as reported previously (van Heesbeen et al., 2014).

3.4 Imaging combined with laser ablation

U2OS cells were imaged using Bruker Opterra Multipoint Scanning Confocal Microscope (Bruker Nano Surfaces, Middleton, WI, USA). The microscopy system and general laser ablation assays used in this paper were described in detail elsewhere (Buda et al., 2017). The system was mounted on a Nikon Ti-E inverted microscope equipped with a Nikon CFI Plan Apo VC 100x/1.4 numerical aperture oil objective (Nikon, Tokyo, Japan). The system was controlled with the Prairie View Imaging Software (Bruker). During imaging, cells were maintained at 37°C in Okolab Cage Incubator (Okolab, Pozzuoli, NA, Italy). In order to obtain the optimal balance between spatial resolution and signal-to-noise ratio, 60 μm pinhole aperture was used. For excitation of GFP and mCherry fluorescence, a 488 and a 561 nm diode laser line were used, respectively. The excitation light was separated from the emitted fluorescence by using Opterra Dichroic and Barrier Filter Set 405/488/561/640. Images were captured with an Evolve 512 Delta EMCCD Camera (Photometrics, Tucson, AZ, USA) using 150-300 ms exposure times. Electron multiplying gain was set on 300-500. Camera readout mode was 20 Mhz. No binning was performed. To bring the xy-pixel size in the image down to 83 nm, a 2x relay lens was placed in front of the camera. Z-stacks were acquired comprising 8-13 focal planes at a 0.5 μm z-spacing using 2xframe averaging. The z-scan mode was unidirectional. Image acquisition was performed for 20-40 time frames at 15-20 s intervals. Severing of microtubule bundles was performed during live imaging using a Mikan femtosecond laser oscillator (Amplitude Systemes, Pessac, France), which was

coupled to the photoactivation module of the microscope, at a wavelength of 1030 nm. The laser power was set to 70-100% which corresponds to ~ 0.7-1W power at the sample plane.

For cutting of k-fibers, the size of the region for ablation was 700-1000 nm and laser exposure time was 800-1000 ms. Laser ablation was performed during the second time frame from start of the imaging in z plane(s) in which a single MT bundle could be discerned. The cut was performed on one of the outermost k-fibers, in one set of experiments 2.5 μm and in the other 1 μm from the kinetochore. Due to the fast reattachment of the ablated k-fibers to neighboring MTs in U2OS cells, multiple sequential cuts were sometimes necessary. For cutting of bridging fibers, the size of the region for ablation was 700-1000 nm and laser exposure time was 800-1000 ms. Laser ablation was performed during the third time frame from the anaphase start in z plane(s) in which a MT bundle could be discerned. For midzone and astral MTs cutting experiments, the single point mode with the fixed size of a region for ablation at 500 nm was used, while the laser exposure time was controlled by holding the mouse button. In both experiments, the laser ablation was performed continuously through all imaged z-planes (10-12 z-planes at 0.5 μm spacing). For photoactivation of fluorescence of PA-GFP after ablation, a 405-nm laser diode (Coherent, Santa Clara, CA, USA) was used. Photoactivation was performed using photoactivation option in software, with duration of pulse set to 80 ms.

U2OS cells in experiment where the cut was performed 2.5 μm from the kinetochore were imaged by using a Zeiss LSM 710 NLO inverted laser scanning microscope with a Zeiss PlanApo × 63/1.4 oil immersion objective (Zeiss, Jena, Germany) heated with an objective heater system (Bioptechs, Butler, PA, USA). During imaging, cells were maintained at 37°C in Tempcontrol 37-2 digital Bachhoffer chamber (Zeiss). For excitation, a 488-nm line of a multiline Argon-Ion laser (0.45 mW; LASOS, Jena, Germany) and helium-neon (HeNe) 594 nm laser (0.11 mW) were used for GFP and RFP/mCherry, respectively. Spectral array detector from 34-Channel QUASAR Detection Unit (Zeiss) was used for detection of fluorescent light. Emission wavelengths for simultaneous image acquisition were selected by the sliding prisms incorporated in the detection unit. GFP and RFP/mCherry emissions were detected in ranges of 490–561 and 597–695 nm respectively. No images were acquired during laser ablation. *xy* pixel size was set to 81 nm. Pinhole diameter was set to 0.7 μm (1 arbitrary unit). Pixel dwell time was 1 μs. Z-stacks were acquired at six focal planes with 0.5-μm spacing. The thickness of the optical sections was 700 nm. Image acquisition was performed for 20–40 time frames with 3.5–4.5 s intervals using unidirectional scanning. A titanium-sapphire (Ti:Sa) femtosecond pulsed laser (Chameleon Vision II, Coherent, Santa Clara, CA,

USA) was utilized at a wavelength of 800 nm for MT severing. The beam was coupled to the bleaching port of the microscope. The pulsed laser light was reflected on the objective with a long pass dichroic mirror LP690. Ablation was performed on user-defined, ellipse-shaped region of interest, ~0.3 μm wide and 1 μm long with the major axis perpendicular to the k-fiber. The system was controlled with the ZEN 2010 software (Zeiss).

Successful severing of the k-fiber in all experiments was identified by rapid depolymerization of the k-fiber fragment attached to the spindle pole, as well as from changes in the orientation of the short k-fiber stub that remained attached to the kinetochore, as described by others (Elting et al., 2014; Sikirzhytski et al., 2014).

3.5 Imaging combined with photoactivation

Photoactivation experiments without laser ablation were performed on Leica TCS SP8 X laser scanning confocal microscope with a HC PL APO 63x/1.4 oil immersion objective (Leica, Wetzlar, Germany) heated with an objective integrated heater system (Okolab, Burlingame, CA, USA). During imaging, cells were maintained at 37 °C in Okolab stage top heating chamber (Okolab, Burlingame, CA, USA). For excitation, a 488-nm line of a visible gas Argon laser and 594-nm line of white light laser (WLL) were used for GFP and mCherry, respectively. GFP and mCherry emissions were detected with HyD (hybrid) detectors in ranges of 498–560 and 608–676 nm respectively. Pinhole diameter was set to 0.8 μm and pixel size was 84 nm. Images were acquired at 5-7 focal planes with 0.5 μm spacing using 1000 Hz bidirectional scanning. Time interval between Z-stacks was 20-30 s. For photoactivation of fluorescence of PA-GFP, a 405-nm laser diode was used. Photoactivation was performed using bleachpoint option in software, with duration of pulse set to 100 ms. The system was controlled with the Leica Application Suite X software (LASX, 1.8.1.13759, Leica, Wetzlar, Germany).

3.6 Data analysis

The time of anaphase onset for each individual cell was defined as the time point immediately prior to the separation of sister chromatid populations as annotated manually using visual inspection based on the distance between the sister kinetochore groups. Time intervals in which the velocities were calculated for different experiments (one, two and three minutes) were chosen based on the criteria that they contain the majority of data. During the measurements of kinetochore velocity with respect to the midpoint we observed that the kinetochore whose k-fiber was severed showed a short delay (30.00±6.43 s, n=39) in the onset of movement with respect to its sister kinetochore. In this case, the beginning of anaphase was defined for each kinetochore individually as they started to move.

Image processing was performed in ImageJ (National Institutes of Health, Bethesda, MD, USA). Quantification and statistical analysis were performed in MatLab (MathWorks, Natick, USA).

Kinetochores were tracked in time using Low Light Tracking Tool (LLTT), an ImageJ plugin (Krull et al., 2014). Tracking of kinetochores in the x, y plane was performed on individual imaging planes or on maximum-intensity projections of up to three planes. The position in z direction was ignored because it had a small contribution to the kinetochore movement. In order to obtain optimal tracking results, it was necessary to define good intensity offset in the channel with fluorescently labeled kinetochores. The intensity offset was defined by measuring the mean intensity around kinetochores in the first frame before ablation using 'freehand selection' tool in Fiji. Sometimes, when photobleaching was prominent, bleach correction using Histogram Matching Method in Fiji was done to compensate for a decrease in background intensity in time. Also, it was necessary to define EMCCD gain and Electrons per A/D count of the used EMCCD camera to correct the measured flux of the object and background noise. The EMCCD-GaussianML tracking algorithm method was used (Krull et al., 2014) because it yielded more precise results compared with Gaussian-ML method, especially in situations when fast movement of the tracked object occurred (on a scale of micron per frame or more). All tracked objects were double checked by eye to ensure that tracking was accurate, because it was inaccurate in situations of an uneven intensity of tracked objects and in situations when multiple similar objects appeared in close proximity. If those cases were predominant, tracking was performed manually. σ value (standard deviation of the Gaussian used to approximate the Point Spread Function (PSF) of the tracked objects) was set to 1 to encompass just the tracked kinetochore.

Velocities of sliding and poleward flux in intact spindle were measured in 20 U2OS cells expressing CENP-A-GFP, mCherry-α-tubulin and photoactivatable (PA)-GFP-tubulin and 5 cells expressing only mCherry-α-tubulin and photoactivatable (PA)-GFP-tubulin. The measurements were done on both inner and outer bundles. Images were first smoothed using Gaussian Blur function in ImageJ with sigma set to 2.0. Segmented line was drawn from one spindle pole, across sister k-fibers and corresponding bridging fiber that spans between them, up to the opposite spindle pole. The intensity profile was taken along this line and positions of the peaks were measured. The thickness of the line was 3-5 pixels. The measurements were performed on maximum-intensity projections of up to three planes. All sliding measurements in protein inactivation/depletion experiments and in their appropriate controls were done in the interval when global kinetochore separation was between 3 and 7 μm. This interval was chosen because velocities of kinetochore and pole separation are linear during that period. Velocities where calculated as a linearly fitted change in the distance of photoactivated spots during 60 s from the initial photoactivation. Measurement of stability of photoactivation of the midzone bundles was calculated as the ratio of the area under the photoactivated midzone bundles in the 60 s after photoactivation and at the moment of photoactivation (0 seconds). The signal intensity of a cross-section of midzone bundles was measured in ImageJ by drawing a 5-pixel-thick line. The intensity profile was taken along the whole midzone region and the mean value of the background signal present in the cytoplasm was subtracted from it.

The attached kinetochore-photoactivated stub tip distance was measured in 9 U2OS cells expressing CENP-A-GFP, mCherry-α-tubulin and photoactivatable (PA)-GFP-tubulin. Images were first smoothed using Gaussian Blur function in ImageJ with sigma set to 1.5. Segmented line was drawn from one kinetochore, across the bridging fiber and the corresponding sister kinetochore to the photoactivated tip of the stub. The intensity profile was taken along this line and positions of the peaks were measured. The thickness of the line was 3-8 pixels. The measurements were performed on maximum-intensity projections of up to three planes.

The contour of displaced element after ablation was tracked in every time frame by using the Multi-point tool in Fiji. Such measurement was done on individual imaging planes or on the maximum-intensity projections of up to five planes. A typical distance between the neighboring points on the contours was ~1 μm. The measurement was done from the spindle pole far from the ablation site along the intact k-fiber to the tip of the k-fiber stub with one extra point on the spindle pole close to the ablation site. From the obtained x and y coordinates, the distances between the points (intact spindle pole-stub tip, intact spindle pole-

attached kinetochore, spindle pole close to ablation-detached kinetochore, attached kinetochore-stub tip, attached kinetochore-midpoint, detached kinetochore-midpoint) were quantitatively described.

To estimate the extent of depolymerization at the newly created minus end of the k-fiber stub, we used the side-effect of ablation laser that sometimes photoactivated PA-GFP-tubulin at the tip of the stub. The photoactivated spot remained stable for 118.13±14.01 s (n=9) during anaphase even though the stub length simultaneously decreased, indicating that the stub did not depolymerize at the minus end. Thus, stub shortening is a result of depolymerization at the plus end, i.e., Pac-Man activity.

Bridging fiber thickness measurement was performed on the side of the spindle where the ablation was performed, in the channel with fluorescently labeled MTs. Such measurement was done on individual imaging planes or on the maximum-intensity projections of up to three planes in the first frame after the ablation and the third frame from the start of the anaphase. In these planes, we could discern sister k-fibers without interference from neighboring fibers. The signal intensity of a cross-section of a bridging fiber (I_b) was measured in Fiji by drawing a 3-pixel-thick line between outermost sister kinetochores and perpendicular to the line joining the centers of the two kinetochores. The intensity profile was taken along this line and the mean value of the background signal, present in the cytoplasm around sister k-fibers (measured in Fiji by drawing a 5-pixel-thick line), was subtracted from it. The signal intensity of the bridging fiber was calculated as the area under the peak closest to the kinetochores using SciDavis (Free Software Foundation, Inc., Boston, MA, USA). The width of this peak was typically 0.7 μm. The signal intensity of the k-fiber and the bridging fiber together (I_{bk}) was measured in a similar manner, 1 μm away from attached kinetochore and perpendicular to and crossing the corresponding k-fiber. The signal intensity I_b was interpreted as the signal of the bridging fiber, and I_{bk} as the sum of the k-fiber signal and the bridging fiber signal (I_b+I_k) because of their lateral connection in that region (Kajtez et al., 2016). Also, due to the limited optical resolution in light microscopy, it was not possible to distinguish separate bridging and k-fiber intensities within the I_{bk}. We observed that after the cut the bridging fiber remained linked to the displaced sister k-fibers during the initial outward-directed movement, as described previously (Kajtez et al., 2016).

Kymographs of CENP-A-GFP and/or mCherry-α-tubulin were generated in maximum-intensity projections of all imaged planes using Low Light Tracking Tool (LLTT), an ImageJ plugin (Krull et al., 2014). For kymographs where displaced kinetochores are presented in magenta, the displaced kinetochores traces where obtained by manually tracking

the pair of sister kinetochores using LLTT. Obtained traces where overlaid with automatic traces of all kinetochore pairs in a cell generated by LLTT and shown in gray. Graphs were generated in Matlab. On the box plots the bottom and top edges of the box indicate the 25th and 75th percentiles, respectively. The whiskers extend to the most extreme data points not considered outliers, and the outliers are plotted individually using the '+' symbol. Outliers are defined as points greater than $q3 + 1.5 \times (q3 - q1)$ or lower than $q1 - 1.5 \times (q3 - q1)$ where q1 and q3 are the 25th and 75th percentiles of the sample data, respectively. Black solid lines indicate median values. p values were obtained using unpaired two-sample Student's t-test (significance level was 5%). When comparing the same parameters cell by cell, we used paired two-sample Student's t-test (significance level was 5%). Regarding data on **Figure** 54, the y-axis coordinates were obtained by linear fitting every four points on average curve for detached kinetochore-midpoint distance. The x-axis coordinates were obtained by averaging every four points from average curve for the stub length.

Images of cells in figures were rotated so the spindle long axis is aligned horizontally, and ImageJ was used to scale the images and adjust brightness and contrast. Kymographs and all quantitative analysis were done on raw images. Smoothing of images was done using Gaussian blur function in Fiji (σ=1.5-2.0). Figures were assembled in Adobe Illustrator CS5 and Adobe Photoshop CS5 (Adobe Systems, Mountain View, CA, USA). Data are given as mean±s.e.m., unless otherwise stated.

4 RESULTS

The discovery of the bridging fiber in metaphase prompted us to investigate its role during anaphase. Accordingly, the further findings described in the results section are published in 2017, in a peer-reviewed scientific journal Developmental Cell as a scientific article entitled "Microtubule sliding within the bridging fiber pushes kinetochore fibers apart to segregate chromosomes" by authors Kruno Vukušić, Renata Buđa, Agneza Bosilj, Ana Milas, Nenad Pavin and Iva M. Tolić. Authors Kruno Vukušić and Renata Buđa contributed equally to this work.

4.1 Development of the laser ablation assay

To determine the function of bridging MTs in chromosome segregation, a pair of sister kinetochores was disconnected by laser ablation, along with the corresponding k-fibers, from one spindle pole in live human U2OS cells stably expressing the centromere protein CENP-A-GFP, mCherry-α-tubulin and photoactivatable PA-GFP-tubulin.

As a first approach, the laser ablation cut was performed during anaphase onset where the outermost k-fiber was severed about 2.5 μm away from the kinetochore (**Figure** 31) in order to follow the movements of one pair of sister kinetochores during the rest of anaphase. Outermost k-fibers were selected for ablation because if they move away from the spindle after the cut (Kajtez et al., 2016), it would be possible to distinguish a single kinetochore pair and the associated MTs from the neighboring MTs in the spindle. Given that the k-fiber and the bridging fiber merge 1-2 μm away from the kinetochore (Kajtez et al., 2016), the distance of 2.5 μm away from the kinetochore was chosen to preserve the connection between the bridging fiber and the k-fiber stub after the cut.

The severed k-fiber at anaphase onset did not move away from the spindle and in 100% of the cells, the k-fiber stub remained integrated in the spindle and indistinguishable from the adjacent MTs soon after laser ablation. There could be two possible explanations for such outcome. Firstly, even if the laser cut of k-fiber was successful, the fibers in anaphase are so bundled that a single k-fiber could not be dissociated from the neighboring MTs. Secondly, due to the MT bundling, the laser cut is unintentionally performed on more than one k-fibers which result in an unsuccessful cut due to the laser inability to sever such great portion of MTs.

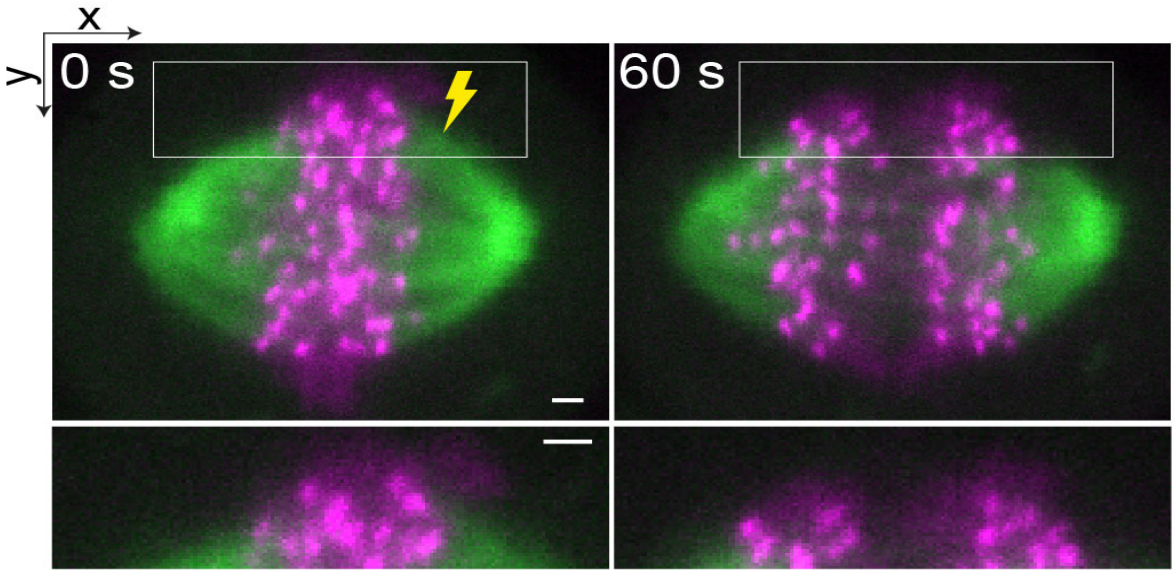

Figure 31 Laser ablation in anaphase. Time-lapse images of the spindle (top row) in a U2OS cell, and enlargements of the boxed region (bottom row). After the k-fiber cut 2.5 μm from the kinetochore (yellow lightning sign) in anaphase, the pair of sister kinetochores did not show displacement from the spindle. Time 0 is the laser ablation onset. Scale bar, 1 μm

In order to maximize the post-severing movement of the kinetochores away from the spindle, a different approach was applied where the laser ablation cut was performed during late metaphase, prior to anaphase onset. The late metaphase was chosen because the spindle maintains a round shape compared to the slightly compressed anaphase spindles and it is easier to distinguish the outermost k-fiber from the neighboring MTs. As previously mentioned, the laser ablation cut was performed about 2.5 μm away from the kinetochore (**Figure** 32).

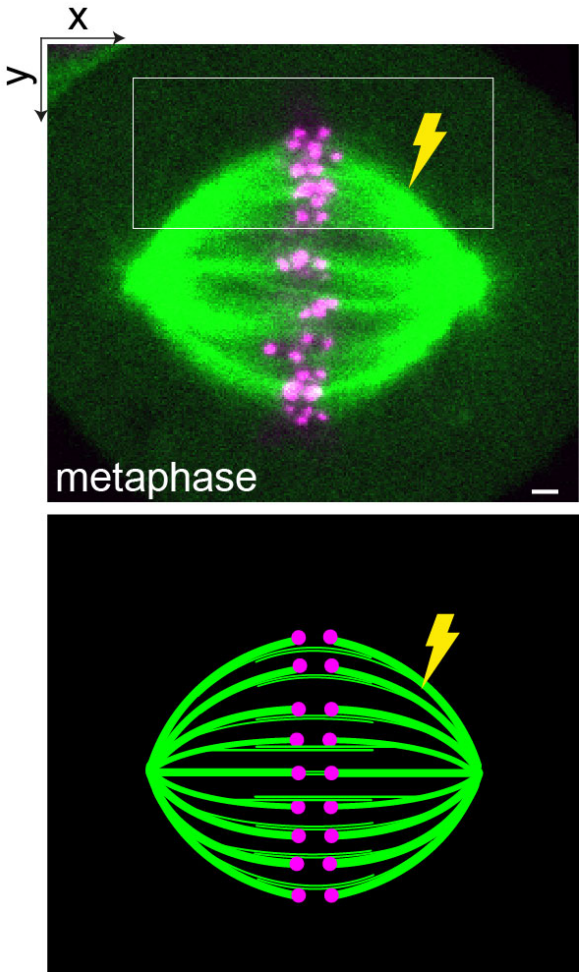

Figure 32 Laser ablation in metaphase. Live image of the spindle (top) in a U2OS cell expressing centromere protein CENP-A-GFP (magenta) and mCherry-α-tubulin (green) and scheme (bottom) show k-fiber cut 2.5 μm from the kinetochore in metaphase (yellow lightning sign). Scale bar, 1 μm.

In 90% of the cells, after severing the outermost k-fiber, the k-fiber stub was pulled back towards the spindle pole during first 15s, before anaphase onset. Such movements were very sudden, which indicates the possible role of the dynein-mediated transport, as showed by others (Elting et al., 2014; Sikirzhytski et al., 2014). Interestingly, in 10% of the cells the k-fiber stub and the kinetochores remained without connection to one spindle pole, usually until mid-anaphase, and the direction of kinetochore and stub movement was away from the pole from which it was disconnected (Figure 33 and Figure 34). More surprisingly, the sister kinetochores of the outermost k-fibers continued to separate after ablation, as well as the rest of the kinetochores in the spindle which kept a connection to both spindle poles intact (**Figure** 34).

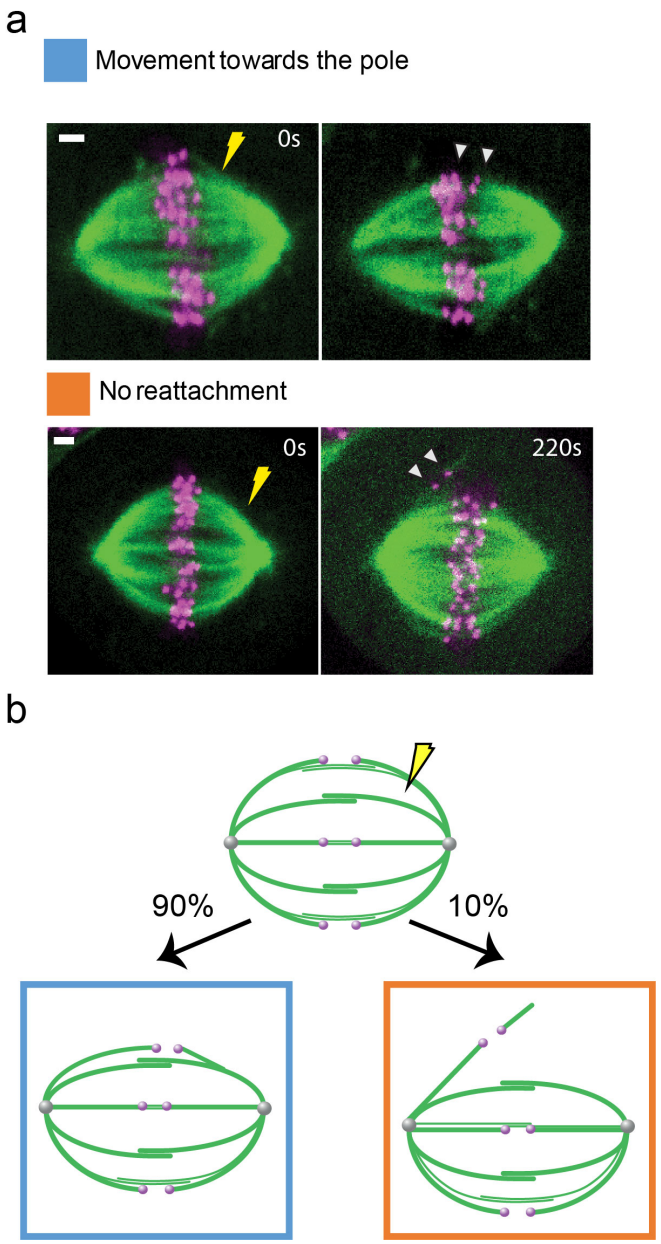

Figure 33 The outcomes after laser ablation in metaphase. (a) Time-lapse images of U2OS spindle show the outcomes after ablation. (b) Only in 10% cases after ablation, sister kinetochores remained detached from the spindle pole.

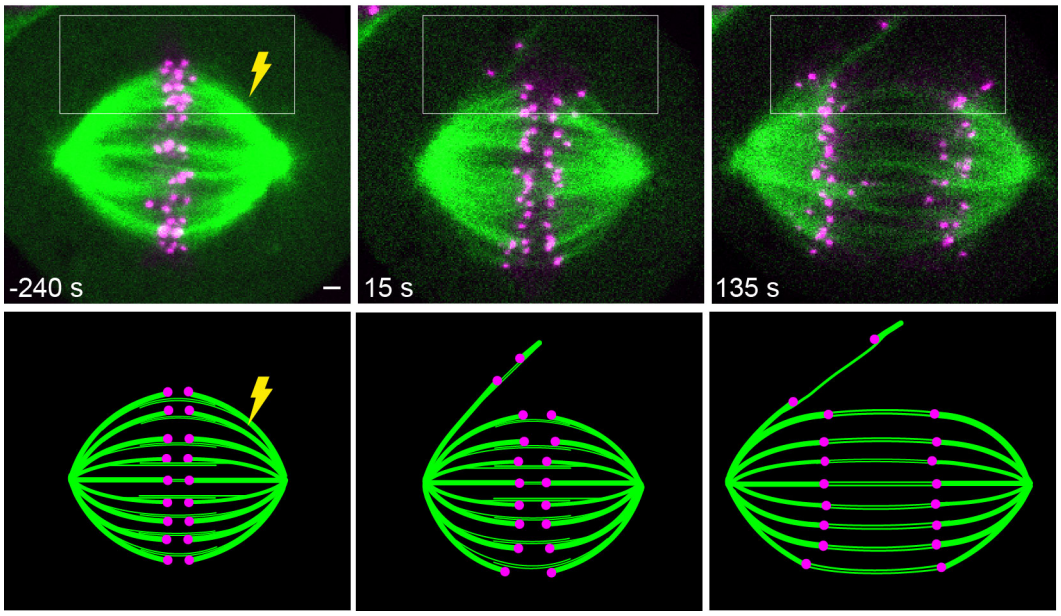

Figure 34 Succesful laser ablation in metaphase. Time-lapse images of the spindle (first row) in a U2OS cell expressing centromere protein CENP-A-GFP (magenta) and mCherry-α-tubulin (green), and enlargements of the boxed region (third row). Schemes are shown under the images. K-fiber was cut 2.5 μm from the kinetochore in metaphase (yellow lightning sign). Time 0 is anaphase start. Scale bar, 1 μm.

This study only considered the population of cells where k-fiber stub remained disconnected from the spindle pole during anaphase, and frames when kinetochores changed direction, quickly approaching spindle poles, were not analyzed. This is due to the fact this phenomenon was observed and described in other studies (Elting et al., 2014; Sikirzhytski et al., 2014). A pair of sister kinetochores successfully disconnected from the spindle will be named displaced kinetochores during further experiments.

To confirm that the bridging fiber between displaced kinetochores indeed remained preserved after anaphase onset, the MT signal intensity between displaced kinetochores was measured during late metaphase and mid-anaphase (**Figure** 35).

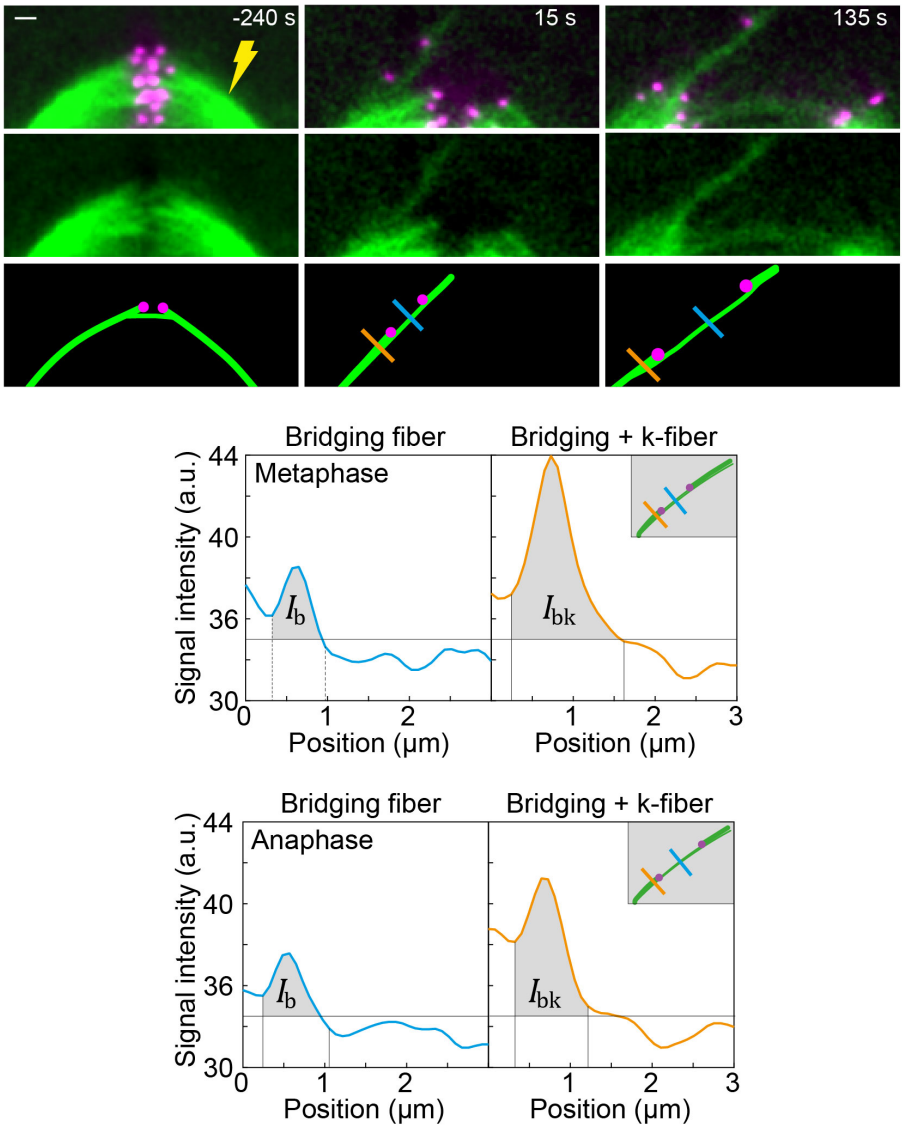

Figure 35 Bridging fiber characterization after the cut. Enlargements of the boxed region from Figure 31. Schemes are shown under the images. K-fiber was cut 2.5 μm from the kinetochore in metaphase (yellow lightning sign). Blue and orange line line represent signal intensity of the bridging fiber and bridging fiber+k-fiber, respectively. Time 0 is anaphase start. (B) mCherry-α-tubulin signal intensity of bridging fiber, I_b (blue, measured along blue line on scheme), and the bundle consisting of bridging and k-fiber, I_{bk} (orange, measured along orange line), after cut in metaphase (left, n=13 cells) and during anaphase (right, n=13 cells). Horizontal lines mark background signal, vertical lines delimit area (grey) where signal was measured.

In addition, the bridging fiber preservation between displaced kinetochores was shown with silicon rhodamine (SiR)-tubulin labeling and α-tubulin immunostaining.

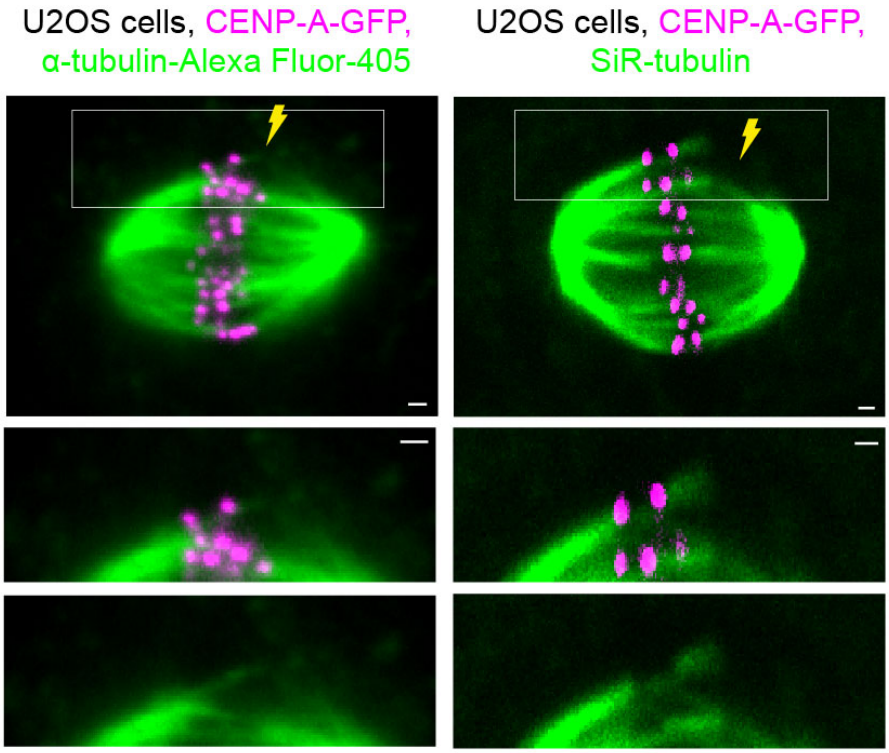

Figure 36 The confirmation of the bridging fiber. Left panel: image of the fixed spindle after ablation (yellow lightning sign) 2.5 um from kinetochore (top row) in a U2OS cell stably expressing centromere protein CENP-A-GFP (magenta) and immunostained for α-tubulin (Alexa Fluor-555 shown in green), and smoothed enlargements of the boxed region in both channels (middle row) and only green channel (bottom row). Right panel: image of the spindle after ablation (yellow lightning sign) 2.5 um from kinetochore (top row) in a U2OS cell stably expressing centromere protein CENP-A-GFP (magenta) and stained with SiR-tubulin (green), and smoothed enlargements of the boxed region in both channels (middle row) and only green channel (bottom row).

To see whether other interpolar MT bundles are found close to the displaced kinetochores, and to confirm that between displaced kinetochores antiparallel microtubules are indeed present, the cells were transfected with protein regulator of cytokinesis 1 (PRC1), which binds to antiparallel overlap regions (Jiang et al., 1998; Kajtez et al., 2016; Mollinari et al., 2002a; Polak et al., 2017). PRC1 was found between the kinetochores

before and after ablation, from metaphase throughout anaphase, whereas other PRC1-labeled overlap bundles were not visible in the vicinity of the displaced kinetochores (**Figure** 37).

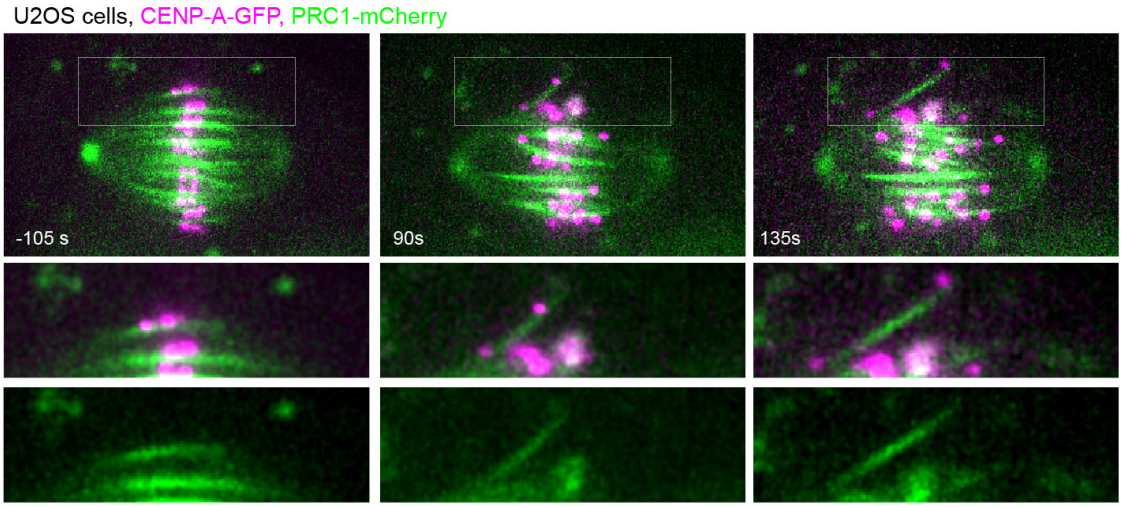

Figure 37 PRC1 labeled bridging fibers. Time-lapse images of the spindle (top row) in a U2OS cell expressing centromere protein CENP-A-GFP (magenta) and PRC1-mCherry (green), and smoothed enlargements of the boxed region in both channels (middle row) and only green channel (bottom row). K-fiber was cut 2.5 μm from the kinetochore in metaphase (yellow lightning sign). Time 0 is anaphase start.

After development of the successful approach for displacement of sister kinetochores with preserved bridging fiber, their movements during anaphase were quantified. It was hypothesized that if displaced kinetochores continue to separate during anaphase even though the connection to one spindle pole is lost, a bridging fiber could play a role in this process.

4.2 Kinetochore segregation after laser ablation

As the displaced sister kinetochores started to separate, similar to the other kinetochore pairs in the spindle (**Figure** 34), displaced kinetochore movements were tracked tracked every 15s, with the Low Light Tracking Tool, until the end of anaphase or until their k-fiber stub became reintegrated into the spindle, whichever occurred first. In order to eliminate the possible damage from laser ablation on displaced kinetochores, control kinetochore pairs from the same spindles were used but whose k-fibers were not severed. Control kinetochores were also tracked every 15s until the end of anaphase. The velocities

were calculated during first 60s of anaphase (early anaphase) because of the certainty that during that time, in all of the cells analyzed, k-fiber stub and displaced kinetochores did not move towards the spindle pole from which they were initially disconnected (**Figure** 38).

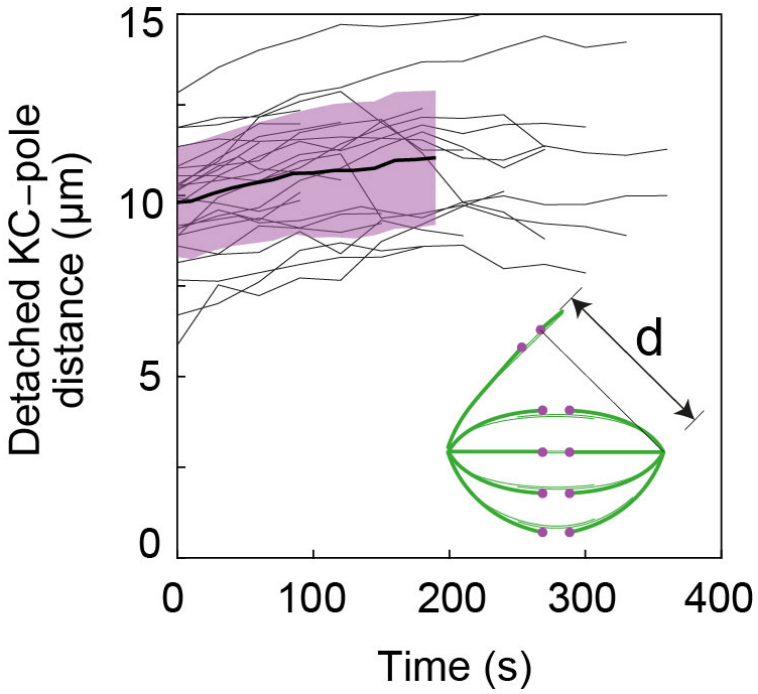

Figure 38 Distance between spindle pole on the side of the ablation and detached kinetochore (see scheme, n=24 cells) over time, where time 0 is anaphase onset. Individual cells (thin lines), mean (thick line), s.d. (pink region). Note that the detached kinetochores are moving away from the spindle pole.

It was found that the distance between displaced sister kinetochores increased during time as they separated at a velocity of 1.53±0.12 µm/min (results are mean±s.e.m. unless otherwise indicated) during the first 60 s after anaphase onset (**Figure** 39a, left panel, Table 1). Excitingly, this velocity was similar to the separation velocity of control kinetochores, 1.77±0.08 µm/min (p=0.51, **Figure** 39a and c, right panel and**Figure** 39b, **Table** 1). The distance for displaced kinetochores was able to increase as long as the k-fiber stub was detectable wile in control cells the distance between kinetochore increased throughout the whole anaphase (**Figure** 39a).

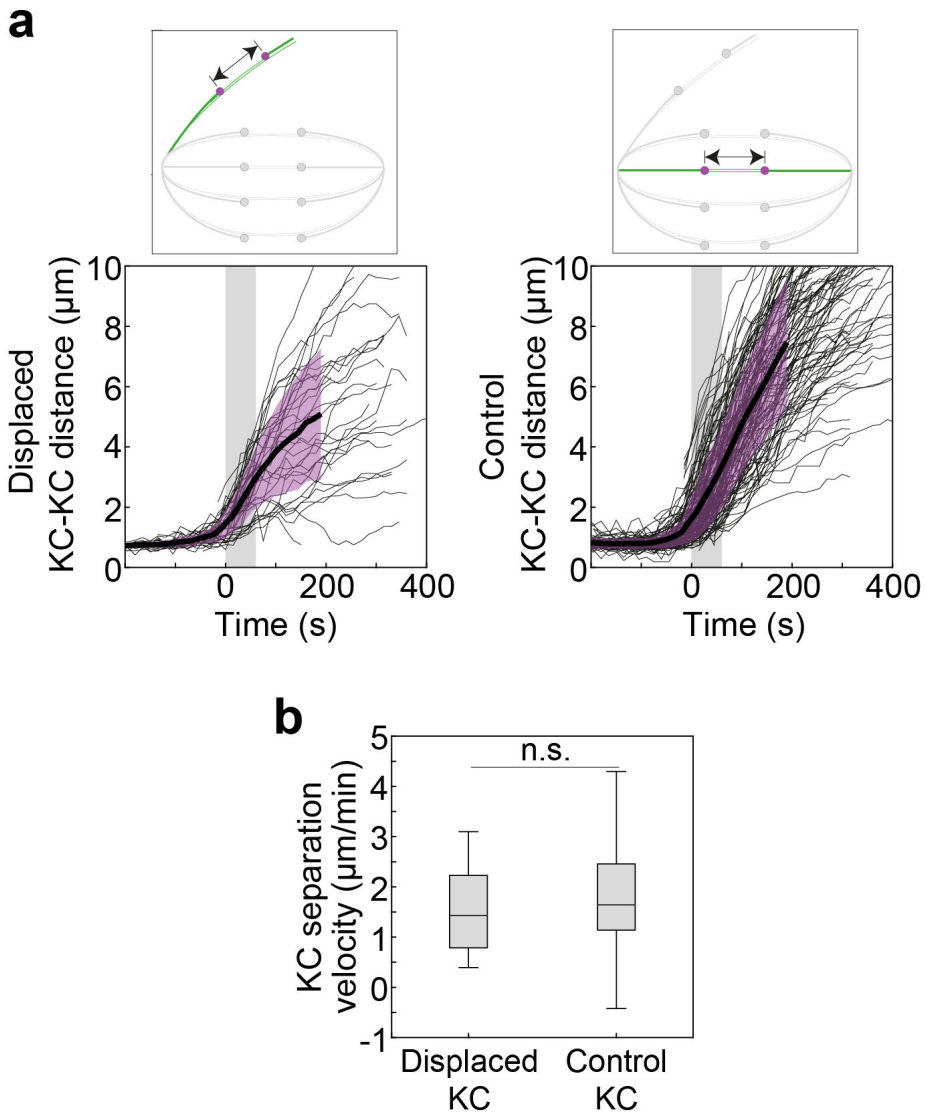

Figure 39 Quantification of displaced kinetochores separation velocities. (a) Distance between displaced (left, n=41 kinetochore pair from 39 cells) and control (right, n=137 kinetochore pairs from 39 cells) sister kinetochores (see schemes) over time, where time 0 is anaphase onset. Individual kinetochore pairs (thin lines), mean (thick line), s.d. (pink region), time interval for velocity measurements (grey region). (b) Box plot of velocities of displaced and control kinetochores.

In addition, the velocity for displaced sister kinetochores in PRC1-mCherry labeled cells was 1.56 µm/min, which did not differ from control kinetochores in the same cells, 1.41 µm/min. The raw data of distances over time indicating the similar incline for displaced and control kinetochores, after anaphase onset, in PRC1-mCherry labeled cells is given in **Figure** 40.

Thus, sister kinetochores segregate with the unchanged velocity from control kinetochores regardless of the detachment from one spindle pole.

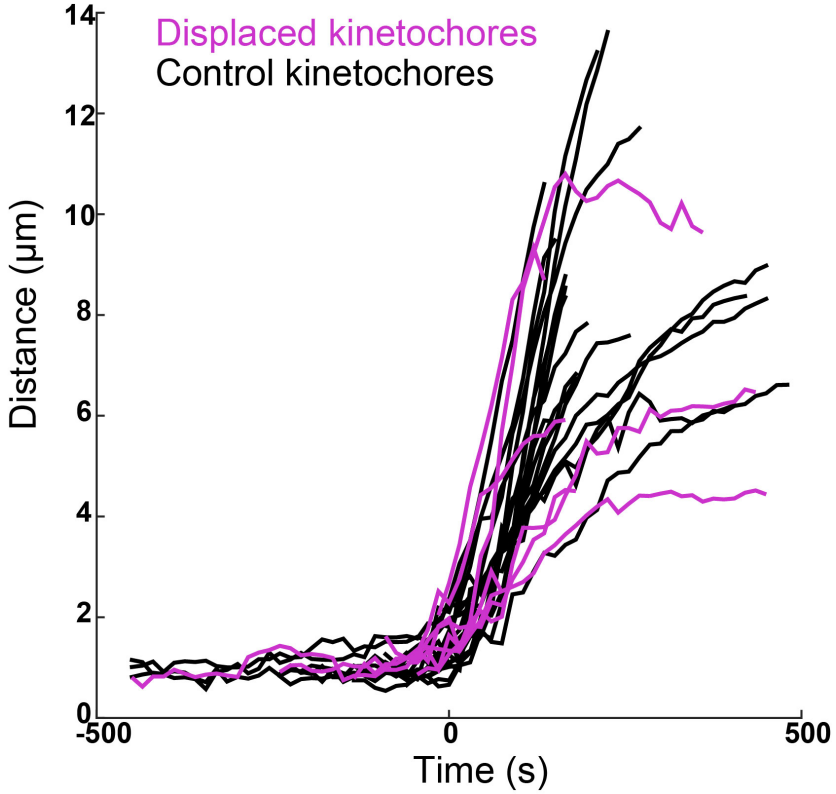

Figure 40 Quantification of displaced kinetochores separation velocities in PRC1 labeled cells. Distance between displaced (magenta, n=7 kinetochore pair) and control (black, n=18 kinetochore pairs) sister kinetochores over time, where time 0 is anaphase onset.

Once the separation of displaced kinetochores was observed and quantified, the contribution of each displaced sister kinetochore to their separation velocity was evaluated. The measured velocities of displaced kinetochores may be a result of movement of both sister kinetochores to the opposite side or f the movement of only the kinetochore with the intact k-fiber, while the other displaced sister kinetochore remained stationary after its k-fiber was severed and the connection to one spindle pole is lost. The latter scenario would imply that, because segregation velocity is similar between displaced and control pairs, movement of kinetochore whose k-fiber is not severed would be faster than in a control situation. To evaluate these scenarios, the midpoint between the displaced sister kinetochores at the beginning of anaphase was set as the fixed reference point from which their distance was measured during the rest of the anaphase. This choice of the reference point was validated

since the displaced sister kinetochore axis remained close to the midpoint during first 60s when the velocity was measured (**Figure** 41).

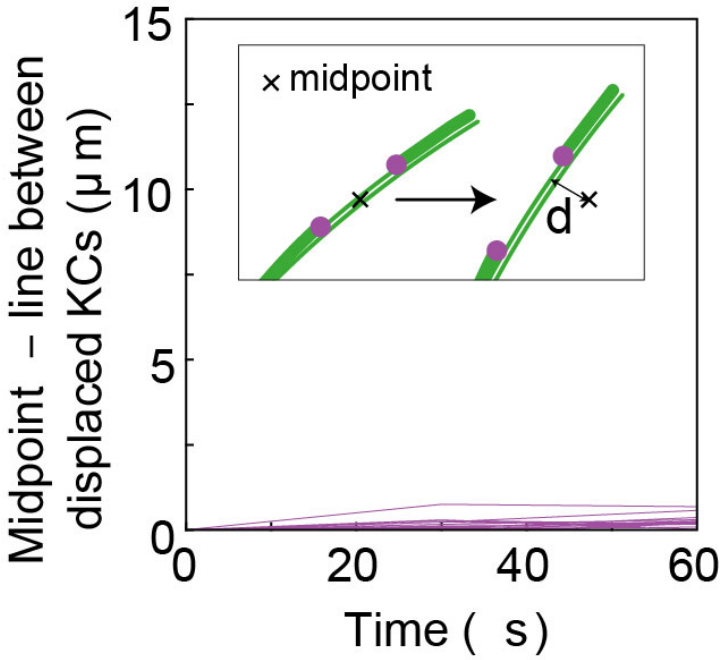

Figure 41 Validation of the midpoint. Distance between line connecting displaced sister kinetochores and their midpoint (see scheme, n=24 cells) defined at the beginning of anaphase over time, where time 0 is anaphase onset.

Even though the kinetochore whose k-fiber was severed showed a short delay (30.00±6.43 s) in the onset of movement with respect to its sister kinetochore (**Figure** 42a), once both sister kinetochores started to move, they moved with similar velocities (v=0.70±0.09 μm/min and 0.80±0.09 μm/min for the kinetochore with the severed and the intact k-fiber, respectively, p=0.19 **Figure** 42b, c and d, **Table** 1). It was concluded that not only the kinetochore with the intact k-fiber, but also the one with the severed k-fiber, contributes to their separation velocity during anaphase.

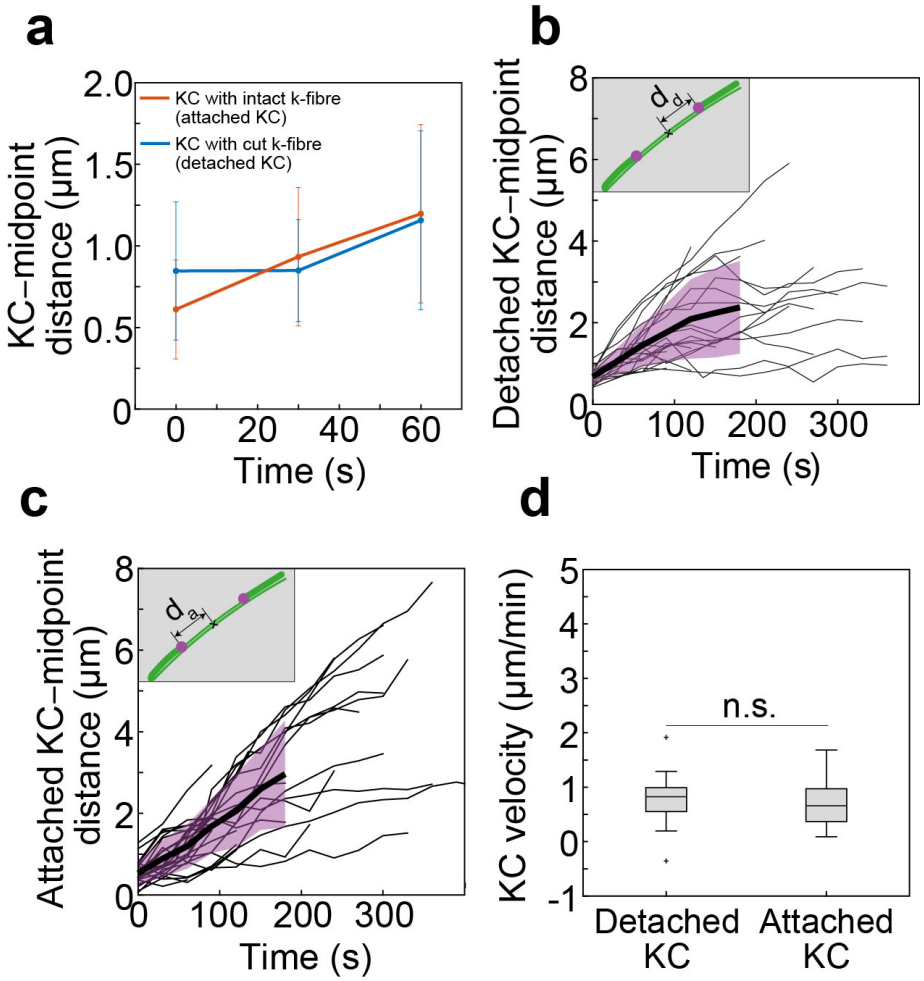

Figure 42 Quantification of velocities for both displaced kinetochores from the midpoint. (a) Average distance between detached (blue line) and attached (orange line) kinetochore from their midpoint (n=24 cells) over time, where time 0 is anaphase onset for attached displaced kinetochore (right panel). Note the delay in the anaphase onset for the detached displaced kinetochore. (b) Distance between detached (left, d_d on scheme, n=24 kinetochore pairs) and (c) attached (right, d_a on scheme, n=24 kinetochore pairs) displaced kinetochores from their midpoint defined at the beginning of anaphase. Individual kinetochore pairs (thin lines), mean (thick line), s.d. (pink region), time interval for velocity measurements (grey region). (d) Box plot (right) represents velocities of detached and attached displaced kinetochores from their midpoint.

4.3 The role of the bridging fiber between displaced kinetochores

Is the bridging fiber indeed crucial for the separation of displaced kinetochores? To test this assumption, a double-ablation assay was developed. First, the outermost k-fiber was severed about 2.5 µm away from the kinetochore in lase metaphase, as described above. Once the displaced sister kinetochores started to separate, we ablated a point between them to sever the bridging fiber (**Figure** 43).

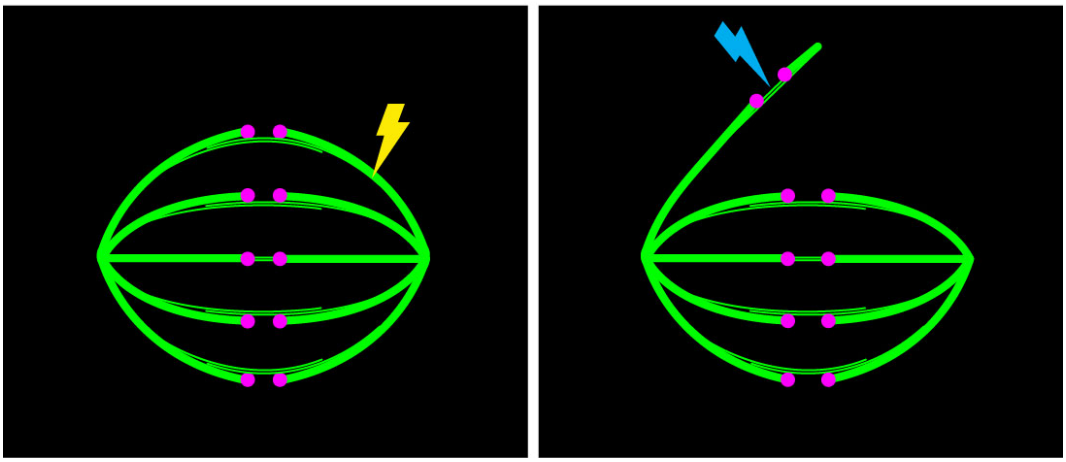

Figure 43 The double-ablation assay. K-fiber was cut 2.5 µm from the kinetochore in metaphase (yellow lightning sign), after the anaphase onset, bridging fiber was cut directly (blue lightning sign).

Even though the kinetochores started to separate after k-fiber ablation, as described previously, the second ablation of the bridging fiber stopped the further separation of displaced kinetochores (**Figure** 44). Interestingly, in 70% of the cells with double ablation, displaced sister kinetochores moved together towards the spindle pole of the intact k-fiber. This joint movement may be due to entanglement of the chromosome arms. In the remaining 30% of the cells, the k-fiber stub and the accompanied kinetochore were suddenly pulled by other spindle MTs towards either spindle pole, as observed previously in metaphase (Elting et al., 2014; Sikirzhytski et al., 2014).

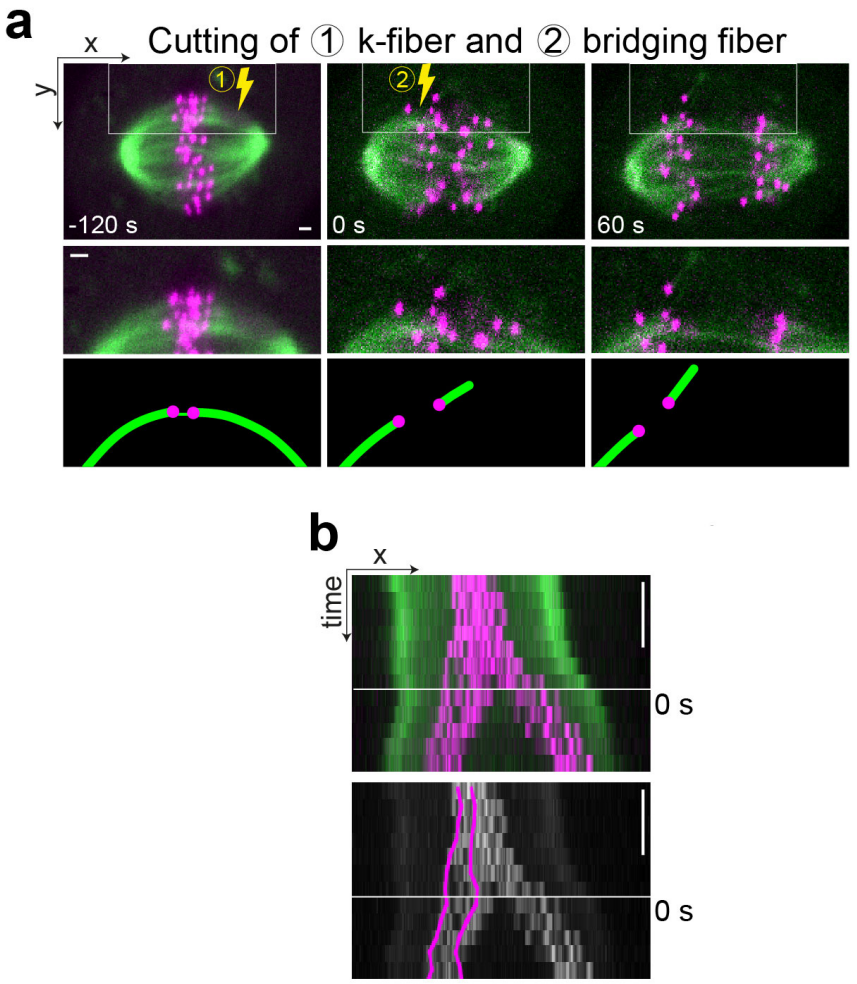

Figure 44 Impaired kinetochore separation after a cut of the bridging fiber. (a) Time-lapse images of the spindle in a U2OS cell: before the k-fiber was cut 2.5 µm from the kinetochore (top left, yellow sign marks the cut), when the bridging fiber was cut (top center, time 0, yellow sign marks the cut) at the beginning of anaphase, and 60 s later (top right). Enlargements of the boxed region (middle row) and schemes (bottom; MTs, green; kinetochores, magenta). (b) Kymograph of the spindle from (a) showing merged channels (top) and traces of displaced kinetochores in magenta and control kinetochores in grey (bottom).

To quantify kinetochore movements in experiments where the bridging fiber was disrupted, the displaced kinetochore segregation velocity during 60 s after the severing was measured, v_s=0.49±0.01 µm/min. This velocity was significantly lower in comparison to the displaced kinetochores with an intact bridging fiber (v_s=1.53±0.12 µm/min, p=1.3x10^{-3}, **Figure** 45) and control sister kinetochores on the unperturbed side of the same spindle (v_s=1.54±0.02 µm/min, p=3.2x10^{-4}, **Figure** 39, **Table** 1). These results show that severing of

the bridging fiber disrupted separation of displaced kinetochores and that the bridging fiber is required for proper segregation of displaced kinetochores.

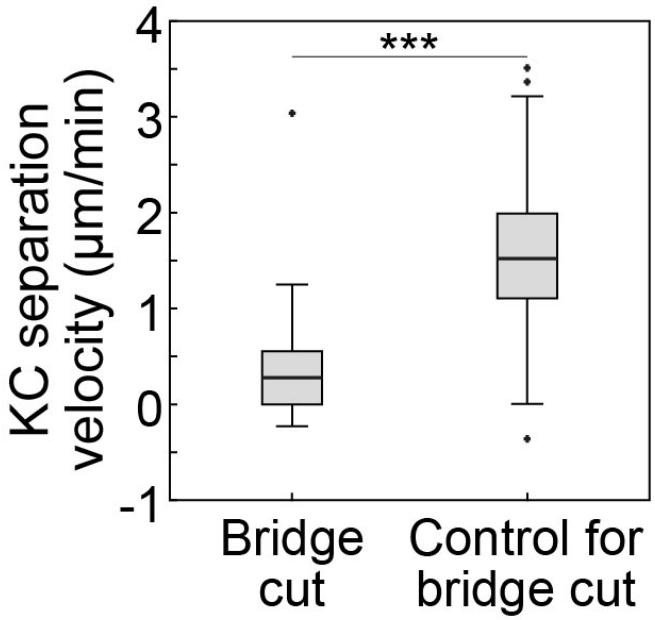

Figure 45 Velocity decrease after the bridging fiber cut. Box plot of velocities of displaced and control kinetochores. ***p<0.001.

Another way to remove the bridging fiber impact on the segregation of displaced kinetochores was the severing of the outermost k-fiber close to the kinetochore (~1.0 µm away) during late metaphase (**Figure** 46). It was expected that such short stubs would become disconnected from the bridging fiber, given that the k-fiber and the bridging fiber merge 1-2 µm away from the kinetochore (Kajtez et al., 2016). In 6 out of 10 cells, a rotational movement of the displaced kinetochores towards the spindle pole of the intact k-fiber was observed where they remained during the rest of the anaphase while the control kinetochores in the spindle continued to separate (**Figure** 46). In the remaining cells, the displaced sister kinetochores did not rotate but their stub reintegrated in the spindle, the distance between them slightly increased but then they continued to move together towards the intact k-fiber (**Figure** 47) as the control kinetochores separated normally, similarly to the 70% of the cells in which the bridging fiber was severed.

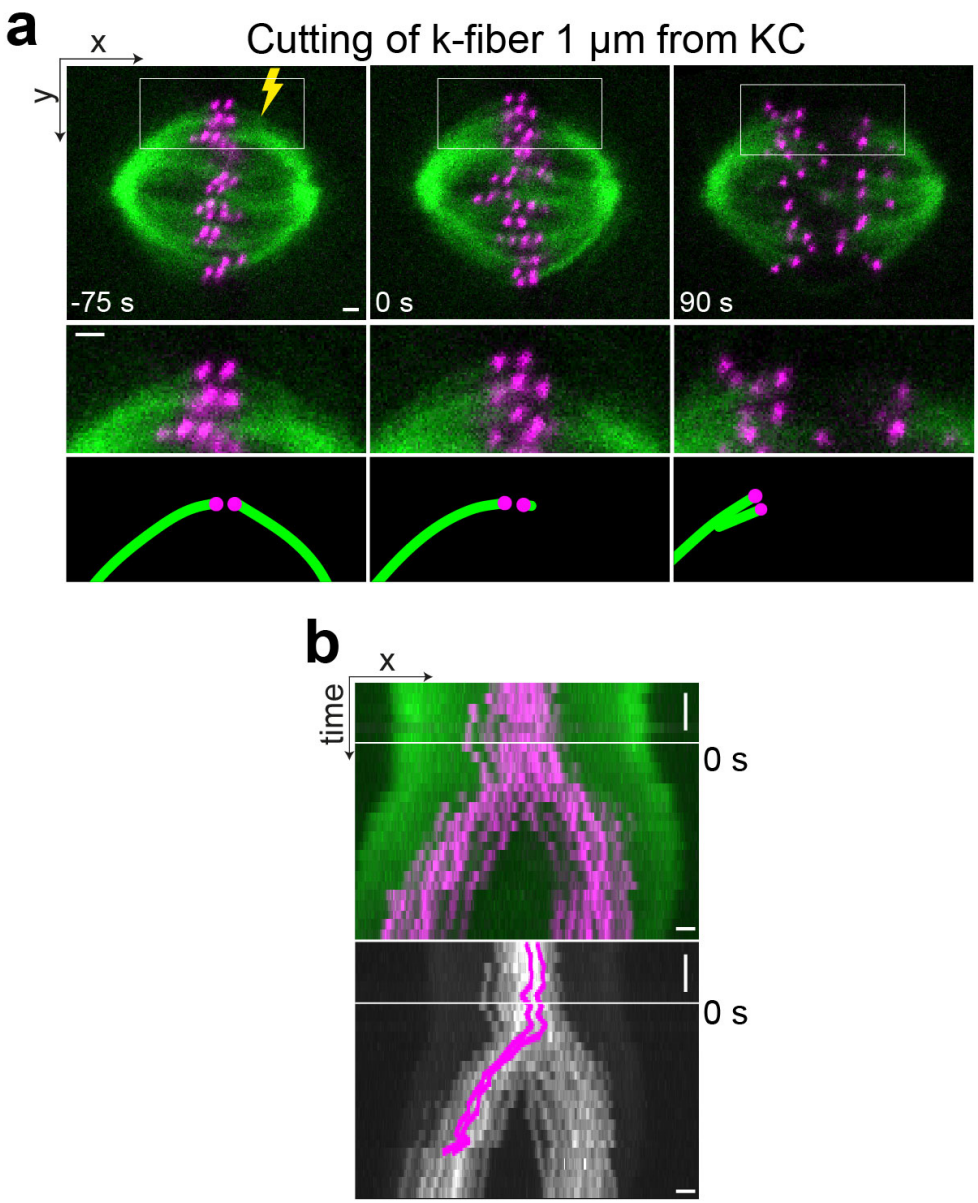

Figure 46 Displaced kinetochores rotational movement after the close cut. (a) Time-lapse images of the spindle in a U2OS cell before the k-fiber was cut 1 µm from the kinetochore (top left, yellow sign marks the cut), at the beginning of anaphase (top center, time 0), and 90 s later (top right). Enlargements of the boxed region (middle row) and schemes (bottom). (b) Kymograph of the spindle from showing merged channels (top) and traces of displaced kinetochores in magenta and control kinetochores in grey (bottom).

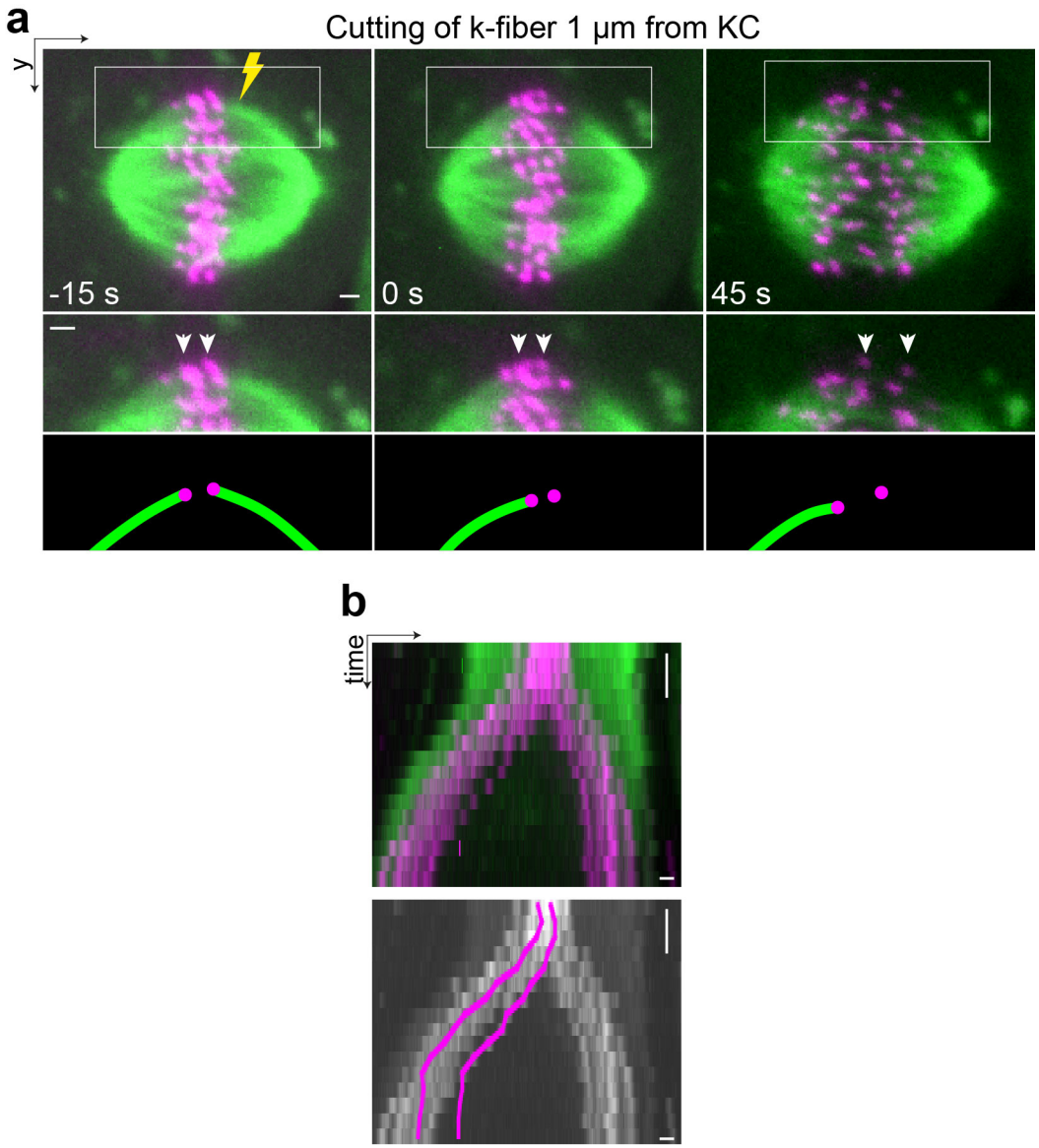

Figure 47 Displaced kinetochores reintegrate into the spindle after a close cut. (a) Time-lapse images of the spindle in a U2OS cell before the k-fiber was cut 1 µm from the kinetochore (top left, yellow sign marks the cut), at the beginning of anaphase (top center, time 0), and 90 s later (top right). Enlargements of the boxed region (middle row) and schemes (bottom row). (b) Kymograph of the spindle from showing merged channels (top) and traces of displaced kinetochores in magenta and control kinetochores in grey (bottom).

The velocity of kinetochores with a short k-fiber stub (<1 μm) was 0.28±0.01 μm/min (Table 1), which was significantly lower in comparison to the displaced kinetochores with a long stub (>2.5 μm, 1.53±0.12 μm/min, $p=1.9x10^{-4}$, **Figure** 48) and control sister kinetochores on the unperturbed side of the same spindle (1.51±0.02 μm/min, $p=3.6x10^{-5}$, **Figure** 39, **Table** 1). These results imply that a short k-fiber stub is not able to keep the connection with the bridging fiber, resulting in impaired kinetochore segregation.

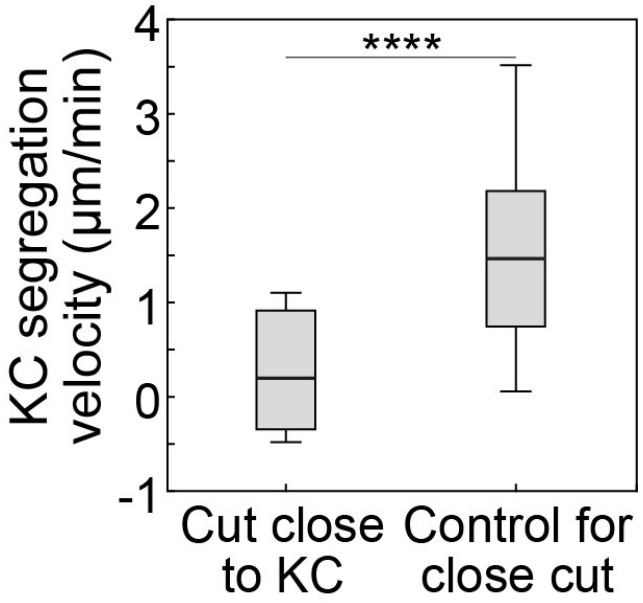

Figure 48 Kinetochore separation velocity decreases after a close cut. Box plot of velocities of displaced and control kinetochores. ****p<0.0001.

4.4 The role of the bridging fiber on a whole spindle scale

Based on the finding that in metaphase almost all interpolar MT bundles are bridging fibers that link a pair of kinetochores (Polak et al., 2017), it was assumed that this is the case also in early anaphase, meaning that almost all MT bundles in the midzone are bridging fibers. To test the contribution of all bridging fibers in mitotic spindle to kinetochore separation, the laser ablation assay to cut the entire midzone region between all sister kinetochores was applied (**Figure** 49a, top). Due to the robustness of the midzone region during anaphase, the laser ablation was performed repeatedly, in every time point during imaging. Midzone ablation resulted in a slower separation of kinetochores and the spindle

poles (**Figure** 49b and c). During the first 3 min of continuous midzone cutting, kinetochores segregated at a velocity of v_s=1.30±0.16 μm/min and the poles at a velocity v_p=0.52±0.10 μm/min (**Figure** 49c, **Table** 1). These values were significantly lower than the respective values for control spindles, v_s=2.30±0.13 μm/min and v_p=1.19±0.07 μm/min ($p=6.6x10^{-3}$ and $4.3x10^{-5}$ respectively, **Figure** 49c, **Table** 1).

The observation that the velocities for kinetochore and spindle pole separation did not reach zero velocities after midzone ablation suggests that either all the bridging fibers were not disrupted and some of the remaining were able to support the separation during anaphase or that there is a potential contribution from astral MTs pulling forces. Continuous ablation most likely did not have a nonspecific impact on anaphase because velocities of the kinetochore poleward movement were indistinguishable from control values suggesting that slower kinetochore and pole separation is indeed the result of midzone disruption (**Figure** 50, Table 1). Together, these findings support the view that bridging fibers are an important part of the machinery that segregates kinetochores and spindle poles.

To evaluate the potential contribution of astral MTs to kinetochore and spindle pole separation, continuous ablation of astral MTs was performed. During the first 3 min of astral cutting, kinetochores segregated at a velocity of v_s=2.40±0.13 μm/min and the poles at a velocity v_p=1.36±0.10 μm/min (**Figure** 49a and b, bottom, **Figure** 49c, **Table** 1). The obtained velocities after astral MTs removal did not differ from control values (**Table** 1), signifying that astral MTs do not play important role in kinetochore and spindle pole separation during early anaphase, unlike bridging MTs. Also, these results confirmed once again that continuous ablation did not have a nonspecific effect on anaphase dynamics (**Figure** 51).

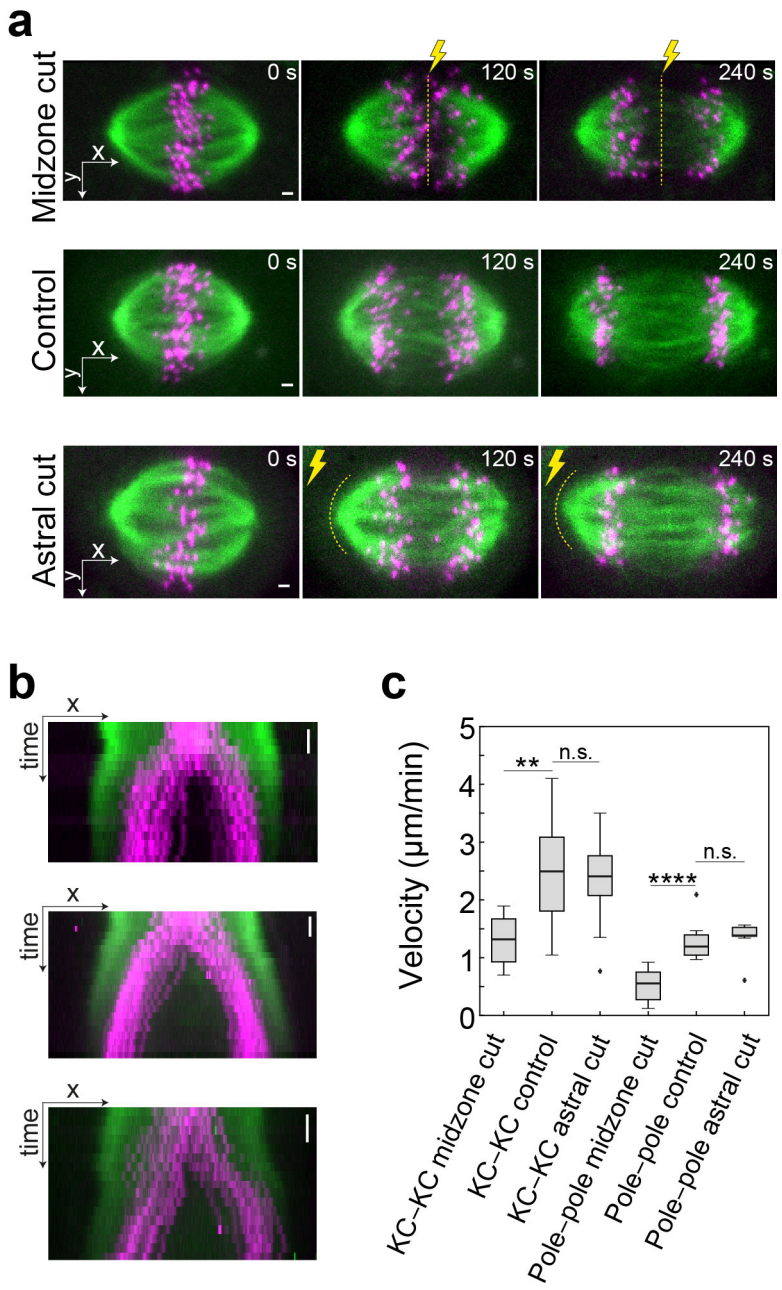

Figure 49 Laser ablation of the midzone and astral MTS. Time-lapse images of the spindle during midzone cut along the dotted yellow line (top), control anaphase spindle (middle) and during astral MT cut along the dotted yellow line (bottom) in a U2OS cell. B) Kymographs of the spindles from (G) showing merged channels. C) Box plot of kinetochore separation velocities (KC-KC) and pole separation velocities (pole-pole) for the conditions from (G). n.s. non-significant. **p<0.01. Scale bars, 1 µm; time bars, 1 min. See also Figure S2.

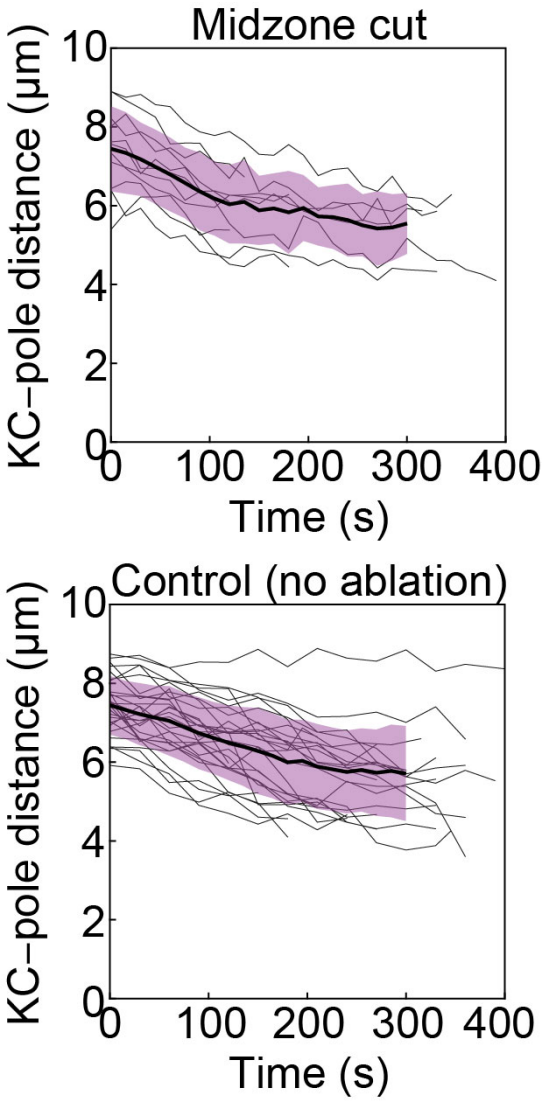

Figure 50 Raw data of poleward movement for cells with midzone cut and the control cells. Distance between kinetochores and the respective spindle poles, in anaphase spindles with midzone cut (top, n=11 cells) and control spindles (bottom, n=24 cells), over time, where time 0 is the beginning of midzone cut. Individual cells (thin lines), mean (thick line), s.d. (pink region).

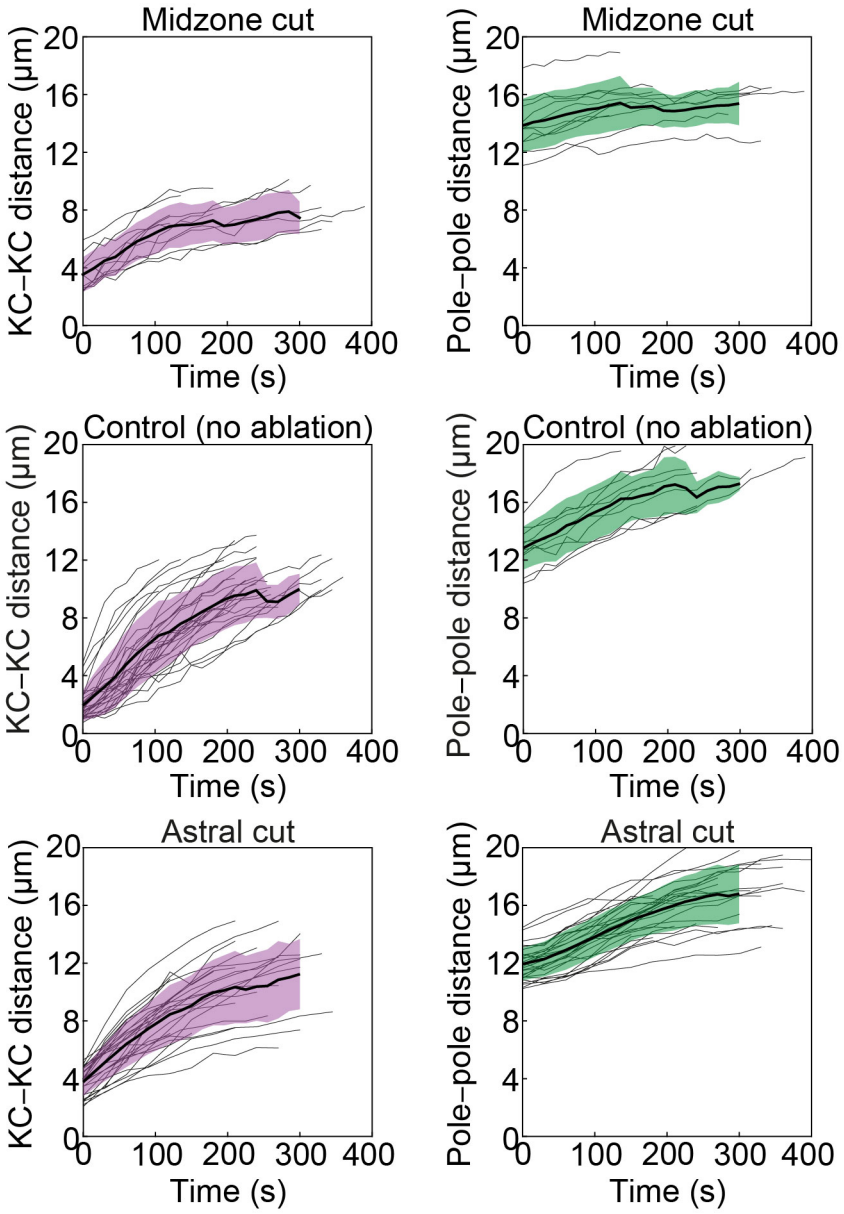

Figure 51 Raw data for kinetochores and spindle poles distances after midzone and astral MTs cut and in control cells. Distance between sister kinetochores (left panel) and spindle poles (right panel), in cells with midzone cut (top row, n=11 cells), astral cut (bottom row, n=29), over time, where time 0 is the beginning of cut and in control spindles (middle row, n=24 cells) over time normalized at an average duration from the beginning of anaphase until the midzone cut. Left panel: individual cells (thin lines), mean (thick line), s.d. (pink region); right panel: s.d. (green region).

4.5 Mechanism of bridging fiber dynamics

The finding that the bridging fiber is required for the segregation of displaced kinetochores prompted the investigation of the role of MT sliding and Pac-Man activity in this process. The changes in the contour length of the structure consisting of the intact k-fiber, bridging fiber and the k-fiber stub of the displaced kinetochores were measured, after severing of the k-fiber ~2.5 µm away from the kinetochore (**Figure** 52a). This contour increased in length at a velocity of 0.80±0.12 µm/min during the first 2 min of anaphase (**Figure** 52b and e, **Table** 1). At the same time, the intact k-fiber shortened at a velocity of 0.57±0.09 µm/min (**Figure** 52c and e), which was similar to that of control k-fibers (**Figure** 52f, **Table** 1) and previous measurements (Yang et al., 2007). The k-fiber stub shortened at the velocity of 0.24±0.12 µm/min during anaphase (**Figure** 52d and e, **Table** 1) but its length did not change during metaphase (**Figure** 52g).

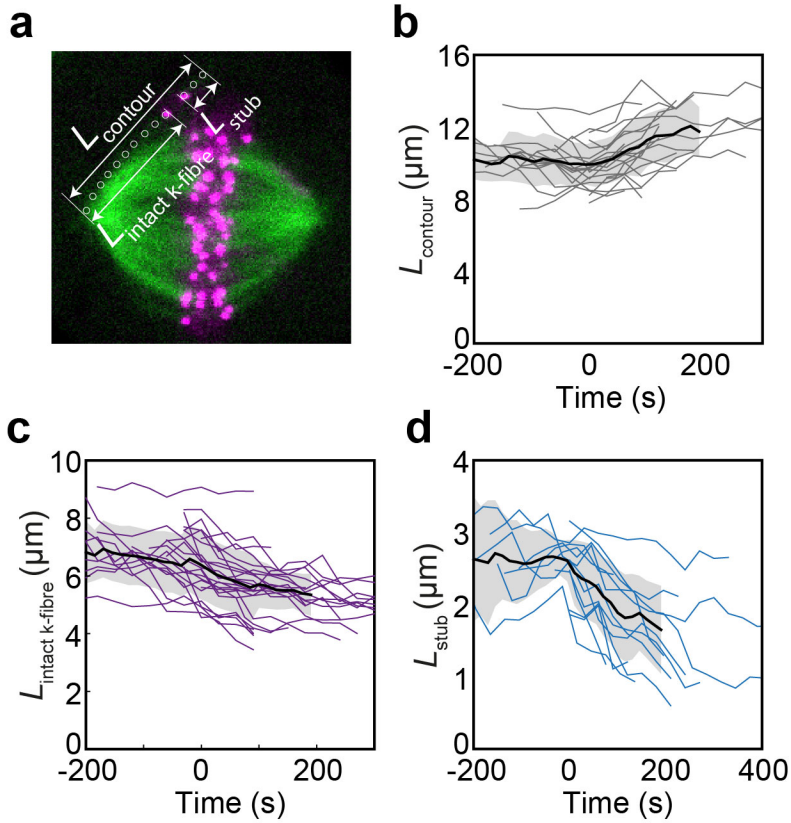

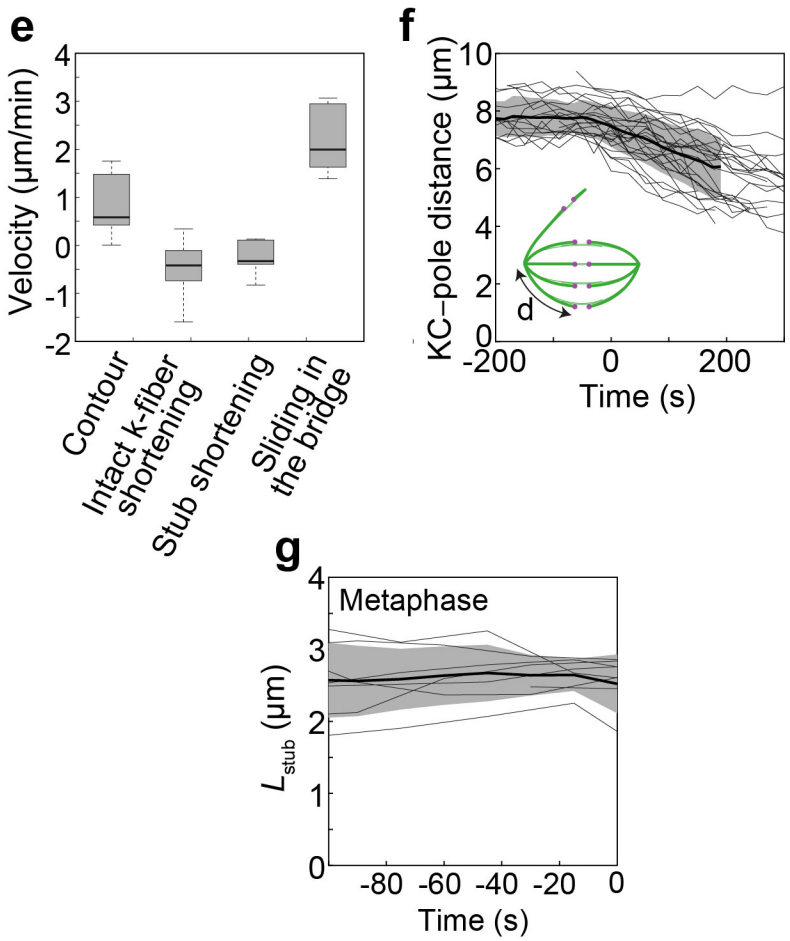

Figure 52 Measurments of the changes in contour length. (a) Image of the spindle in a U2OS cell showing tracking of the contour length of the intact k-fiber, $L_{\text{intact k-fiber}}$, k-fiber stub resulting from the ablation, L_{stub}, and the total contour, L_{contour}. (b)-(d) L_{contour} (n=14), $L_{\text{intact k-fiber}}$ (n=24), and L_{stub} (n=24), measured as shown in (a), over time. Individual kinetochore pairs (thin lines), mean (thick line), s.d. (shaded region). (e) Box plot of velocities for given parameters. (f) Distance between intact spindle pole and control kinetochores (see scheme, n=24 cells) over time. (g) L_{stub} (n=9 cells) during metaphase, measured as shown in (a), over time. Time 0 is anaphase onset.

Intriguingly, after k-fiber ablation, a photoactivated spot at the stub-tip minus end was observed. We observed that this newly created photoactivated spot remained stable even though the stub shortened during anaphase indicating that the stub shortening is a result of only depolymerization at the plus end, i.e., Pac-Man activity (**Figure** 53). When the stub

shortening was analyzed by measuring the distance between the photoactivated spot and the associated kinetochore (Figure 53), a similar value (0.22±0.11 µm/min, p=0.77) was obtained as in previous measurements in contour length (**Figure** 52d and e).

Because intact k-fiber and the stub shortened and the net increase in the contour length was still observed, it was concluded that the elongation of the total contour is most likely a consequence of the sliding apart of MTs in the bridging fiber.

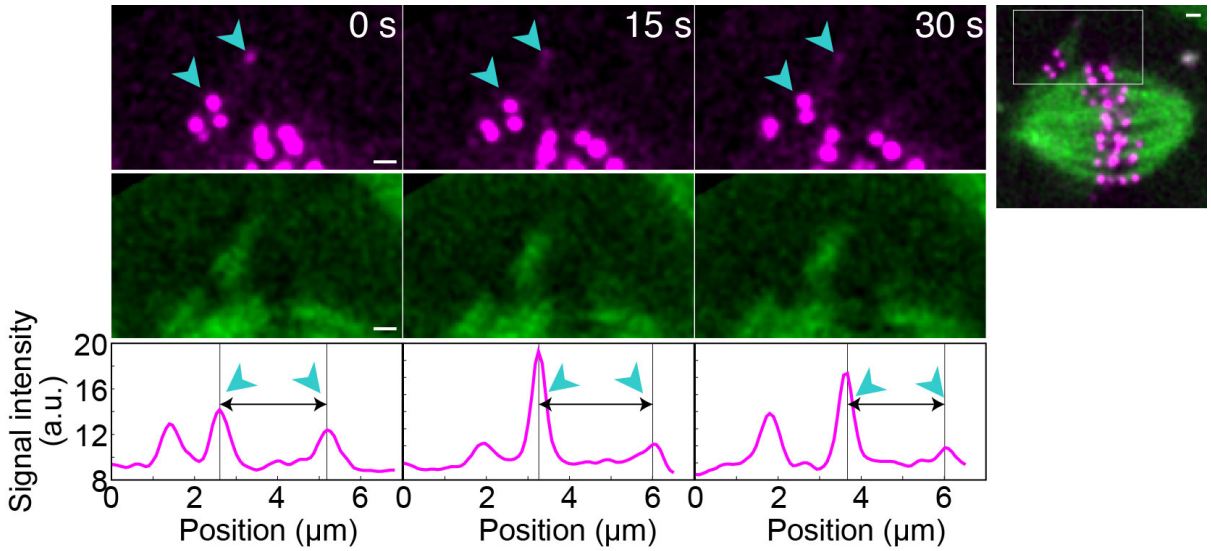

Figure 53 Photoactivation of the k-fiber stub tip. Spindle after k-fiber ablation (right, yellow lightning sign), smoothed enlargements of the boxed region in the channel showing CENP-A-GFP and PA-GFP-tubulin (green and magenta, top row) and mCherry-α-tubulin channel (green, middle row) after photoactivation of the k-fiber stub at time 0. Blue arrowheads mark the photoactivated spot and the detached kinetochore. Signal intensities of the PA-GFP-tubulin between the detached kinetochore and the stub tip (blue arrowheads) in the respective frames above (bottom row). Vertical lines mark the signal intensity peaks, arrows show the approaching of the detached kinetochore to the photoactivated spot.

Moreover, it was observed that the velocity of the kinetochore with the severed k-fiber correlates with the stub length decrease most likely because the k-fiber is not linked to the bridging fiber up to ~1 µm from the kinetochore (**Figure** 54) (Kajtez et al., 2016; Milas and Tolic, 2016).

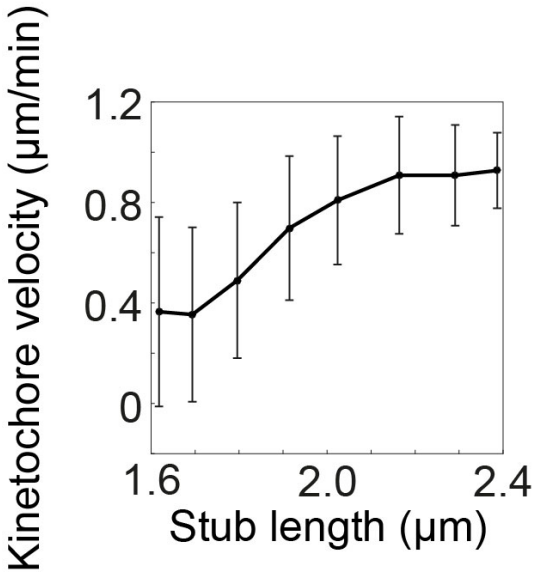

Figure 54 The correlation between a detached kinetochore-midpoint velocity and the length of the k-fiber stub (n=8 cells).

To test directly whether bridging MTs, linked to displaced kinetochores, slide apart during anaphase, PA-GFP-tubulin in the bridging fiber after sister kinetochores started to separate was photoactivated (**Figure** 55).

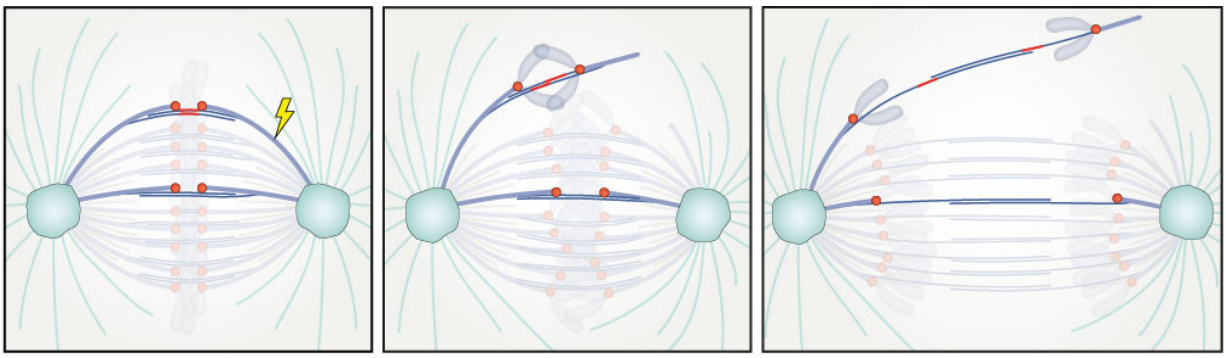

Figure 55 Experimental setup for photoactivation of the bridging fiber between displaced kinetochores. Schemes show laser ablation (yellow) of one k-fiber and photoactivation of the bridging fiber (red marks).

If the MTs in the bridging fiber slide apart, the photoactivated spot should split into two spots that move away from each other. Indeed, as the kinetochores separated, it was

observed that the photoactivated spot separated into two spots at a velocity 2.13±0.33 µm/min, **Figure** 56, **Table** 1). It was concluded that the bridging fibers slide apart during anaphase in order to separate the displaced sister kinetochores.

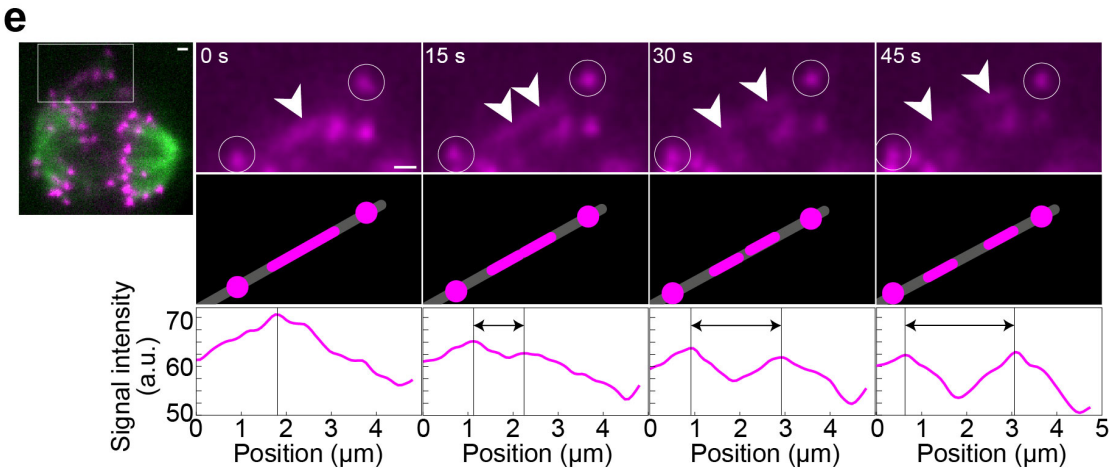

Figure 56 Photoactivation of the bridging fiber between displaced kinetochores. Spindle after k-fiber ablation (left), smoothed enlargements of the boxed region in the channel showing CENP-A-GFP and PA-GFP-tubulin (magenta, top row) after photoactivation of the bridging fiber at time 0. White arrowheads mark the photoactivated spot, which splits into two spots. Circles mark the kinetochores. Schemes (middle row) show the kinetochores and the photoactivated regions in magenta and MTs in grey. Signal intensities of the PA-GFP-tubulin between the displaced sister kinetochores in the respective frames above (bottom row). Vertical lines mark the signal intensity peaks, arrows show the separation of the photoactivated spots.

4.6 k-fibers and the bridging fiber dynamics in the intact spindle

To see if the MTs in the bridging fibers slide apart in intact spindles as well, PA-GFP-tubulin in a line across the entire spindle midzone during anaphase was photoactivated, without performing laser ablation (**Figure** 57). It was observed that in intact spindles, as the anaphase continued, the initial photoactivated spot separated into two spots (v=2.08±0.18 µm/min, **Figure** 57, **Table** 1), similar to the spot between displaced kinetochores (p=0.77,**Figure** 52e), indicating that the bridging MTs slide apart in intact spindles during anaphase.

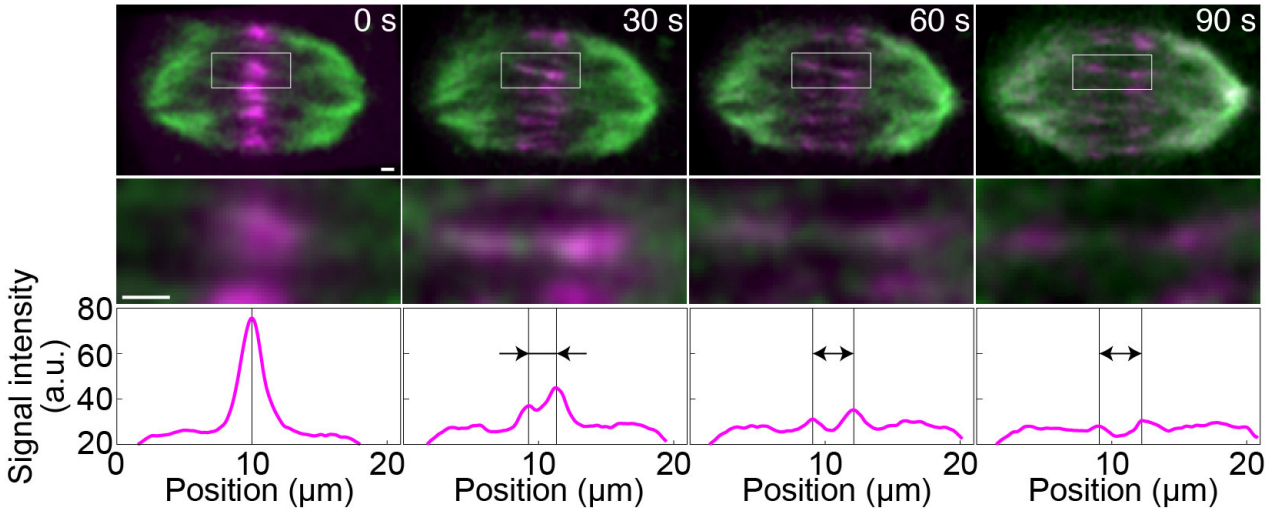

Figure 57 Photoactivation of bridging fibers in intact spindles. Smoothed time-lapse images (top) of the anaphase spindle after photoactivation of PA-GFP-tubulin at time 0 in bridging fibers. Enlargements of the boxed region (middle row) and signal intensity of PA-GFP-tubulin (bottom row) measured across the whole spindle. Vertical lines mark the signal intensity peaks; arrows show the separation of the photoactivated spots in the bridging fiber.

As the bridging MTs slide apart, the associated k-fibers may slide with respect to or together with them. To distinguish between these possibilities, k-fibers and bridging fibers in the same spindle were photoactivated (**Figure** 58a). It was found that the photoactivated spots on the k-fiber moved apart at a similar velocity as the spots on the bridging fiber (1.88±0.19 µm/min and 2.08±0.18 µm/min, respectively, p=0.44, **Figure** 58b, **Table** 1). Importantly, the two velocities were similar inside single cells, despite a significant variation in the rates of sliding among different cells (**Figure** 58c).

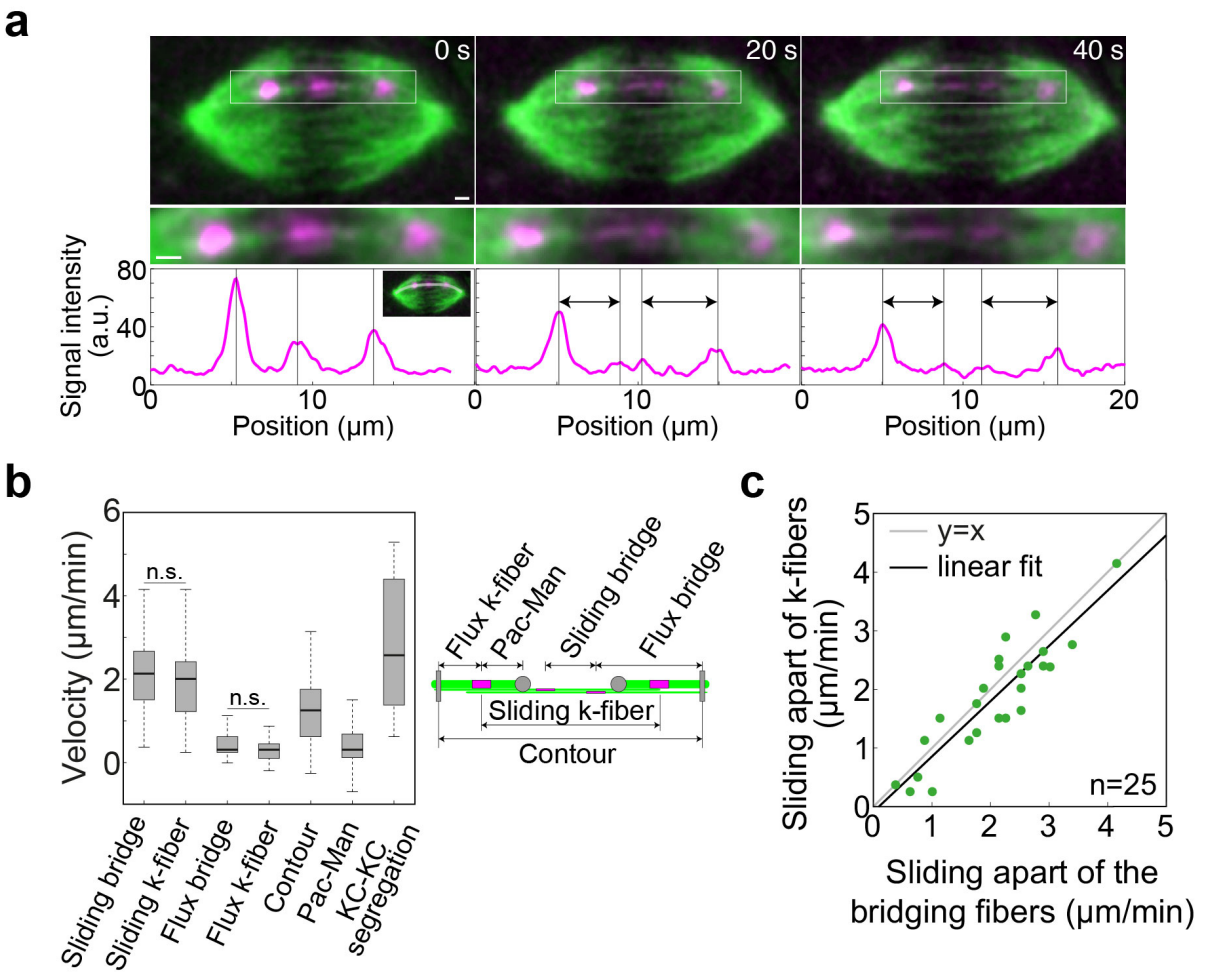

Figure 58 (a) Photoactivation of bridging fibers and k-fibers in intact spindles. Smoothed time-lapse images (top) of the anaphase spindle after photoactivation both bridging fibers and k-fibers. Enlargements of the boxed region (middle row) and signal intensity of PA-GFP-tubulin (bottom row) measured along the gray line shown in inset. Vertical lines mark the signal intensity peaks; arrows show the distance between the photoactivated spots on the bridging and k-fiber. (b) Box plot of velocities measured for parameters shown in scheme. (c) Correlation between velocities of sliding apart of bridging fibers and k-fibers; n, number of cells.

By measuring the velocity of the photoactivated spots with respect to the spindle pole, it was found that the bridging fiber and the attached k-fiber undergo poleward flux at a similar velocites (0.42±0.06 μm/min and 0.32±0.05 μm/min, respectively, p=0.19, **Figure** 58b, **Table** 1). The flux velocity of the k-fibers is in agreement with previous indirect estimation of poleward flux velocity in anaphase (Ganem et al., 2005). Pac-Man depolymerization, measured as the velocity at which the kinetochore approached the photoactivated spot, occurred at the rate of 0.43±0.13 μm/min. During the same time period, the kinetochores

segregated at a velocity of 2.76±0.27 μm/min (n=20, **Figure** 58b). In addition, it was found that the lengthening velocity of the contour consisting of the sister k-fibers and the bridging fiber (1.23±0.17 μm/min) was slower than the velocity of sliding of the bridging fibers itself, as expected in the presence of poleward flux (**Figure** 58b). In the same cells, spindle poles separated at a velocity of 1.36±0.27 μm/min (**Table** 1). Taken together, these results indicate that bridging fibers and k-fibers remain laterally linked and slide together during anaphase in intact spindles.

4.7 Eg5 and KIF15 do not affect anaphase velocities

To identify the proteins that can drive or regulate MT sliding in the bridging fiber, a candidate approach was used based on the protein ability to slide antiparallel MTs or on the protein localization in the spindle midzone during anaphase. A first tested candidate was Eg5 /KIF11 (kinesin-5) which slides antiparallel MTs and contributes to spindle assembly (Blangy et al., 1995; Kapitein et al., 2005). After inactivation of Eg5 by S-Trityl-l-cysteine (STLC, see Methods), kinetochore separation velocity and pole separation velocity were similar to those in untreated cells (p1=0.12, p2=0.44, **Figure** 59a and d, **Table** 1). It was concluded that Eg5 is not crucial for kinetochore and spindle pole separation in U2OS cells.

Next, KIF15/Hklp2 (kinesin-12) was tested because it is functionally redundant with Eg5 (Tanenbaum et al., 2009). However, depletion of KIF15 by siRNA (see Methods) affected neither kinetochore separation nor pole separation velocities (p1=0.17, p2=0.83, **Figure** 59b and d, **Table** 1). Moreover, the combined depletion of KIF15 by siRNA and inhibition of Eg5 by STLC did not show a significant effect on kinetochore and pole velocities (p1=0.67, p2=0.58, **Figure** 59c and d, **Table** 1). Taken together, these results indicate that Eg5 and KIF15 are not the primary motors driving kinetochore and spindle pole separation.

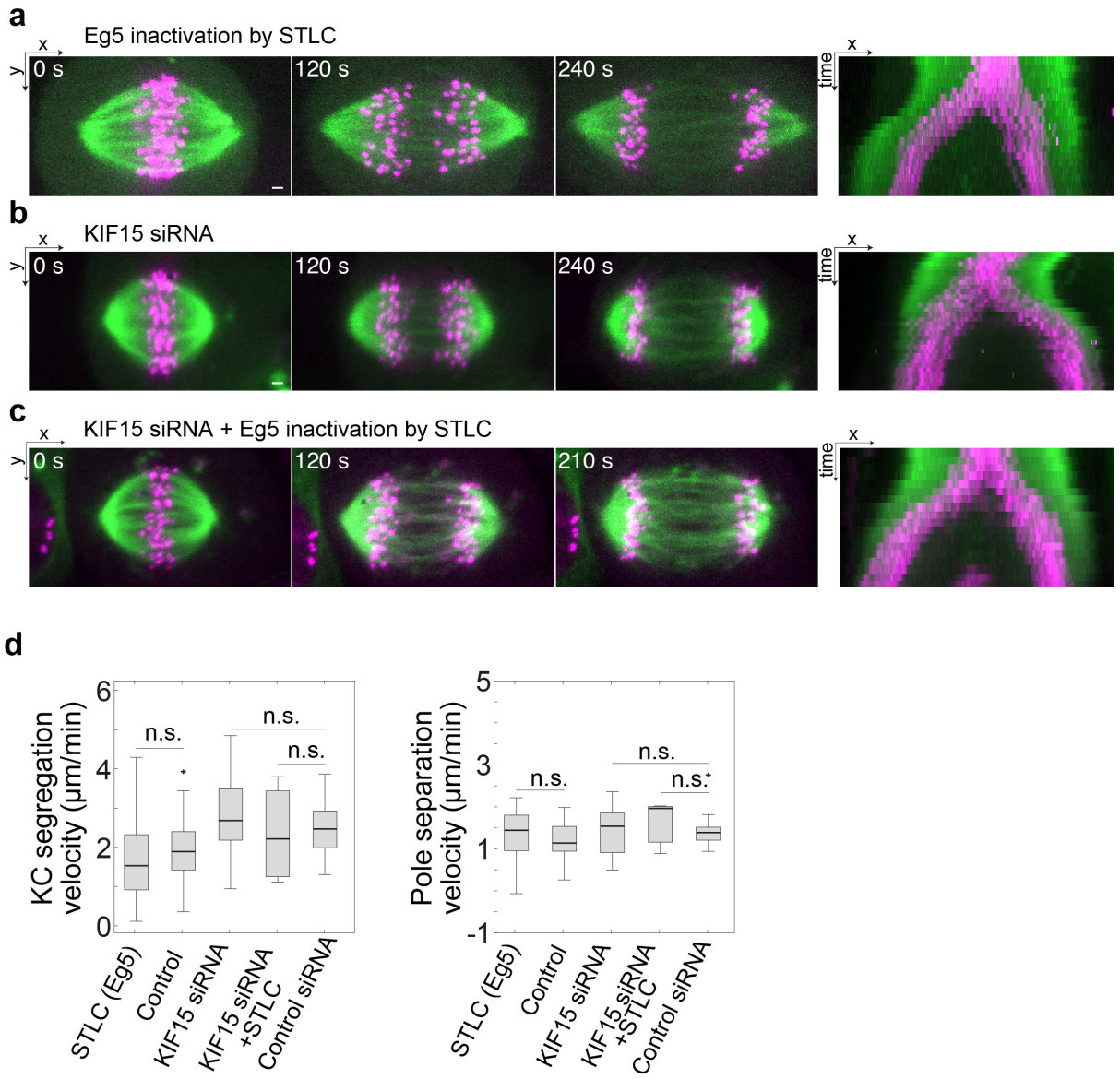

Figure 59 Depletion of Eg5 and KIF15 does not affect kinetochore and spindle pole separation. (a) Time-lapse images of the anaphase spindle in a U2OS cell treated with STLC. Kymographs in merged channels are shown at the right. (b) Time-lapse images of the anaphase spindles in a U2OS cell treated with Kif15 siRNA. Kymographs in merged channels are shown at the right. (c) Time-lapse images of anaphase spindles in a U2OS cell treated with STLC and Kif15 siRNA. Kymographs in merged channels are shown at the right. (d) Box plot shows kinetochore and spindle pole separation velocities for conditions from a – c ; n.s. non-significant.

Next, the photoactivation of the spindle midzone after inactivation of Eg5 by STLC, depletion of KIF15 by siRNA and combined depletion of KIF15 by siRNA and inhibition of Eg5 by STLC was performed to determine the effect of given protein candidates on sliding of

bridging MTs. It was observed that the photoactivated spot in the spindle midzone separated into two spots at a velocity similar to that of the control cells (**Figure** 60, **Table** 1). These results suggest that Eg5 and KIF15, individually or combined, are not required for the sliding of bridging MTs in early anaphase.

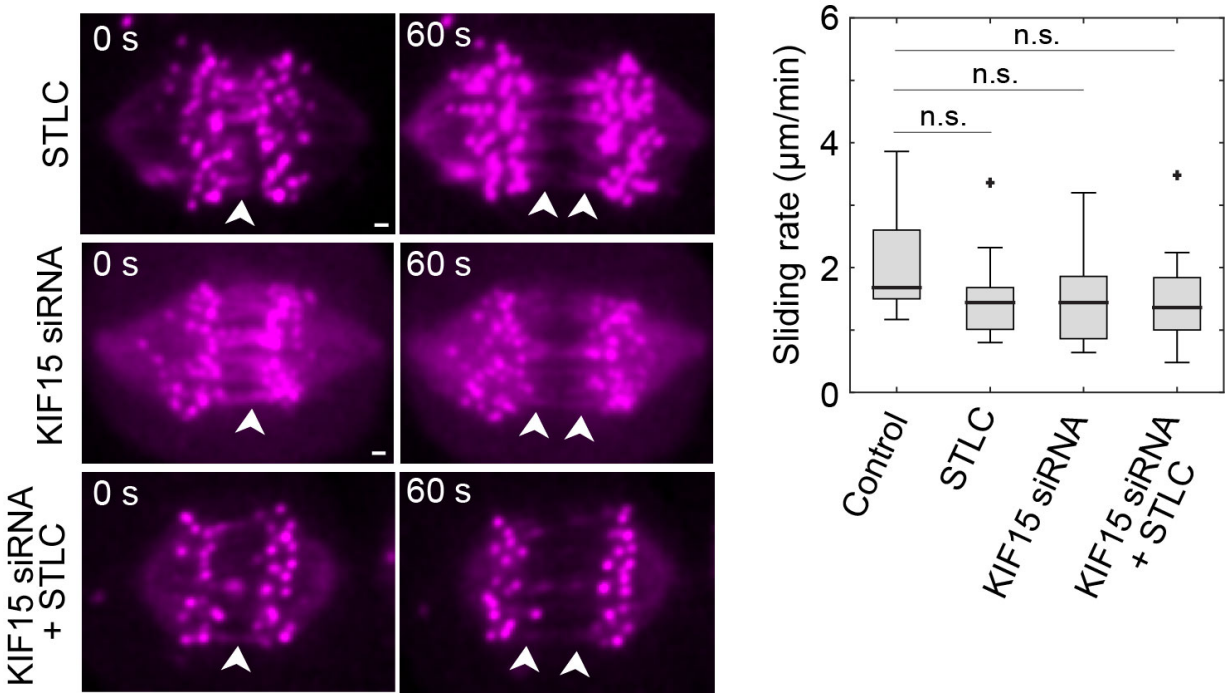

Figure 60 Depletion of Eg5 and KIF15 does not affect sliding velocity. Smoothed time-lapse images (left panel) of the anaphase spindle after photoactivation of PA-GFP-tubulin at time of photoactivation (0s) and after photoactivation (60s) in the bridging fibers in STLC treated spindles (top row), KIF15 depleted spindles (middle row), Kif15 depleted and STLC treated spindles (bottom row). White arrowheads mark the photoactivated spot, which splits into two spots. Box plot (right panel) of sliding rates for control spindles and for the conditions from. n.s. non-significant.

4.8 Kinetochore segregation and pole separation is slower after depletion of MKLP1 and faster after depletion of KIF4a

MKLP1/KIF23 (kinesin-6) slides antiparallel MTs *in vitro* (Nislow et al., 1992) and is a part of the centralspindlin complex which helps bundle midzone MTs for cytokinesis in human cells (Hu et al., 2011). In *Schizosaccharomyces pombe*, the kinesin-6 Klp9p drives anaphase B spindle elongation (Fu et al., 2009). Interestingly, it was observed that depletion of MKLP1 by siRNA resulted in a 27% decrease in kinetochore separation velocity and a

38% decrease in pole separation velocity (vs=1.78±0.15 µm/min, vp=0.90±0.12 µm/min) in comparison with cells treated with control siRNA (vs=2.44±0.09 µm/min, vp=1.45±0.12 µm/min) measured during first 2 minutes of anaphase (see Methods, $p1=8.8x10^{-4}$, $p2=4.7x10^{-3}$, **Figure** 61a and b, **Table** 1).

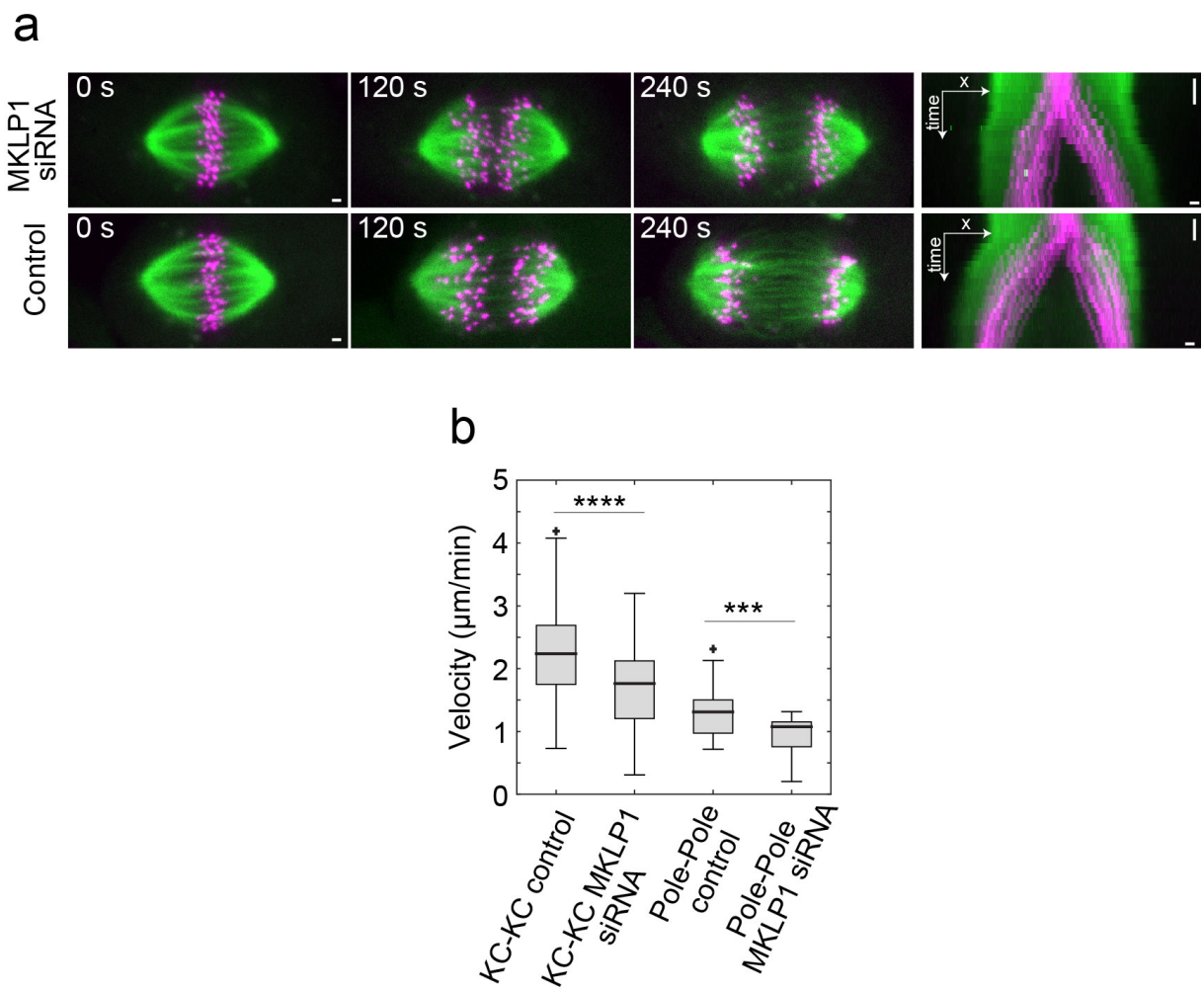

Figure 61 Slower kinetochore and spindle pole separation velocities after MKLP1 depletion. (a) Time-lapse images of the anaphase spindle in a U2OS cell treated with MKLP1 siRNA (top) and non-targeting siRNA (bottom). Kymographs in merged channels are shown at the right. (b) Box plot of kinetochores and poles separation velocities for the conditions from a). ****p<0.0001

The decrease in kinetochore and spindle pole separation velocites during anaphase could be a result of the reduced sliding velocities of the bridging fibers. Once again, we decided to photoactivate the spindle midzone after MKLP1 depletion. Surprisingly, the sliding velocity was not measurable because the photoactivated spots were not detectable after

1 min as they were in controls (n=10 for both conditions, **Figure** 62a and b), suggesting a higher MT turnover. Thus, it was not possible to distinguish the role of MKLP1 in microtubule sliding from its role in stabilization of bridging MTs. These results indicate that MKLP1 contributes to the stabilization of the midzone which consequentially affects kinetochore separation velocity in early anaphase.

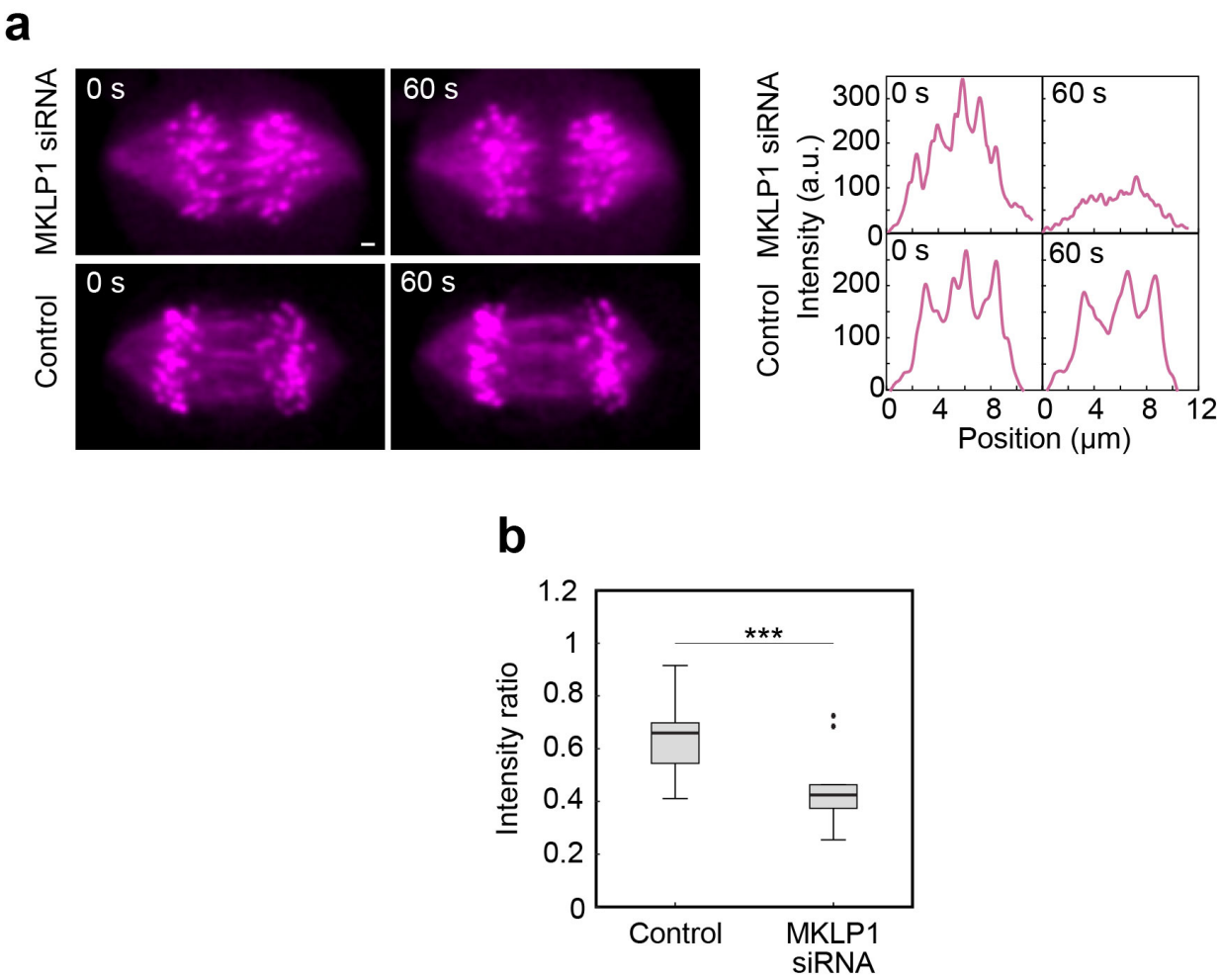

Figure 62 MKLP1 depletion affects the midzone stability. (a) Smoothed time-lapse images (left panel) of the anaphase spindle after photoactivation of PA-GFP-tubulin at time of photoactivation (0s) and after photoactivation (60s) in the bridging fibers in MKLP1 depleted spindles (top row) and control spindles (bottom row). Signal intensity of PA-GFP-tubulin (right panel), measured across the midzone, at time of photoactivation (0s) and after photoactivation (60s) in the bridging fibers in MKLP1 depleted spindles (top row) and control spindles (bottom row). (b) Box plot of signal intensity ratio (signal in the midzone 60s after photoactivation/signal in the midzone at time of photoactivation) for the conditions from a). ***$p<0.001$

The chromokinesin KIF4a (kinesin-4) is important for proper spindle midzone formation, regulates midzone MT dynamics and the length of antiparallel overlaps during anaphase (Zhu and Jiang, 2005). Surprisingly, a 78% increase in kinetochore separation velocity and a 48% increase in pole separation velocity after KIF4a depletion by siRNA was found in comparison with cells treated with control siRNA (**Figure** 63a and b). During first 2 minutes, kinetochores in cells treated with KIF4a siRNA separated at a velocity of 4.34±0.18 µm/min, and the spindle poles at a velocity of 2.15±0.17 µm/min (**Figure** 63b). These values were significantly higher than the respective values in cells treated with control siRNA ($p1=3.2x10^{-14}$, $p2=2.8x10^{-3}$, **Figure** 63b, **Table** 1). Taken together, it was concluded that KIF4a modulates the process of anaphase by limiting kinetochore and spindle pole separation velocities, possibly by controlling the length of the antiparallel bridging MT overlaps and their dynamics.

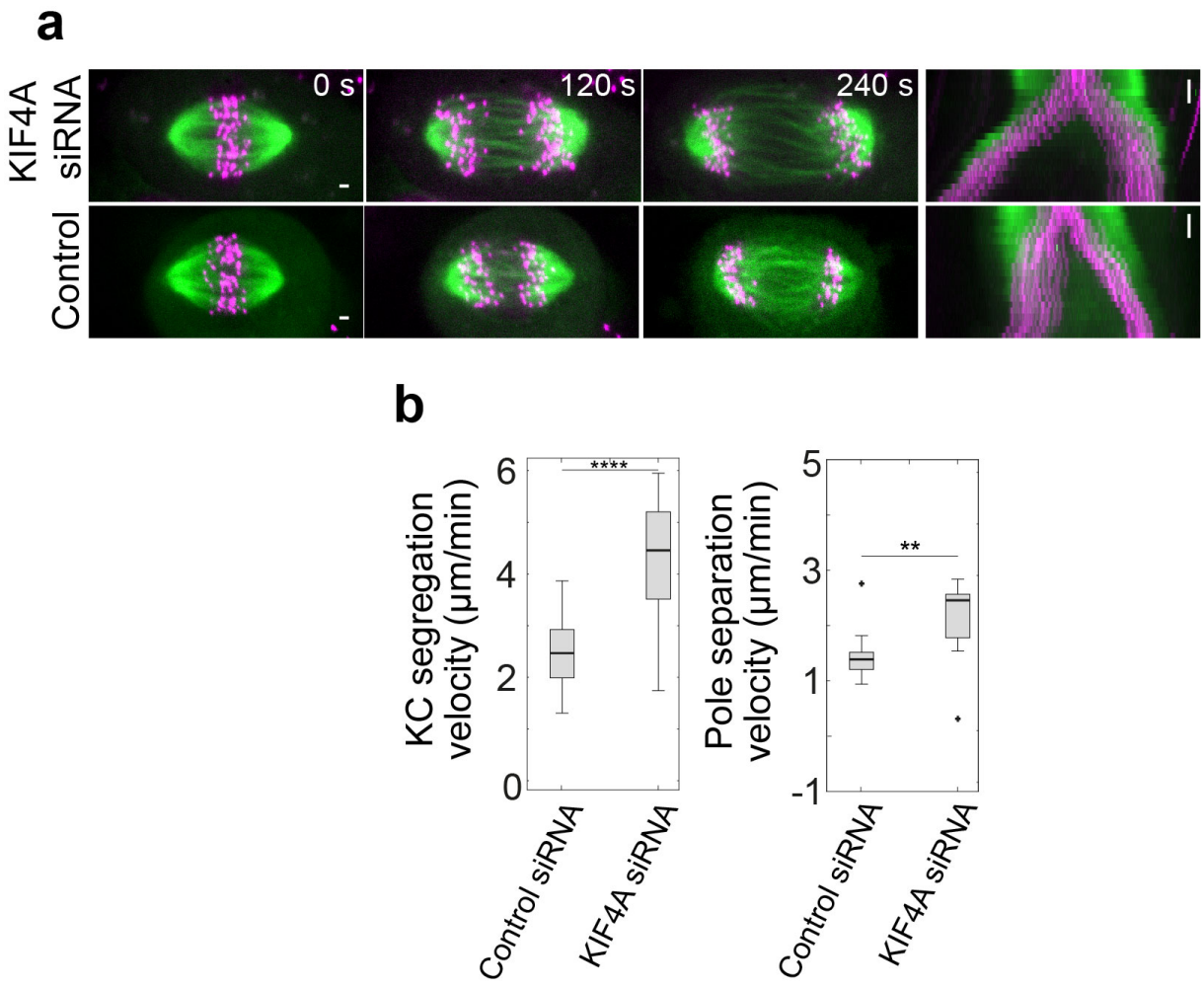

Figure 63 KIF4a depletion increases kinetochore and spindle pole separation velocities. (a) Time-lapse images of the anaphase spindle in a U2OS cell treated with KIF4a siRNA (top)

and non-targeting siRNA (bottom). Kymographs in merged channels are shown at the right. (b) Box plot of kinetochores and poles separation velocities for the conditions from a). **p<0.01, ****p<0.0001

Table 1. List of velocities obtained from experimental measurements

	Parameter	Mean ± s.e.m [μmmin^{-1}] (number of cells, number of kinetochore pairs)		p-value
Experiment		Displaced	Control	
[c]Cut 2.5 μm (Figures 39, 42 and 52)	Kinetochore - Kinetochore	1.53 ± 0.12 (39 ,41)	1.77 ± 0.08 (39, 137)	0.51
	Kinetochore - Midpoint	0.76 ± 0.09 (24, n.a.)[a]	n.a.	0.33
		0.65 ± 0.08 (24, n.a.)[b]		
	Intact pole - Kinetochore	0.57 ± 0.09 (24, n.a.)[a]	0.47 ± 0.05 (24, n.a.)	0.34
	Intact pole - Stub tip	0.80 ± 0.12 (24, n.a.)	n.a.	n.a.
	Kinetochore - Stub tip	0.24 ± 0.12 (14, n.a.)[b]	n.a.	n.a.
	Sliding in the bridging fiber	2.13 ± 0.33 (5, n.a.)	2.08 ± 0.18 (25, n.a.)	0.77
[c]Cut 2.5 μm + Bridge cut (Figure 45)	Kinetochore - Kinetochore	0.49 ± 0.01 (14, 14)	1.54 ± 0.02 (14, 55)	3.2x10^{-4}
[c]Cut 1μm (Figure 48)	Kinetochore - Kinetochore	0.28 ± 0.01 (10, 10)	1.51 ± 0.02 (10, 30)	3.6x10^{-5}
[d]Midzone cut (Figure 49)		Midzone cut	Control	
	Kinetochore - Kinetochore	1.30 ± 0.16 (11,11)	2.30 ± 0.13 (24, 24)	6.6x10^{-3}
	Pole - Pole	0.52 ± 0.10 (11, n.a.)	1.19 ± 0.07 (24, n.a.)	4.3x10^{-5}
	Pole - Kinetochore	0.57 ± 0.08 (11, n.a.)	0.50 ± 0.05 (24, n.a.)	0.57
[d]Astral cut (Figure 49)		Astral cut	Control	
	Kinetochore - Kinetochore	2.40 ± 0.13 (10,29)	2.30 ± 0.13 (24, 24)	0.21
	Pole - Pole	1.36 ± 0.10 (10, n.a.)	1.19 ± 0.07 (24, n.a.)	0.57
[c]Intact spindle (Figure 58)		Bridging fiber	k-fiber	
	Sliding	2.08 ± 0.18 (25, n.a.)	1.88 ± 0.19 (25, n.a.)	0.44
	Polward flux	0.42 ± 0.06 (25, n.a.)	0.32 ± 0.05 (25, n.a.)	0.19
	Sliding	STLC	Control	
		1.55 ± 0.47 (11, n.a.)	2.0 ± 0.63 (10, n.a.)	0.21
		KIF15 siRNA		
		1.54 ± 0.43 (11, n.a.)	2.0 ± 0.63 (13, n.a.)	0.21
		STLC+KIF15 siRNA		
		1.53 ± 0.44 (11, n.a.)	2.0 ± 0.63 (10, n.a.)	0.19
		MKLP1 siRNA	Control	
	Kinetochore - Kinetochore	1.63 ± 0.19 (14, 50)	2.25 ± 0.26 (23, 72)	6x10^{-6}
	Pole - Pole	0.91 ± 0.11 (14, n.a.)	1.31 ± 0.15 (23, n.a.)	0.0048

TABLE LEGEND

Superscripts are as follows: [a]attached displaced kinetochore, [b]detached displaced kinetochore, [c]measured in 1 min interval, [d]measured in 3 min interval. n.a., not applicable.

5 DISCUSSION

The forces driving chromosome segregation in human cells remain one of the most challenging questions in the field of mitosis. Even though anaphase duration is short, it is of the absolute importance for the genome fidelity that there are no mistakes (Worrall et al., 2018). The foundation of the understanding of anaphase mechanisms is primarily based on the proper characterization of all structures in the mitotic spindle that are contributing to proper temporal and spatial chromosome distribution during anaphase (Maiato and Lince-Faria, 2010).

In accordance to the previous study in metaphase, our work confirmed that a novel structure, termed bridging fiber (Kajtez et al., 2016), remained preserved during anaphase and is able to segregate chromosomes independently of the connection to the spindle pole possibly by exerting pushing forces on k-fibers to which it is attached. This was a surprising result because, according to the current view, the processes that contribute to kinetochore separation require kinetochores to be linked, directly or indirectly, with the spindle poles in order to generate the forces for chromosome segregation (Vukusic et al., 2019b).

The pioneering ablation experiments in cricket and grasshopper spindles showed that chromosomes continue to move poleward after centrosome removal as long as the k-fiber stub is longer than 1 μm (Nicklas, 1989; Nicklas et al., 1982). However, during these experiments the ablation was performed on all of the k-fibers in order to detach them from the spindle pole. Consequentially, newly formed k-fiber stubs focused into a newly formed pole making the role of kinetochore-pole connection hard to determine. Also, recent study in human cells showed that after laser ablation of a whole region between chromosomes and spindle pole did not stop chromosome poleward movement (Yu et al., 2019b) which is similar to our experiments where single k-fibers were detached from a pole. Furthermore, studies have shown that some k-fibers are ending in the vicinity of the adjacent k-fibers or non-kinetochore MTs rather than at a pole in the human cells. When they generated short k-fibers by laser ablation, chromosomes moved poleward during anaphase through interaction with adjacent spindle MTs (Sikirzhytski et al., 2014) and this fast movement is mediated by dynein-NuMa complexes at minus-ends of these fibers (Elting et al., 2014). On the contrary, in our study the k-fiber stub was oriented away from the spindle pole and the rest of the spindle MTs. The kinetochore attached to the stub moved away from its sister kinetochore and the pole to which it was originally connected, before ablation. Therefore, we concluded that kinetochores segregated without any connection, direct or indirect, to one spindle pole suggesting that the

forces for chromosome segregation are not generated from the forces acting on the spindle poles. In agreement with these results, direct pushing of spindle poles is not likely because there are no interpolar MTs directly contacting spindle poles in human spindles (Yu et al., 2019a). Similar experiments in which centrosomes in *Caenorhabditis elegans* were destroyed by laser ablation showed that chromosomes can segregate without centrosomes, most likely by outward forces generated by midzone MTs that push against chromosomes (Nahaboo et al., 2015). This model differs from ours where the bridging MTs push the k-fibers apart, rather than pushing directly on the chromosomes.

Moreover, transport of chromosomes towards the spindle poles is enabled by shortening of k-fibers through Pac-Man and poleward flux mechanisms. Our work provides the first direct measurements of the contributions of Pac-Man and poleward flux to the poleward kinetochore velocity in human cells, which are 60% and 40%, respectively. These contributions are similar to those in *Drosophila* S2 cells (Matos et al., 2009), but different than in *Xenopus* egg extracts where poleward flux dominates (Desai et al., 1998) and in fission yeast where poleward flux does not occur (Mallavarapu et al., 1999). Besides, the flux velocities measured here are in qualitative agreement with previous results for k-fibers in newt lung cells (Mitchison and Salmon, 1992) and for interpolar MTs in PtK1 cells (Saxton and McIntosh, 1987).

Collectively, our measurements show that anaphase B spindle elongation is driven by MT sliding and anaphase A poleward kinetochore movement and that these processes contribute roughly equally to kinetochore segregation. The experiments in which the midzone and astral MTs were severed showed that interpolar fibers are required for proper spindle pole separation, whereas the contribution of cortical pulling forces is not significant. Comparable results were obtained after laser ablation of a spindle midzone in human cells where abrupt and complete cessation of chromosome segregation was observed (Yu et al., 2019b). Also, this mechanism is similar to pole-pole separation by outward sliding of interpolar MTs in diatoms, fission yeast, grasshopper and *Drosophila* embryos (Brust-Mascher et al., 2009; Khodjakov et al., 2004; Leslie and Pickett-Heaps, 1983; Nicklas, 1989; Tolic-Norrelykke et al., 2004). Furthermore, the results supporting the irrelevance of cortical pulling in spindle elongation include the inhibition of actin/myosin forms since their structure and dynamics are implicated in organization of the cell cortex (Maiato and Lince-Faria, 2010), a place where astral MTs make contact with a stabile structure to exert forces on the spindle (Aist et al., 1991). While spindle positioning, cytokinesis, and cell elongation can be inhibited by addition of actin-drugs, Cytochalasin D (Fernandez et al., 2011) or Lantrunculin A (Charnley et al.,

2013), no effect on spindle pole separation was observed in human cells (Wheatley et al., 1997). On the contrary, in other model organisms such as Ptk2 (Aist et al., 1993), *C. elegans* (Grill et al., 2001) and *Nectria haematococca* (Aist et al., 1991), the same ablation experiments of interpolar MTs accelerated pole separation during anaphase B. This suggests that in latter astral MTs might have a role in spindle elongation through cortical pulling (Scholey et al., 2016), while midzone MTs are dispensable and instead act as a brake in spindle elongation. Our results support a view that the pushing forces from the midzone interpolar fibers, combined with the regulation of MT dynamics at the kinetochore and the pole, define the speed of chromosome and centrosome separation in human cells, as previously discussed (Betterton and McIntosh, 2013).

The motor proteins required for chromosome segregation in human cells are largely unknown (Maiato and Lince-Faria, 2010). Our experiments suggest that MKLP1 contributes to chromosome and pole separation by affecting the stability of midzone MTs which was previously observed in cytokinesis (Glotzer, 2009). We speculate that this protein takes part in bundling and potentially sliding of antiparallel MTs in early anaphase, similarly to its role in Anaphase B in fission yeast (Fu et al., 2009). Our results are in agreement with previous work showing that the centralspindlin complex is contributing to midzone elongation during cytokinesis in human cells (Hu et al., 2011). On the contrary, our most recent work showed that after MKLP1 depletion in RPE1 cells, anaphase rates were not affected due to reduced midzone MTs stability (Vukušić et al., 2019a). This suggests that MKLP1 affects anaphase dynamics through different mechanism. Here, it should be noted that U2OS cell line, used in this study, contains mCherry-α-tubulin tag that is not present in RPE1 cell line used in the recent study and that this tag itself could somehow affect MT stability and the arrangement of MKLP1 motor proteins causing the discrepancy in anaphase rates between RPE1 and U2OS cell line.

Inhibition of Eg5, the motor that drives spindle elongation in yeast (Khmelinskii et al., 2009), *Xenopus* (Shirasu-Hiza et al., 2004), and *Drosophila* (Brust-Mascher et al., 2009), did not affect anaphase in our experiments. This result is consistent with the previous observations that this motor had no effect on midzone elongation in HeLa cells (Hu et al., 2011) and is barely detectable on midzone MTs in early anaphase mammalian cells (Gable et al., 2012), but different from the observed accelerated spindle elongation in STLC treated mammalian LLC-Pk1 cells (Collins et al., 2014). Conversely, acute inhibition of Eg5 with 10 μM FCPT, that induces a rigor like state of the motor to the MT, caused a significant decrease in spindle elongation velocity in human cells (Afonso et al., 2014). This could be due to the

increased friction in the antiparallel region or potentially the overcrowding of rigor state binded motors. Also, it is possible that these motors work in cooperation with some other motor or non-motor element in anaphase, but that awaits further research. Depletion of KIF15 alone or together with inhibition of Eg5 did not affect anaphase movement, although it was previously suggested that both Eg5 and KIF15 slide antiparallel MTs (Tanenbaum et al., 2009; van Heesbeen et al., 2014). Yet, recent work suggests that KIF15 crosslinks mainly parallel MTs (Drechsler and McAinsh, 2016), making it a less likely candidate for antiparallel sliding.

Depletion of the chromokinesin KIF4a revealed an impact on chromosome and pole separation in a way suggesting that KIF4a limits the anaphase rates. Previous works showed that KIF4a depletion causes longer PRC1-labeled antiparallel midzone overlaps (Zhu and Jiang, 2005) and longer midzones between the chromosomes, although the midzone elongated at a similar rate as in untreated cells (Hu et al., 2011). Possible mechanisms by which KIF4a restricts spindle elongation and kinetochore segregation include regulation of MT dynamics (Wandke et al., 2012), interaction with PRC1 (Zhu and Jiang, 2005), and confining of the overlap zone length (Vukusic et al., 2019b). However, recent work on non-tumor RPE1 cell line showed that depletion of KIF4a does not affect affect anaphase rates as in U2OS cell line (Vukušić et al., 2019a). Such difference in KIF4a depletion effect could be a result of a variance in protein level expression between tumor and non-tumor cell lines which could be useful in further studies focused on the weak points of tumor cells.

Along with the motor proteins, our theory relies on a connection between the bridging fiber and k-fibers, which is established by parallel non-motor cross-linkers. It was shown that parallel cross-linkers called "the mesh" connect MTs in a k-fiber (Nixon et al., 2015). However, these proteins could also crosslink k-fiber MTs and bridging MTs in the regions of their parallel overlap. Similarly, the antiparallel cross-linker PRC1 is present in the bridging fibers (Kajtez et al., 2016; Polak et al., 2017). These cross-linkers will be an important subject for future studies.

Our experiments and theory revisit the old ideas that force for anaphase movement is generated by MT sliding and transmitted along the entire k-fiber. Östergren proposed that forces are produced all along the k-fiber rather than only at its ends (Östergren, 1951). In a seminal paper from 1969, McIntosh and co-workers proposed that MT sliding moves the chromosomes during anaphase (McIntosh et al., 1969). Crosslinking between k-fibers and interpolar MTs in anaphase has been discussed in several works (Goode, 1981; Maiato and Lince-Faria, 2010; Margolis et al., 1978; Matos et al., 2009; Mitchison, 2005). Yet, these

ideas have not been directly tested and remained largely unappreciated. Our work revisits the concept of forces resulting from crosslinking k-fiber and non-k-fiber MTs, demonstrating that these forces work together with the forces generated by k-fiber shortening to segregate chromosomes in human cells.

6 CONCLUSION

In this study, by combining live-cell imaging, laser cutting of MT bundles, photoactivatable GFP experiments and inhibition of candidate motor proteins, we found that sliding of the MTs in the bridging fiber pushes sister k-fibers apart, thereby separating sister kinetochores.

The disruption of chromosome connection to one spindle pole by applying laser ablation assay, showed that chromosomes can segregate properly only if bridging MTs remained preserved between their sister kinetochore fibers. Also, photoactivation of the bridging fiber between displaced kinetochores demonstrated that bridging MTs slide apart in order to separate kinetochores. Furthermore, after photoactivation of all bridging MTs in the spindle during anaphase, it was estimated that bridging MTs slide apart in an intact spindle as well. Likewise, the removal of most bridging MTs in the mitotic spindle impaired chromosome segregation and spindle pole separation confirming that bridging MTs are necessary to push spindle poles and sister k-fibers and kinetochores along with the adjacent chromosomes. To directly elucidate between the contribution of bridging and astral MTs, laser ablation was performed on astral MTs, which did not affect anaphase dynamics and confirmed the predominance of bridging MTs outward pushing. Taken together, these results support the idea that the forces for chromosome segregation and spindle pole separation are primarily generated from the spindle midzone neglecting the role of astral MTs in these processes.

Additionally, our measurements and velocity calculations showed that anaphase B spindle elongation, driven by MT sliding, and anaphase A poleward kinetochore movement contribute roughly equally to cumulative kinetochore segregation velocity.

Finally, depletion or inactivation experiments in tumor U2OS cell line suggest that MKLP1/KIF23 (kinesin-6) contributes to chromosome segregation, KIF4a (kinesin-4) restricts it, whereas Eg5/KIF11 (kinesin-5) and KIF15/Hklp2 (kinesin-12) do not have a significant effect.

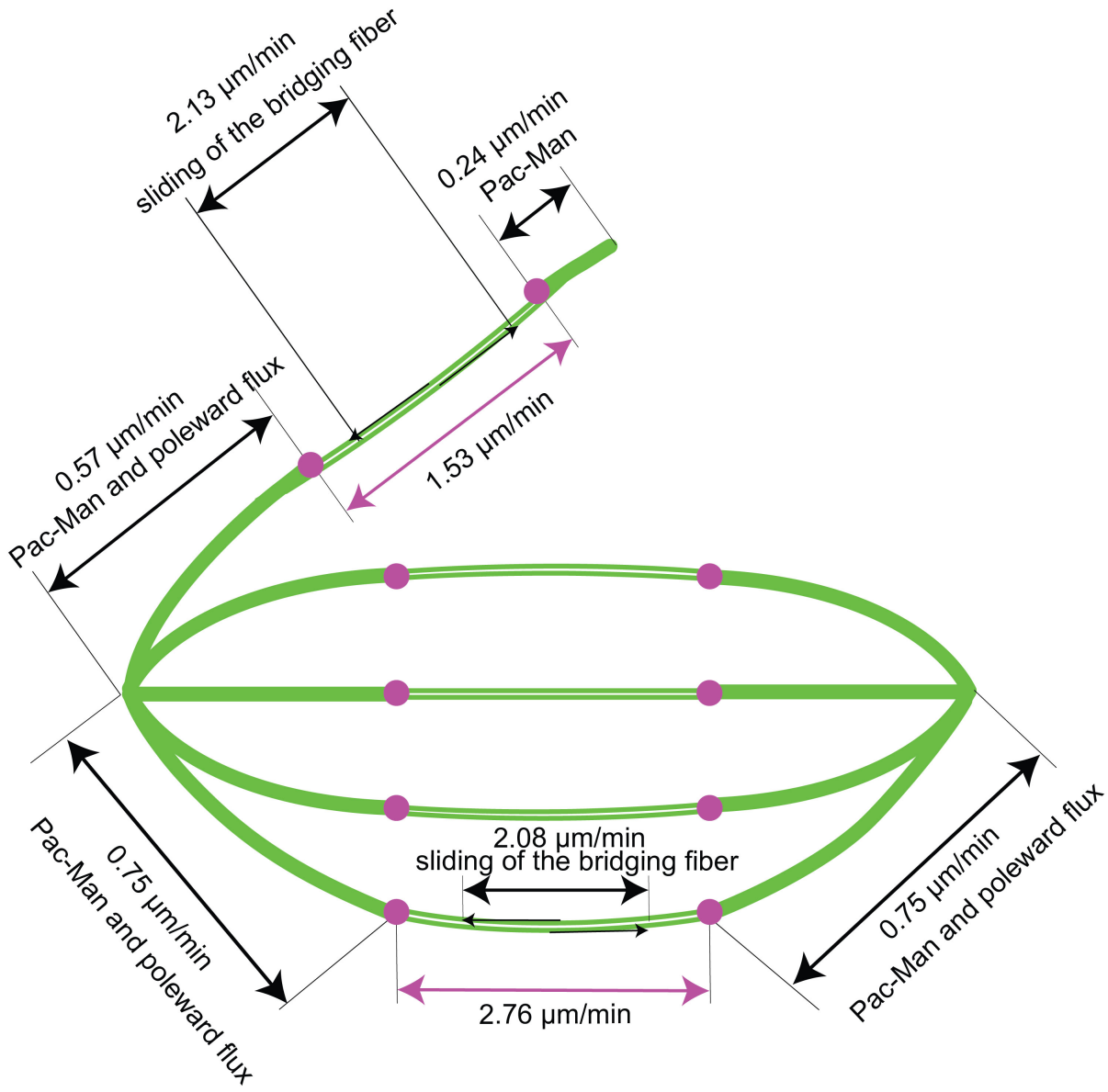

Figure 64 The scheme represents equal contribution of k-fiber depolymerization and sliding to kinetochore separation. Vertical grey lines indicate spindle poles. Round grey circles indicate kinetochores.

7 LITERATURE

Afonso, O., Matos, I., Pereira, A.J., Aguiar, P., Lampson, M.A., and Maiato, H. (2014). Feedback control of chromosome separation by a midzone Aurora B gradient. Science *345*, 332-336.

Aist, J.R., Bayles, C.J., Tao, W., and Berns, M.W. (1991). Direct experimental evidence for the existence, structural basis and function of astral forces during anaphase B in vivo. J Cell Sci *100 (Pt 2)*, 279-288.

Aist, J.R., Liang, H., and Berns, M.W. (1993). Astral and spindle forces in PtK2 cells during anaphase B: a laser microbeam study. J Cell Sci *104 (Pt 4)*, 1207-1216.

Alberts, B., Johnson, A., Lewis, J., Morgan, D., Raff, M., Roberts, K., and Walter, P. (2014). Molecular biology of the cell, 6th edn (Garland Science, New York).

Ananthanarayanan, V., Schattat, M., Vogel, S.K., Krull, A., Pavin, N., and Tolic-Norrelykke, I.M. (2013). Dynein motion switches from diffusive to directed upon cortical anchoring. Cell *153*, 1526-1536.

Antal, T., Krapivsky, P.L., and Redner, S. (2007). Dynamics of Microtubule Instabilities. J Stat Mech, L05004.

Asashima, M., Ikeuchi, M., Ishiura, S., Ide, T., Irimura, T., Ohya, Y., Kamimura, S., Kodama, T., Komazaki, S., Sasagawa, N.*, et al.* (2010). Fundamental Concept of Biology. In A comprehensive approach to Life Science, C.T.U.o. Tokio, ed.

Asbury, C.L. (2017). Anaphase A: Disassembling Microtubules Move Chromosomes toward Spindle Poles. Biology (Basel) *6*.

Bannigan, A., Lizotte-Waniewski, M., Riley, M., and Baskin, T.I. (2008). Emerging molecular mechanisms that power and regulate the anastral mitotic spindle of flowering plants. Cell Motil Cytoskeleton *65*, 1-11.

Barnum, K.J., and O'Connell, M.J. (2014). Cell cycle regulation by checkpoints. Methods Mol Biol *1170*, 29-40.

Belar, K. (1929). Beitrage zur Kausalanalyse der Mitose : II. Untersuchungen an den Spermatocyten von Chorthippus (Stenobothrus) lineatus Panz. Wilhelm Roux Arch Entwickl Mech Org *118*, 359-484.

Betterton, M.D., and McIntosh, J.R. (2013). Regulation of chromosome speeds in mitosis. Cell Mol Bioeng *6*, 418-430.

Blangy, A., Lane, H.A., d'Herin, P., Harper, M., Kress, M., and Nigg, E.A. (1995). Phosphorylation by p34cdc2 regulates spindle association of human Eg5, a kinesin-related motor essential for bipolar spindle formation in vivo. Cell *83*, 1159-1169.

Botvinick, E.L., Venugopalan, V., Shah, J.V., Liaw, L.H., and Berns, M.W. (2004). Controlled ablation of microtubules using a picosecond laser. Biophys J *87*, 4203-4212.

Bringmann, H., and Hyman, A.A. (2005). A cytokinesis furrow is positioned by two consecutive signals. Nature *436*, 731-734.

Britannica, T.E.o.E. (2019). Microtubule (Encyclopædia Britannica, inc.).

Brito, D.A., Strauss, J., Magidson, V., Tikhonenko, I., Khodjakov, A., and Koonce, M.P. (2005). Pushing forces drive the comet-like motility of microtubule arrays in Dictyostelium. Mol Biol Cell *16*, 3334-3340.

Brust-Mascher, I., Sommi, P., Cheerambathur, D.K., and Scholey, J.M. (2009). Kinesin-5-dependent poleward flux and spindle length control in Drosophila embryo mitosis. Mol Biol Cell *20*, 1749-1762.

Buda, R., Vukusic, K., and Tolic, I.M. (2017). Dissection and characterization of microtubule bundles in the mitotic spindle using femtosecond laser ablation. Methods Cell Biol *139*, 81-101.

Cameron, L.A., Yang, G., Cimini, D., Canman, J.C., Kisurina-Evgenieva, O., Khodjakov, A., Danuser, G., and Salmon, E.D. (2006). Kinesin 5-independent poleward flux of kinetochore microtubules in PtK1 cells. J Cell Biol *173*, 173-179.

Cande, W.Z. (1982). Nucleotide requirements for anaphase chromosome movements in permeabilized mitotic cells: anaphase B but not anaphase A requires ATP. Cell *28*, 15-22.

Carlier, M.F., Pantaloni, D., and Korn, E.D. (1987). The mechanisms of ATP hydrolysis accompanying the polymerization of Mg-actin and Ca-actin. J Biol Chem *262*, 3052-3059.

Cassimeris, L.U., Walker, R.A., Pryer, N.K., and Salmon, E.D. (1987). Dynamic instability of microtubules. Bioessays *7*, 149-154.

Charnley, M., Anderegg, F., Holtackers, R., Textor, M., and Meraldi, P. (2013). Effect of Cell Shape and Dimensionality on Spindle Orientation and Mitotic Timing. PLoS One *8*, e66918.

Cojoc, G., Roscioli, E., Zhang, L., Garcia-Ulloa, A., Shah, J.V., Berns, M.W., Pavin, N., Cimini, D., Tolic, I.M., and Gregan, J. (2016). Laser microsurgery reveals conserved viscoelastic behavior of the kinetochore. J Cell Biol *212*, 767-776.

Collins, E., Mann, B.J., and Wadsworth, P. (2014). Eg5 restricts anaphase B spindle elongation in mammalian cells. Cytoskeleton (Hoboken) *71*, 136-144.

Colombelli, J., Reynaud, E.G., Rietdorf, J., Pepperkok, R., and Stelzer, E.H. (2005a). In vivo selective cytoskeleton dynamics quantification in interphase cells induced by pulsed ultraviolet laser nanosurgery. Traffic *6*, 1093-1102.
Colombelli, J., Reynaud, E.G., and Stelzer, E.H. (2005b). Subcellular nanosurgery with a pulsed subnanosecond UV-A laser. Med Laser Appl *20*, 217-222.
Cooper, G.M. (2000). Structure and Organization of Actin Filaments. In The Cell: A Molecular Approach, S. Associates, ed. (Sunderland (MA)).
Cooper, G.M., and Hausman, R.E. (2003). The cell: a molecular approach. (Sunderland: Sinauer Associates).
des Georges, A. (2008). Regulation of Tubulin dynamics by the +Tip tracking protein Mal3. In MRC Laboratory of Molecular Biology
Hughes Hall (University of Cambridge).
Desai, A., Maddox, P.S., Mitchison, T.J., and Salmon, E.D. (1998). Anaphase A chromosome movement and poleward spindle microtubule flux occur At similar rates in Xenopus extract spindles. J Cell Biol *141*, 703-713.
Dominguez, R., and Holmes, K.C. (2011). Actin structure and function. Annu Rev Biophys *40*, 169-186.
Drechsler, H., and McAinsh, A.D. (2016). Kinesin-12 motors cooperate to suppress microtubule catastrophes and drive the formation of parallel microtubule bundles. Proc Natl Acad Sci U S A *113*, E1635-1644.
Dumont, J., Oegema, K., and Desai, A. (2010). A kinetochore-independent mechanism drives anaphase chromosome separation during acentrosomal meiosis. Nat Cell Biol *12*, 894-901.
Elting, M.W., Hueschen, C.L., Udy, D.B., and Dumont, S. (2014). Force on spindle microtubule minus ends moves chromosomes. J Cell Biol *206*, 245-256.
Erickson, H.P., and O'Brien, E.T. (1992). Microtubule dynamic instability and GTP hydrolysis. Annu Rev Biophys Biomol Struct *21*, 145-166.
Feher, J. (2012). Cell Structure. In Quantitative Human Physiology, J. Feher, ed. (Academic Press), pp. 75-90.
Ferenz, N.P., Gable, A., and Wadsworth, P. (2010). Mitotic functions of kinesin-5. Semin Cell Dev Biol *21*, 255-259.
Fernandez, P., Maier, M., Lindauer, M., Kuffer, C., Storchova, Z., and Bausch, A.R. (2011). Mitotic spindle orients perpendicular to the forces imposed by dynamic shear. PLoS One *6*, e28965.

Fontijn, R.D., Goud, B., Echard, A., Jollivet, F., van Marle, J., Pannekoek, H., and Horrevoets, A.J. (2001). The human kinesin-like protein RB6K is under tight cell cycle control and is essential for cytokinesis. Mol Cell Biol *21*, 2944-2955.

Fu, C., Ward, J.J., Loiodice, I., Velve-Casquillas, G., Nedelec, F.J., and Tran, P.T. (2009). Phospho-regulated interaction between kinesin-6 Klp9p and microtubule bundler Ase1p promotes spindle elongation. Dev Cell *17*, 257-267.

Fuchs, E., and Coulombe, P.A. (1992). Of mice and men: genetic skin diseases of keratin. Cell *69*, 899-902.

Gable, A., Qiu, M., Titus, J., Balchand, S., Ferenz, N.P., Ma, N., Collins, E.S., Fagerstrom, C., Ross, J.L., Yang, G.*, et al.* (2012). Dynamic reorganization of Eg5 in the mammalian spindle throughout mitosis requires dynein and TPX2. Mol Biol Cell *23*, 1254-1266.

Galderisi, U., Jori, F.P., and Giordano, A. (2003). Cell cycle regulation and neural differentiation. Oncogene *22*, 5208-5219.

Ganem, N.J., Upton, K., and Compton, D.A. (2005). Efficient mitosis in human cells lacking poleward microtubule flux. Curr Biol *15*, 1827-1832.

Glotzer, M. (2004). Cleavage furrow positioning. J Cell Biol *164*, 347-351.

Glotzer, M. (2009). The 3Ms of central spindle assembly: microtubules, motors and MAPs. Nat Rev Mol Cell Biol *10*, 9-20.

Goode, D. (1981). Microtubule turnover as a mechanism of mitosis and its possible evolution. Biosystems *14*, 271-287.

Goodman, S.R. (2008). The Cell Cycle and Cancer. In Medical Cell Biology S.R. Goodman, ed. (Academic Press), pp. 273-289.

Gorbsky, G.J., Sammak, P.J., and Borisy, G.G. (1987). Chromosomes move poleward in anaphase along stationary microtubules that coordinately disassemble from their kinetochore ends. J Cell Biol *104*, 9-18.

Goudarzi, M., Banisch, T.U., Mobin, M.B., Maghelli, N., Tarbashevich, K., Strate, I., van den Berg, J., Blaser, H., Bandemer, S., Paluch, E.*, et al.* (2012). Identification and regulation of a molecular module for bleb-based cell motility. Dev Cell *23*, 210-218.

Grill, S.W., Gonczy, P., Stelzer, E.H., and Hyman, A.A. (2001). Polarity controls forces governing asymmetric spindle positioning in the Caenorhabditis elegans embryo. Nature *409*, 630-633.

Grill, S.W., Howard, J., Schaffer, E., Stelzer, E.H., and Hyman, A.A. (2003). The distribution of active force generators controls mitotic spindle position. Science *301*, 518-521.

Grill, S.W., and Hyman, A.A. (2005). Spindle positioning by cortical pulling forces. Dev Cell *8*, 461-465.
Grishchuk, E.L., Molodtsov, M.I., Ataullakhanov, F.I., and McIntosh, J.R. (2005). Force production by disassembling microtubules. Nature *438*, 384-388.
Guarino, E., Cojoc, G., Garcia-Ulloa, A., Tolic, I.M., and Kearsey, S.E. (2014). Real-time imaging of DNA damage in yeast cells using ultra-short near-infrared pulsed laser irradiation. PLoS One *9*, e113325.
Hauf, S., Waizenegger, I.C., and Peters, J.M. (2001). Cohesin cleavage by separase required for anaphase and cytokinesis in human cells. Science *293*, 1320-1323.
Hickson, G.R., Echard, A., and O'Farrell, P.H. (2006). Rho-kinase controls cell shape changes during cytokinesis. Curr Biol *16*, 359-370.
Hiramoto, Y., and Nakano, Y. (1988). Micromanipulation studies of the mitotic apparatus in sand dollar eggs. Cell Motil Cytoskeleton *10*, 172-184.
Hohmann, T., and Dehghani, F. (2019). The Cytoskeleton-A Complex Interacting Meshwork. Cells *8*.
Howard, J., and Hyman, A.A. (2007). Microtubule polymerases and depolymerases. Curr Opin Cell Biol *19*, 31-35.
Howard, J., and Hyman, A.A. (2009). Growth, fluctuation and switching at microtubule plus ends. Nat Rev Mol Cell Biol *10*, 569-574.
Hu, C.K., Coughlin, M., Field, C.M., and Mitchison, T.J. (2011). KIF4 regulates midzone length during cytokinesis. Curr Biol *21*, 815-824.
Inoue, S., and Ritter, H., Jr. (1975). Dynamics of mitotic spindle organization and function. Soc Gen Physiol Ser *30*, 3-30.
Jiang, W., Jimenez, G., Wells, N.J., Hope, T.J., Wahl, G.M., Hunter, T., and Fukunaga, R. (1998). PRC1: a human mitotic spindle-associated CDK substrate protein required for cytokinesis. Mol Cell *2*, 877-885.
Kajtez, J., Solomatina, A., Novak, M., Polak, B., Vukusic, K., Rudiger, J., Cojoc, G., Milas, A., Sumanovac Sestak, I., Risteski, P.*, et al.* (2016). Overlap microtubules link sister k-fibres and balance the forces on bi-oriented kinetochores. Nat Commun *7*, 10298.
Kapitein, L.C., Peterman, E.J., Kwok, B.H., Kim, J.H., Kapoor, T.M., and Schmidt, C.F. (2005). The bipolar mitotic kinesin Eg5 moves on both microtubules that it crosslinks. Nature *435*, 114-118.

Khmelinskii, A., Roostalu, J., Roque, H., Antony, C., and Schiebel, E. (2009). Phosphorylation-dependent protein interactions at the spindle midzone mediate cell cycle regulation of spindle elongation. Dev Cell *17*, 244-256.
Khodjakov, A., La Terra, S., and Chang, F. (2004). Laser microsurgery in fission yeast; role of the mitotic spindle midzone in anaphase B. Curr Biol *14*, 1330-1340.
Kiyomitsu, T., and Cheeseman, I.M. (2012). Chromosome- and spindle-pole-derived signals generate an intrinsic code for spindle position and orientation. Nat Cell Biol *14*, 311-317.
Kiyomitsu, T., and Cheeseman, I.M. (2013). Cortical dynein and asymmetric membrane elongation coordinately position the spindle in anaphase. Cell *154*, 391-402.
Klingner, C., Cherian, A.V., Fels, J., Diesinger, P.M., Aufschnaiter, R., Maghelli, N., Keil, T., Beck, G., Tolic-Norrelykke, I.M., Bathe, M.*, et al.* (2014). Isotropic actomyosin dynamics promote organization of the apical cell cortex in epithelial cells. J Cell Biol *207*, 107-121.
Koshland, D.E., Mitchison, T.J., and Kirschner, M.W. (1988). Polewards chromosome movement driven by microtubule depolymerization in vitro. Nature *331*, 499-504.
Kozlowski, C., Srayko, M., and Nedelec, F. (2007). Cortical microtubule contacts position the spindle in C. elegans embryos. Cell *129*, 499-510.
Kruger, L.K., Sanchez, J.L., Paoletti, A., and Tran, P.T. (2019). Kinesin-6 regulates cell-size-dependent spindle elongation velocity to keep mitosis duration constant in fission yeast. Elife *8*.
Krull, A., Steinborn, A., Ananthanarayanan, V., Ramunno-Johnson, D., Petersohn, U., and Tolic-Norrelykke, I.M. (2014). A divide and conquer strategy for the maximum likelihood localization of low intensity objects. Opt Express *22*, 210-228.
La Terra, S., English, C.N., Hergert, P., McEwen, B.F., Sluder, G., and Khodjakov, A. (2005). The de novo centriole assembly pathway in HeLa cells: cell cycle progression and centriole assembly/maturation. J Cell Biol *168*, 713-722.
Lauvrak, S.U., Munthe, E., Kresse, S.H., Stratford, E.W., Namlos, H.M., Meza-Zepeda, L.A., and Myklebost, O. (2013). Functional characterisation of osteosarcoma cell lines and identification of mRNAs and miRNAs associated with aggressive cancer phenotypes. Br J Cancer *109*, 2228-2236.
Lee, G.M. (1989). Characterization of mitotic motors by their relative sensitivity to AMP-PNP. J Cell Sci *94 (Pt 3)*, 425-441.
Lee, Y.M., and Kim, W. (2004). Kinesin superfamily protein member 4 (KIF4) is localized to midzone and midbody in dividing cells. Exp Mol Med *36*, 93-97.

Leslie, R.J., and Pickett-Heaps, J.D. (1983). Ultraviolet microbeam irradiations of mitotic diatoms: investigation of spindle elongation. J Cell Biol *96*, 548-561.
Lodish, H., Berk, A., Zipursky, S.L., Matsudaira, P., Baltimore, D., and Darnell, J. (2000). Molecular Cell Biology, 4 edn (New York).
Longhese, M.P., Clerici, M., and Lucchini, G. (2003). The S-phase checkpoint and its regulation in Saccharomyces cerevisiae. Mutat Res *532*, 41-58.
Lowery, J., Kuczmarski, E.R., Herrmann, H., and Goldman, R.D. (2015). Intermediate Filaments Play a Pivotal Role in Regulating Cell Architecture and Function. J Biol Chem *290*, 17145-17153.
Luders, J., and Stearns, T. (2007). Microtubule-organizing centres: a re-evaluation. Nat Rev Mol Cell Biol *8*, 161-167.
Maghelli, N., and Tolic-Norrelykke, I.M. (2010). Optical trapping and laser ablation of microtubules in fission yeast. Methods Cell Biol *97*, 173-183.
Maghelli, N., and Tolic-Norrelykke, I.M. (2011). Laser ablation of the microtubule cytoskeleton: setting up and working with an ablation system. Methods Mol Biol *777*, 261-271.
Magidson, V., Loncarek, J., Hergert, P., Rieder, C.L., and Khodjakov, A. (2007). Laser microsurgery in the GFP era: a cell biologist's perspective. Methods Cell Biol *82*, 239-266.
Maiato, H., Khodjakov, A., and Rieder, C.L. (2005). Drosophila CLASP is required for the incorporation of microtubule subunits into fluxing kinetochore fibres. Nat Cell Biol *7*, 42-47.
Maiato, H., and Lince-Faria, M. (2010). The perpetual movements of anaphase. Cell Mol Life Sci *67*, 2251-2269.
Maiato, H., Rieder, C.L., and Khodjakov, A. (2004). Kinetochore-driven formation of kinetochore fibers contributes to spindle assembly during animal mitosis. J Cell Biol *167*, 831-840.
Mallavarapu, A., Sawin, K., and Mitchison, T. (1999). A switch in microtubule dynamics at the onset of anaphase B in the mitotic spindle of Schizosaccharomyces pombe. Curr Biol *9*, 1423-1426.
Malumbres, M. (2020). Control of the Cell Cycle. In Abeloff's Clinical Oncology N. J.E., A. J.O., K. M.B., D. J.H., and T. J.E., eds., pp. 56-73.e55.
Margolis, R.L., Wilson, L., and Keifer, B.I. (1978). Mitotic mechanism based on intrinsic microtubule behaviour. Nature *272*, 450-452.
Mastronarde, D.N., McDonald, K.L., Ding, R., and McIntosh, J.R. (1993). Interpolar spindle microtubules in PTK cells. J Cell Biol *123*, 1475-1489.

Matos, I., Pereira, A.J., Lince-Faria, M., Cameron, L.A., Salmon, E.D., and Maiato, H. (2009). Synchronizing chromosome segregation by flux-dependent force equalization at kinetochores. J Cell Biol *186*, 11-26.
McDonald, K.L., O'Toole, E.T., Mastronarde, D.N., and McIntosh, J.R. (1992). Kinetochore microtubules in PTK cells. J Cell Biol *118*, 369-383.
McIntosh, J.R. (2016). Mitosis. Cold Spring Harb Perspect Biol *8*.
McIntosh, J.R., Hepler, P.K., and Van Wie, D.G. (1969). Model for mitosis. Nature *224*, 659-663.
McIntosh, J.R., and Landis, S.C. (1971). The distribution of spindle microtubules during mitosis in cultured human cells. J Cell Biol *49*, 468-497.
McIntosh, J.R., Molodtsov, M.I., and Ataullakhanov, F.I. (2012). Biophysics of mitosis. Q Rev Biophys *45*, 147-207.
Nikon Microscopy (2020). Human Bone Osteosarcoma Epithelial Cells (U2OS Line).
Milas, A., and Tolic, I.M. (2016). Relaxation of interkinetochore tension after severing of a k-fiber depends on the length of the k-fiber stub. Matters (Zur), doi:10.19185/matters.201603000025
Milas, A., and Tolić, I.M. (2016). Relaxation of interkinetochore tension after severing of a k-fiber depends on the length of the k-fiber stub. Matters Select.
Mishima, M., Pavicic, V., Gruneberg, U., Nigg, E.A., and Glotzer, M. (2004). Cell cycle regulation of central spindle assembly. Nature *430*, 908-913.
Mitchison, T., Evans, L., Schulze, E., and Kirschner, M. (1986). Sites of microtubule assembly and disassembly in the mitotic spindle. Cell *45*, 515-527.
Mitchison, T.J. (1989). Polewards microtubule flux in the mitotic spindle: evidence from photoactivation of fluorescence. J Cell Biol *109*, 637-652.
Mitchison, T.J. (2005). Mechanism and function of poleward flux in Xenopus extract meiotic spindles. Philos Trans R Soc Lond B Biol Sci *360*, 623-629.
Mitchison, T.J., and Salmon, E.D. (1992). Poleward kinetochore fiber movement occurs during both metaphase and anaphase-A in newt lung cell mitosis. J Cell Biol *119*, 569-582.
Moll, R., Divo, M., and Langbein, L. (2008). The human keratins: biology and pathology. Histochem Cell Biol *129*, 705-733.
Mollinari, C., Kleman, J.-P., Jiang, W., Schoehn, G., Hunter, T., and Margolis, R.L. (2002a). PRC1 is a microtubule binding and bundling protein essential to maintain the mitotic spindle midzone. The Journal of Cell Biology *157*, 1175-1186.

Mollinari, C., Kleman, J.P., Jiang, W., Schoehn, G., Hunter, T., and Margolis, R.L. (2002b). PRC1 is a microtubule binding and bundling protein essential to maintain the mitotic spindle midzone. J Cell Biol *157*, 1175-1186.

Mollinari, C., Kleman, J.P., Saoudi, Y., Jablonski, S.A., Perard, J., Yen, T.J., and Margolis, R.L. (2005). Ablation of PRC1 by small interfering RNA demonstrates that cytokinetic abscission requires a central spindle bundle in mammalian cells, whereas completion of furrowing does not. Mol Biol Cell *16*, 1043-1055.

Musacchio, A., and Desai, A. (2017). A Molecular View of Kinetochore Assembly and Function. Biology (Basel) *6*.

Musacchio, A., and Salmon, E.D. (2007). The spindle-assembly checkpoint in space and time. Nat Rev Mol Cell Biol *8*, 379-393.

Nahaboo, W., Zouak, M., Askjaer, P., and Delattre, M. (2015). Chromatids segregate without centrosomes during Caenorhabditis elegans mitosis in a Ran- and CLASP-dependent manner. Mol Biol Cell *26*, 2020-2029.

Nezi, L., and Musacchio, A. (2009). Sister chromatid tension and the spindle assembly checkpoint. Curr Opin Cell Biol *21*, 785-795.

Nicklas, R.B. (1989). The motor for poleward chromosome movement in anaphase is in or near the kinetochore. J Cell Biol *109*, 2245-2255.

Nicklas, R.B., Kubai, D.F., and Hays, T.S. (1982). Spindle microtubules and their mechanical associations after micromanipulation in anaphase. J Cell Biol *95*, 91-104.

Niforou, K.M., Anagnostopoulos, A.K., Vougas, K., Kittas, C., Gorgoulis, V.G., and Tsangaris, G.T. (2008). The proteome profile of the human osteosarcoma U2OS cell line. Cancer Genomics Proteomics *5*, 63-78.

Nislow, C., Lombillo, V.A., Kuriyama, R., and McIntosh, J.R. (1992). A plus-end-directed motor enzyme that moves antiparallel microtubules in vitro localizes to the interzone of mitotic spindles. Nature *359*, 543-547.

Nixon, F.M., Gutierrez-Caballero, C., Hood, F.E., Booth, D.G., Prior, I.A., and Royle, S.J. (2015). The mesh is a network of microtubule connectors that stabilizes individual kinetochore fibers of the mitotic spindle. Elife *4*.

Nixon, F.M., Honnor, T.R., Clarke, N.I., Starling, G.P., Beckett, A.J., Johansen, A.M., Brettschneider, J.A., Prior, I.A., and Royle, S.J. (2017). Microtubule organization within mitotic spindles revealed by serial block face scanning electron microscopy and image analysis. J Cell Sci *130*, 1845-1855.

Ohi, R., Coughlin, M.L., Lane, W.S., and Mitchison, T.J. (2003). An inner centromere protein that stimulates the microtubule depolymerizing activity of a KinI kinesin. Dev Cell *5*, 309-321.
Östergren, G. (1951). The mechanism of co-orientation in bivalents and multivalents. Hereditas *37*, 85-156.
Pavin, N., and Tolic, I.M. (2016). Self-Organization and Forces in the Mitotic Spindle. Annu Rev Biophys *45*, 279-298.
Pavin, N., and Tolic-Norrelykke, I.M. (2013). Dynein, microtubule and cargo: a menage a trois. Biochem Soc Trans *41*, 1731-1735.
Polak, B., Risteski, P., Lesjak, S., and Tolic, I.M. (2017). PRC1-labeled microtubule bundles and kinetochore pairs show one-to-one association in metaphase. EMBO Rep *18*, 217-230.
Pollard, T.D., Earnshaw, W.C., Lippincott-Schwartz, J., and Johnson, G.T. (2017). Intermediate Filaments. In Cell Biology T.D. Pollard, W.C. Earnshaw, J. Lippincott-Schwartz, and G.T. Johnson, eds. (Elsevier), pp. 613-622.
PosthumaDeBoer, J., Witlox, M.A., Kaspers, G.J., and van Royen, B.J. (2011). Molecular alterations as target for therapy in metastatic osteosarcoma: a review of literature. Clin Exp Metastasis *28*, 493-503.
Raabe, I., Vogel, S.K., Peychl, J., and Tolic-Norrelykke, I.M. (2009). Intracellular nanosurgery and cell enucleation using a picosecond laser. J Microsc *234*, 1-8.
Reinhardt, D., Frenz, M., Mandel, T., and Kuhlemeier, C. (2005). Microsurgical and laser ablation analysis of leaf positioning and dorsoventral patterning in tomato. Development *132*, 15-26.
Rieder, C.L., Cole, R.W., Khodjakov, A., and Sluder, G. (1995). The checkpoint delaying anaphase in response to chromosome monoorientation is mediated by an inhibitory signal produced by unattached kinetochores. J Cell Biol *130*, 941-948.
Rumpf, C., Cipak, L., Schleiffer, A., Pidoux, A., Mechtler, K., Tolic-Norrelykke, I.M., and Gregan, J. (2010). Laser microsurgery provides evidence for merotelic kinetochore attachments in fission yeast cells lacking Pcs1 or Clr4. Cell Cycle *9*, 3997-4004.
Sacristan, C., and Kops, G.J. (2015). Joined at the hip: kinetochores, microtubules, and spindle assembly checkpoint signaling. Trends Cell Biol *25*, 21-28.
Saunders, A.M., Powers, J., Strome, S., and Saxton, W.M. (2007). Kinesin-5 acts as a brake in anaphase spindle elongation. Curr Biol *17*, R453-454.
Sawin, K.E., LeGuellec, K., Philippe, M., and Mitchison, T.J. (1992). Mitotic spindle organization by a plus-end-directed microtubule motor. Nature *359*, 540-543.

Saxton, W.M., and McIntosh, J.R. (1987). Interzone microtubule behavior in late anaphase and telophase spindles. J Cell Biol *105*, 875-886.
Scholey, J.M., Civelekoglu-Scholey, G., and Brust-Mascher, I. (2016). Anaphase B. Biology (Basel) *5*.
Sharp, D.J., McDonald, K.L., Brown, H.M., Matthies, H.J., Walczak, C., Vale, R.D., Mitchison, T.J., and Scholey, J.M. (1999). The bipolar kinesin, KLP61F, cross-links microtubules within interpolar microtubule bundles of Drosophila embryonic mitotic spindles. J Cell Biol *144*, 125-138.
Shen, N., Datta, D., Schaffer, C.B., LeDuc, P., Ingber, D.E., and Mazur, E. (2005). Ablation of cytoskeletal filaments and mitochondria in live cells using a femtosecond laser nanoscissor. Mech Chem Biosyst *2*, 17-25.
Shirasu-Hiza, M., Perlman, Z.E., Wittmann, T., Karsenti, E., and Mitchison, T.J. (2004). Eg5 causes elongation of meiotic spindles when flux-associated microtubule depolymerization is blocked. Curr Biol *14*, 1941-1945.
Sikirzhytski, V., Magidson, V., Steinman, J.B., He, J., Le Berre, M., Tikhonenko, I., Ault, J.G., McEwen, B.F., Chen, J.K., Sui, H.*, et al.* (2014). Direct kinetochore-spindle pole connections are not required for chromosome segregation. J Cell Biol *206*, 231-243.
Simunic, J., and Tolic, I.M. (2016). Mitotic Spindle Assembly: Building the Bridge between Sister K-Fibers. Trends Biochem Sci *41*, 824-833.
Stark, G.R., and Taylor, W.R. (2004). Analyzing the G2/M checkpoint. Methods Mol Biol *280*, 51-82.
Steinmeyer, J.D., Gilleland, C.L., Pardo-Martin, C., Angel, M., Rohde, C.B., Scott, M.A., and Yanik, M.F. (2010). Construction of a femtosecond laser microsurgery system. Nat Protoc *5*, 395-407.
Stiess, M., Maghelli, N., Kapitein, L.C., Gomis-Ruth, S., Wilsch-Brauninger, M., Hoogenraad, C.C., Tolic-Norrelykke, I.M., and Bradke, F. (2010). Axon extension occurs independently of centrosomal microtubule nucleation. Science *327*, 704-707.
Stringham, E.G., Marcus-Gueret, N., Ramsay, L., and Schmidt, K. (2012). Live Cell Imaging of the Cytoskeleton. In Methods in Enzymology, P.M. Conn, ed. (Academic Press), pp. 203-217.
Stumpff, J., von Dassow, G., Wagenbach, M., Asbury, C., and Wordeman, L. (2008). The kinesin-8 motor Kif18A suppresses kinetochore movements to control mitotic chromosome alignment. Dev Cell *14*, 252-262.

Su, K.C., Barry, Z., Schweizer, N., Maiato, H., Bathe, M., and Cheeseman, I.M. (2016). A Regulatory Switch Alters Chromosome Motions at the Metaphase-to-Anaphase Transition. Cell Rep *17*, 1728-1738.

Tanenbaum, M.E., Macurek, L., Janssen, A., Geers, E.F., Alvarez-Fernandez, M., and Medema, R.H. (2009). Kif15 cooperates with eg5 to promote bipolar spindle assembly. Curr Biol *19*, 1703-1711.

Tarau, I.S., Berlin, A., Curcio, C.A., and Ach, T. (2019). The Cytoskeleton of the Retinal Pigment Epithelium: from Normal Aging to Age-Related Macular Degeneration. Int J Mol Sci *20*.

Tolic, I.M. (2018). Mitotic spindle: kinetochore fibers hold on tight to interpolar bundles. Eur Biophys J *47*, 191-203.

Tolic, I.M., and Pavin, N. (2016). Bridging the gap between sister kinetochores. Cell Cycle *15*, 1169-1170.

Tolic-Norrelykke, I.M., Sacconi, L., Thon, G., and Pavone, F.S. (2004). Positioning and elongation of the fission yeast spindle by microtubule-based pushing. Curr Biol *14*, 1181-1186.

Uehara, R., Kamasaki, T., Hiruma, S., Poser, I., Yoda, K., Yajima, J., Gerlich, D.W., and Goshima, G. (2016). Augmin shapes the anaphase spindle for efficient cytokinetic furrow ingression and abscission. Mol Biol Cell *27*, 812-827.

Valentine, M.T., and Gilbert, S.P. (2007). To step or not to step? How biochemistry and mechanics influence processivity in Kinesin and Eg5. Curr Opin Cell Biol *19*, 75-81.

van Heesbeen, R.G., Tanenbaum, M.E., and Medema, R.H. (2014). Balanced activity of three mitotic motors is required for bipolar spindle assembly and chromosome segregation. Cell Rep *8*, 948-956.

Vanneste, D., Takagi, M., Imamoto, N., and Vernos, I. (2009). The role of Hklp2 in the stabilization and maintenance of spindle bipolarity. Curr Biol *19*, 1712-1717.

Verhey, K.J., and Hammond, J.W. (2009). Traffic control: regulation of kinesin motors. Nat Rev Mol Cell Biol *10*, 765-777.

Vogel, A., Lorenz, K., Horneffer, V., Huttmann, G., von Smolinski, D., and Gebert, A. (2007). Mechanisms of laser-induced dissection and transport of histologic specimens. Biophys J *93*, 4481-4500.

Vogel, A., Noack, J., Hüttman, G., and Paltauf, G. (2005). Mechanisms of femtosecond laser nanosurgery of cells and tissues. Appl Phys B *81*, 1015-1047.

Vogel, S.K., Pavin, N., Maghelli, N., Julicher, F., and Tolic-Norrelykke, I.M. (2009). Self-organization of dynein motors generates meiotic nuclear oscillations. PLoS Biol *7*, e1000087.
Vukusic, K., Buda, R., Bosilj, A., Milas, A., Pavin, N., and Tolic, I.M. (2017). Microtubule Sliding within the Bridging Fiber Pushes Kinetochore Fibers Apart to Segregate Chromosomes. Dev Cell *43*, 11-23 e16.
Vukušić, K., Buđa, R., Ponjavić, I., Risteski, P., Tolić, I.M. (2019a) Chromosome segregation is driven by joint microtubule sliding action of kinesins KIF4A and EG5. BioRxiv
Vukusic, K., Buda, R., and Tolic, I.M. (2019b). Force-generating mechanisms of anaphase in human cells. J Cell Sci *132*.
Walczak, C.E., Cai, S., and Khodjakov, A. (2010). Mechanisms of chromosome behaviour during mitosis. Nat Rev Mol Cell Biol *11*, 91-102.
Wandke, C., Barisic, M., Sigl, R., Rauch, V., Wolf, F., Amaro, A.C., Tan, C.H., Pereira, A.J., Kutay, U., Maiato, H*., et al.* (2012). Human chromokinesins promote chromosome congression and spindle microtubule dynamics during mitosis. J Cell Biol *198*, 847-863.
Watanabe, W., Arakawa, N., Matsunaga, S., Higashi, T., Fukui, K., Isobe, K., and Itoh, K. (2004). Femtosecond laser disruption of subcellular organelles in a living cell. Opt Express *12*, 4203-4213.
Waters, J.C., and Salmon, E. (1997). Pathways of spindle assembly. Curr Opin Cell Biol *9*, 37-43.
Wayne, R. (2010). In Plant Cell Biology, R. Wayne, ed. (Academic Press), pp. 319-338.
Wegner, A., and Isenberg, G. (1983). 12-fold difference between the critical monomer concentrations of the two ends of actin filaments in physiological salt conditions. Proc Natl Acad Sci U S A *80*, 4922-4925.
Wendell, K.L., Wilson, L., and Jordan, M.A. (1993). Mitotic block in HeLa cells by vinblastine: ultrastructural changes in kinetochore-microtubule attachment and in centrosomes. J Cell Sci *104 (Pt 2)*, 261-274.
Wheatley, S.P., Hinchcliffe, E.H., Glotzer, M., Hyman, A.A., Sluder, G., and Wang, Y. (1997). CDK1 inactivation regulates anaphase spindle dynamics and cytokinesis in vivo. J Cell Biol *138*, 385-393.
Worrall, J.T., Tamura, N., Mazzagatti, A., Shaikh, N., van Lingen, T., Bakker, B., Spierings, D.C.J., Vladimirou, E., Foijer, F., and McClelland, S.E. (2018). Non-random Mis-segregation of Human Chromosomes. Cell Rep *23*, 3366-3380.
Wu, X., Yin, H., and Li, Q. (2019). Ablation and Patterning of Carbon Nanotube Film by Femtosecond Laser Irradiation. Applied Sciences *9*, 3045.

Yanagida, M. (2014). The role of model organisms in the history of mitosis research. Cold Spring Harb Perspect Biol *6*, a015768.
Yang, W.V. (2018). The Cell Cycle. In Physiology of the Gastrointestinal Tract H.M. S., ed., pp. 197-219.
Yang, Z., Tulu, U.S., Wadsworth, P., and Rieder, C.L. (2007). Kinetochore dynein is required for chromosome motion and congression independent of the spindle checkpoint. Curr Biol *17*, 973-980.
Yanik, M.F., Cinar, H., Cinar, H.N., Chisholm, A.D., Jin, Y., and Ben-Yakar, A. (2004). Neurosurgery: functional regeneration after laser axotomy. Nature *432*, 822.
Yu, C.H., Redemann, S., Wu, H.J., Kiewisz, R., Yoo, T.Y., Farhadifar, R., Miller-Reichert, T., and Needleman, D. (2019a). Central spindle microtubules are strongly coupled to chromosomes during both anaphase A and anaphase B. BioRxiv *537290*.
Yu, C.H., Redemann, S., Wu, H.Y., Kiewisz, R., Yoo, T.Y., Conway, W., Farhadifar, R., Muller-Reichert, T., and Needleman, D. (2019b). Central-spindle microtubules are strongly coupled to chromosomes during both anaphase A and anaphase B. Mol Biol Cell *30*, 2503-2514.
Zhu, C., and Jiang, W. (2005). Cell cycle-dependent translocation of PRC1 on the spindle by Kif4 is essential for midzone formation and cytokinesis. Proc Natl Acad Sci U S A *102*, 343-348.

8 BIOGRAPHY

Renata Buđa was born on December 29, 1989 in Zagreb. She graduated in 2014 from the Faculty of Food Technology and Biotechnology, University of Zagreb, where she was listed among the top 10% of graduate students of Bioprocess Engineering. During her studies, she spent six months at an internship at the University of Edinburgh (UK), where she completed her undergraduate thesis under the mentorship of Teuta Pilizota and Bozidar Šantek. Since 2015 she has been working as a PhD at the Ruđer Bošković (IRB) within the ERC project, at the Division of Molecular Biology under the mentorship of Iva Tolić. At the same time, she has enrolled in the postgraduate study of Biology at the Faculty of Science in Zagreb. As part of her work at the IRB, she has spent six months at the Max Planck Institute in Dresden (Germany). She participated in four conferences where she gave an oral presentation of the scientific results in three of them (The EMBO Meeting 2016 in Mannheim, Kinetochore Workshop 2017 in Edinburgh and the Science Symposium in Split 2018) and in one of them in the form of a scientific poster (EMBL Symposium, Heidelberg, 2016). She has published five scientific papers in international journals and has won two awards: the Dean's Award for Plants - A New Generation of Organic Chemists (2012) and the Rudjer Boskovic Institute Annual Award for Microtubule Sliding within the Bridging Fiber Pushes Kinetochore Fibers Apart to Segregate Chromosomes ”(2018).

Publications:

1. Buđa, Renata*; Liu, Yunxiao*; Yang, Jin*; Hegde, Smitha*; Stevenson, Keiran; Bai, Fan; Pilizota, Teuta. Dynamics of Escherichia coli’s passive response to a sudden decrease in external osmolarity. *Proceedings of the National Academy of Sciences of the United States of America* (2016).

2. Buđa, Renata*; Vukušić, Kruno*; Tolić, Iva Marija. Dissection and characterization of microtubule bundles in the mitotic spindle using femtosecond laser ablation. *Methods in cell biology* (2017).

3. Vukušić, Kruno*; Buđa, Renata*; Bosilj, Agneza; Milas, Ana; Pavin, Nenad; Tolić, Iva Marija. Microtubule Sliding within the Bridging Fiber Pushes Kinetochore Fibers Apart to Segregate Chromosomes. *Developmental cell* (2017).

4. Pavoković, Dubravko; Buđa, Renata; Andrašec, Fran; Roje, Marin; Cvjetko Bubalo, Marina; Radojčić Redovniković, Ivana. Plant-mediated asymmetric reduction of 1-(3, 4-dimethylphenyl) ethanone, *Tetrahedron : asymmetry* (2017).

5. Vukušić, Kruno*; Buđa, Renata*; Ponjavić, Ivana*; Risteski, Patrik; Tolić, Iva Marija. Chromosome segregation is driven by joint microtubule sliding action of kinesins KIF4A and EG5. *bioRxiv* (2019).

* These authors contributed equally.